The Primary Sodium Binding Site of Human Concentrative Nucleoside Transporter 3, hCNT3

by

Sandra Gawad Gad

A thesis submitted in partial fulfillment of the requirements for the degree of

Master of Science
Biophysics

Department of Physiology
University of Alberta

Abstract

Nucleosides are essential for RNA and DNA synthesis. They also play a central role in other cellular metabolic pathways, and modulate a diverse array of physiological processes, including renal and cardiovascular function and neurotransmission. Due to their hydrophilic nature, specialized integral membrane proteins known as nucleoside transporters (NTs) are required for transport across cell membranes. In humans, the cation-coupled concentrative nucleoside transporter (CNT) family is represented by three members, hCNT1, hCNT2, and hCNT3. hCNT3, the most functionally versatile hCNT, is a cation-nucleoside symporter that transports both purine and pyrimidine nucleosides, as well as anticancer and antiviral nucleoside drugs. Produced as a recombinant protein in the *Xenopus* oocyte heterologous expression system, hCNT3 has been shown to have a Na^+:uridine coupling ratio of 2:1, in contrast to hCNT1/2 which have Na^+:uridine coupling ratios of 1:1. One of the two Na^+-binding sites of hCNT3 also accepts H^+. Recently, the crystal structure of a bacterial hCNT ortholog (vcCNT from *Vibrio cholerae*) has been reported. Based upon the crystal structure of vcCNT and previous mutagenesis studies of hCNTs, four amino acid residues (N336, V339, T370, and I371) were postulated to coordinate Na^+ (and hydronium ion) binding within the primary cation-binding site of hCNT3. To test this hypothesis, electrophysiological studies were performed on oocytes producing wild-type hCNT3 or engineered forms of the transporter in which each of the four residues were individually mutated to cysteine. The results show marked changes in Na^+- andH^+-coupling consistent with these residues forming the primary cation-binding site of hCNT3. Mutation of the corresponding residues in hCNT1 and characterization of wild-type and mutant forms of vcCNT in oocytes provide supporting evidence for this conclusion.

Contributions

Technologist Mrs. Amy M. L. Ng and Research Associate Dr. Sylvia Y. M. Yao constructed the mutants studied in this thesis. Honours student Shauna Regan performed the hCNT1 electrophysiology experiments described in Chapter 5, and Graduate student Cody Wu undertook the corresponding hCNT1 radioisotope studies. Honours student Cindy Wu performed the vcCNT radioisotope experiments in Appendix I. I was involved in the planning and design of each of these studies. Research Associate Dr. Kyla M. Smith provided guidance with electrophysiology, and all of the hCNT3 electrophysiological experiments and data described in Chapters 3 and 4 were undertaken and collected by myself. Finally, Drs. S.A. and J.M. Baldwin of the Astbury Centre for Structural Molecular Biology, School of Biomedical Sciences, University of Leeds, Leeds, UK used homology modelling and FATCAT alignment to construct the predicted 3D and topology models of hCNTs. The Baldwin laboratory also provided the vcCNT cDNA used in Appendix I.

Acknowledgements

Firstly, I would sincerely thank my supervisor Dr. James Young for providing me with the opportunity to work for him. I am very grateful for all the knowledge and many insightful discussions and suggestions Dr. Young has provided me over the past three years. He is a great researcher, and a better mentor.

"We learn by example and by direct experience because
there are real limits to the adequacy of verbal instruction."
— Malcolm Gladwell, Blink

I would also like to especially thank Dr. Kyla Smith for her abundant knowledge, patience, and teaching ability that have been unbelievably inspirational. For that I am forever indebted to her.

I am also very grateful to Dr. Edward Karpinski for all of his technical help and support throughout my thesis. As well, I would like to thank each of my committee members.

Finally, I would also like to thank the each member of the laboratory team for fostering a wholesome environment for me to excel.

Last, but not least, I would like to thank my Mom and friends for their unconditional love and support.

Table of Contents

List of Tables

List of Figures

List of Abbreviations and Symbols

AIDS	acquired immune deficiency syndrome
ATP	adenosine triphosphate
AZT	3'-azido-3'-deoxythymidine; zidovudine
BBB	blood-brain barrier
BCSFB	blood-cerebrospinal fluid barrier
CaCNT	CNT family member from *Candida albicans*
cDNA	complementary DNA
ChCl	choline chloride
CNS	central nervous system
CNT	concentrative nucleoside transporter
ddC	2', 3'-dideoxycytidine; zalcitabine
DNA	deoxyribonucleic acid
ENT	equilibrative nucleoside transporter
g	gram
gemcitabine	2'-deoxy-2',2'-difluorocytidine; dFdC
h	human
hr	hour
hepes	4-(2-hydroxyehtyl)-1-piperazineethanesulfonic acid
hf	hagfish
HP	hairpin loop
Hz	hertz
IH	interfacial helix
I	nucleoside- induced current
I_{max}	predicted current maximum
K_{50}	cation concentration at half-maximal unidirectional flux; apparent affinity for cation
K_m	permeant concentration at half-maximal unidirectional flux; apparent affinity for permeant
l	liter

M	molar
MES	2-(N-morpholino)ethanesulfonic acid
min	minute
mM	millimolar
mRNA	messenger RNA
mV	millivolt
n	Hill coefficient
NBMPR	nitrobenzylthioinosine; nitrobenzylmercaptopurine riboside
nd	not determined
NT	nucleoside transporter
NupC	CNT family member from *Escherichia coli*
p	pico; 10^{-12}
PCMBS	*p*-chloromercuribenzene sulfonate
RNA	ribonucleic acid
'SCAM	substituted cysteine accessibility method
SDS	sodium dodecyl sulphate
SE	standard error of the fitted estimate
SEM	standard error of the mean
SLC	solute carrier
T	absolute temperature
TEVC	two-microelectrode voltage clamp
TM	transmembrane domain
V	nucleoside- induced flux
V_h	holding potential
V_m	membrane potential
V_{max}	maximum transport rate
vc	*Vibrio cholerae*
°C	degrees Celsius
Ω	Ohms
µ	micro; 10^{-6}

Chapter 1:

General Introduction

Physiological Role of Nucleosides

Nucleosides are important physiological molecules involved in numerous cellular processes, including DNA and RNA synthesis, cell signaling, enzyme regulation, and metabolism. Naturally occurring nucleosides include the purine nucleosides adenosine, guanosine, and inosine and the pyrimidine nucleosides cytidine, thymidine, and uridine. Nucleosides are metabolic precursors of nucleotides, including high-energy compounds such as ATP, and are thus precursors for the synthesis of DNA or RNA (Baldwin *et al.,* 1999; King*et al*., 2006; Jordheim *et al.,* 2013).

Purinergic nucleosides, in particular adenosine, are important for signaling cascades; they control a number of G-protein coupled receptors of the P1 family (A1, A2A, A2B, and A3), particularly in heart and neurogenic tissue (McIntosh and Lasely, 2012). Through interaction with cell surface purinergic receptors, adenosine is involved in the regulation of coronary bloodflow, platelet aggregation, renal function, and neurotransmission and neuromodulation (Damaraju *et al.,* 2003; Wang *et al*., 2013). Nucleoside transporters (NTs) play a key role in the regulation of extracellular concentrations of adenosine available to bind to receptors and thereby modulate various physiological processes (Damaraju *et al*., 2003). The importance of adenosine is shown by its ability to be transported by all known human NTs (Young *et al*., 2013).

Nucleosides are hydrophilic molecules and, thus, their passive diffusion across biological membranes is limited. Specialized NTs are therefore required in order for nucleosides to cross plasma membranes or move between intracellular compartments (Cass *et al*., 1998). The cellular uptake of nucleosides is essential for the synthesis of nucleic acid precursors by salvage pathways. Nucleoside salvage pathways are energetically more favorable than *de novo* biosynthetic pathways and thus NTs have key roles in nucleoside and nucleotide homeostasis. Additionally, some cell types, such as bone marrow cells, enterocytes, erythrocytes, and certain cells in the CNS, are deficient in *de novo* biosynthetic pathways and thus rely solely on salvage pathways involving nucleoside transport into cells (Damaraju *et al*., 2003; King *et al*., 2006).

Nucleosides are also vital for metabolic activity (Young *et al.,* 2013). In the brain, for example, the blood-brain barrier (BBB) and the blood-cerebrospinal fluid barrier (BCSFB) represent the main obstacles for nutrient and drug movement between the CNS and the peripheral circulation (Parkinson *et al*., 2011). Nucleoside access and drug exposure are made

possible by the presence of multiple NTs present in the BBB endothelial cells of the vasculature and the BCSFB epithelial cells (Parkinson *et al.,* 2011; Young *et al.,* 2013). The presence of altered nucleoside levels is implicated in a number of conditions including epilepsy, neurodegenerative disorders, various psychiatric conditions, and cerebrovascular ischemia (Parkinson *et al.,* 2011).

Nucleoside analog drugs or nucleoside inhibitor drugs represent an area of current and potential therapy for a variety of conditions, including ischemia, cancer, viral infections, treatment of chronic pain, ethanol-mediated/anxiety- like behaviors, and epilepsy (Pastor-Anglada *et al*., 2005). Examples of chemotherapeutic antiviral and anticancer drugs include AZT (zidovudine; 3'-azido-3'-deoxythymidine) and gemcitabine (2', 2'-difluorodeoxycytidine), respectively (Damaraju *et al*., 2003; Young *et al*., 2013). AZT, a thymidine analog, is used in the treatment of acquired immune deficiency syndrome (AIDS). After transport into the cell, AZT is phosphorylated to its triphosphate analogue which inhibits the enzyme viral reverse transcriptase, and, ultimately, viral DNA replication (King *et al.,* 2006). Gemcitabine, a pyrimidine analog of deoxycytidine, is employed in the treatment of solid tumors, including non-small cell lung, breast, bladder, pancreatic, ovarian and other cancers (Mackey *et al*., 1998; Damaraju *et al*., 2003). The triphosphate form of gemcitabine replaces one of the building blocks of nucleic acids, in this case dCTP, during DNA replication. This process arrests tumor growth. Gemcitabine alsoacts by inhibiting the enzyme ribonucleotide reductase (Mackey *et al*., 1998; Damaraju *et al*.,2003). The diphosphate form of gemcitabine binds to the enzyme's active site and inactivates the enzyme irreversibly, so that DNA replication and repair cannot occur (Mackey *et al*., 1998;Damaraju *et al*., 2003).

Nucleoside Transporter Proteins

Various nucleoside transport processes have been described in eukaryotic and prokaryotic cells. Molecular cloning strategies and heterologous expression systems, along with genome sequencing projects and bioinformatics analysis, have led to the identification of a diverse array of structurally distinct nucleoside transport protein families. The importance of nucleosides is highlighted by the multiplicity of nucleoside transport protein families in different organisms, including the H^+:nucleoside symporter family, the Tsx channel-forming protein family, the

uracil/allantoin permease family, the nucleoside permease family, the organic cation transporter family, and the organic anion transporter family (Pastor-Anglada *et al*., 2005). In humans, the proteins responsible for the uptake of nucleosides across cell membranes belong to two structurally unrelated protein families: the concentrative nucleoside transporters (CNTs) and the equilibrative nucleoside transporters (ENTs) (Baldwin *et al*., 1999; Young *et al*., 2013), and are further discussed below.

The Equilibrative Nucleoside Transporter (ENT) Family

Members of the equilibrative nucleoside transporter family (ENT), also designated in humans as the Solute Carrier 29 (SLC29) family, are transmembrane glycoproteins that localize to the plasma membrane and, as well, intracellular membranes (Young *et al*., 2008). ENT family members have 11 transmembrane (TM) α-helices, and are present in most, if not all, cell types (Young *et al.,* 2008, 2013). ENTs mediate the bidirectional transport of hydrophilic physiological nucleosides and nucleoside analogs down their concentration gradients across cellular membranes (Young *et al*., 2008, 2013). Some members of the ENT family, described below, are activated at low pH, and thus may be capable of H^+-coupled active transport of nucleosides (Young *et al.,* 2013). ENTs are widely distributed amongst eukaryotes, including mammals, protozoa, nematodes, insects, fungi, and plants, but appear to be absent from prokaryotes (Young *et al.,* 2013).

cDNAs encoding ENTs from a variety of different eukaryotes have been isolated and the proteins functionally characterized. There are four human ENT (hENT) isoforms: hENT1, hENT2, hENT3, and hENT4 (Young *et al*., 2008, 2013). Of these, hENT1 and hENT2 are the most extensively characterized, and are distinguished functionally on the basis of sensitivity to inhibition by nanomolar concentrations of nitrobenzylthioinosine (nitrobenzylmercaptopurine riboside; NBMPR), with hENT1 being NBMPR-sensitive and hENT2 being NBMPR-insensitive (Baldwin *et al.,* 2004).

hENT1 (SLC29A1)

The human ENT1 gene has been localized to the p21.1 - 21.2 region of chromosome 6 (Coe *et al*., 1997). During the late 1990s, Griffiths *et al.* (1997a) used N-terminus amino acid sequence information from the purified human erythrocyte ENT1 to isolate and clone the cDNA encoding hENT1. hENT1 is 456 amino acid residues in length, and shares 78 % identity in amino acid sequence to its rat (rENT1) and mouse (mENT1) homologues (Kiss *et al*., 2000; Visser *et al.,* 2002). hENT1 is capable of transporting a broad range of purine andpyrimidine nucleosides and corresponding nucleobases (hypoxanthine, thymine, adenine and, to a lesser extent, uracil and guanine) (Griffiths *et al*., 1997a; Yao *et al*., 2011) (Figure 1-1). When produced in *Xenopus laevis* oocytes, nucleoside transport mediated by hENT1 was saturable and conformed to Michaelis-Menten kinetics with an apparent K_m value of 0.4 mM for uridine (Griffiths *et al*., 1997a; Yao *et al*., 2011). Nucleobases were transported by hENT1 with lower affinity than nucleosides (Yao *et al*., 2011). hENT1, in common with other NTs, does not transport nucleotides such as ATP (Kiss *et al*., 2000; Baldwin *et al.* 2004; Wang *et al*., 2013).

hENT1 is ubiquitously distributed in human tissues, such as liver, heart, spleen, kidney, lung, and intestine at varying levels of expression (Visser *et al.,* 2002; Baldwin *et al.,* 2004). Interestingly, hENT1 and hENT2 are highly expressed in vascular endothelium, with hENT1 being expressed at levels twice those seen with hENT2, implying its implication in controlling adenosine signaling in conditions of hypoxia (Podgorska *et al.,* 2005; Loffler *et al.*, 2007). The membrane abundance of hENT1 may function as an important biomarker in the clinical efficacy of gemcitabine treatment of pancreatic cancer (Damaraju *et al.,* 2009; Spratlin and Mackey,2010).

hENT2 (SLC29A2)

The human ENT2 gene is localized to position 13q on chromosome 11 (Griffiths *etal*., 1997b; Baldwin *et al.,* 2004; Young *et al*., 2013). Due to its high homology with hENT1, cDNA encoding hENT2 was isolated shortly after hENT1 using a functional complementat ion approach (Griffiths *et al*., 1997b; Baldwin *et al.,* 2004). hENT2 is 456 amino acid residues in length and 46 % identical in sequence to hENT1 (Griffiths *et al*., 1997b). Similar to hENT1, hENT2 mRNA is expressed in a variety of tissues, including liver, lung, brain, kidney, heart, pancreas, placenta

and, predominantly, in skeletal muscle (Hyde *et al*., 2001; Baldwin *et al.,* 2004). In a similar manner to hENT1, hENT2 transports a broad range of purine and pyrimidine nucleosides. When produced in *Xenopus laevis* oocytes, an apparent K_m value for uridine of 0.5 mM was reported for hENT2 (Griffiths *et al*., 1997b; Baldwin *et al.,* 2004; Yao *et al*., 2011) (Figure1-1). With the exception of uridine and inosine, hENT2 mediates transport of other nucleosides with lower apparent affinities than hENT1 (Ward *et al*., 2000). hENT2 is also able to efficiently transport a wide range of natural purine and pyrimidine nucleobases, although cytosine is only weakly transported by hENT2 (Yao *et al*., 2002a; Young *et al*., 2008). The apparent affinities of hENT2 for nucleobases are lower than for the corresponding nucleosides (Young *et al.,* 2008). hENT2 is hypothesised to be important during muscle exercise and recovery, based upon its ability to transport the nucleobase hypoxanthine, its high affinity for inosine, and its abundance in skeletal muscle (Griffiths *et al*., 1997b; Baldwin *et al.,* 2004).

hENT3 (SLC29A3)

The gene encoding hENT3 is located at position 22.1 of chromosome 10 (Young *et al.,* 2013). hENT3 is 475 amino acid residues in length and is 29 % identical in amino acid sequence to hENT1 (Baldwin *et al*., 2005; Young *et al*., 2008). This transporter was discovered following completion of the human genome project. Similar to hENT1 and hENT2, hENT3 is present in a wide range of tissues, but is especially abundant in the placenta (Hyde *et al*., 2001; Young *et al*., 2008). hENT3 is predominantly localized to intracellular membranes, particularly lysosomal membranes (Baldwin *et al*., 2005; Young *et al*., 2008). Unlike hENT1, but similar to hENT2, hENT3 is NBMPR-insensitive (Baldwin *et al*., 2005). hENT3 demonstrates a broad selectivity for nucleosides and nucleobases (Baldwin *et al*., 2005; Young *et al*., 2008). It does not, however, mediate the transport of hypoxanthine (Young *et al*., 2008). Transport mediated by hENT3 is strongly dependent upon pH, suggesting potential H^+-coupling (Baldwin *et al*., 2005; Young *et al.,* 2008; Wang *et al.,* 2013).

hENT4 (SLC29A4)

The gene encoding hENT4 is located at position 22.1 on chromosome 7 and, like hENT3, was discovered by genome database analysis (Coe *et al*., 2002; Young *et al*., 2008; Young *et al*., 2013; Wang *et al.,* 2013). hENT4 is 530 amino acid residues in length and exhibits a very low amino acid sequence identity to hENT1 (18 %) (Young *et al*., 2008). hENT4 is distributed in a wide range of tissues such as brain, skeletal muscle, heart, intestine, pancreas, kidney, liver, bone marrow, and lymph node (Engel *et al*., 2004; Barnes *et al*., 2006).

Originally identified as an adenosine-specific transporter, hENT4 has now been shown to transport monoamines (Wang *et al.,* 2013; Young *et al.,* 2013). hENT4 has the lowest affinity for adenosine compared to the other hENT isoforms, and is only weakly inhibited by NBMPR (Baldwin *et al*., 2005). Like hENT3, the transport of adenosine is only observed at acid pH, again suggesting the possibility of H^+-coupling (Baldwin *et al.,* 2005; Wang *et al.,* 2013).

The Conce ntrative Nucle oside Transporte r (CNT) Family

Members of the concentrative nucleoside transporter family, also classified in humans as the Solute Carrier 28 (SLC28) family, are found in epithelia such as small intestine, kidney, and liver, and other specialized cells (Young *et al*., 2008). The human genome contains three SLC28 family genes (SLC28A1, SLC28A2, and SLC28A3) that encode three CNT proteins (hCNT1, hCNT2, and hCNT3, respectively) (Baldwin *et al*., 1997; Larrayoz *et al*., 2004; Young *et al*., 2013). CNTs are integral membrane proteins that mediate the active transport of nucleosides across cellular membranes, moving nucleosides against their concentration gradients bycoupling to cations moving down their electrochemical gradients. These transporters differ in their nucleoside and cation selectivities, and cation stoichiometries (Young *et al*., 2013) (Figure 1-1). CNT proteins are found in numerous eukaryotes, including mammals, lower vertebrates, fungi, and nematodes (Young *et al.,* 2013) and, unlike ENTs, are also found in prokaryotes (Young *et al*., 2013). A number of CNT familymembers from both eukaryotes and prokaryotes have been characterized functionally.

hCNT1 (SLC28A1)

The gene encoding the human CNT1 protein is located at position q25 - 26 on chromosome 15 (Ritzel *et al*., 1997). It consists of 650 amino acid residues (Ritzel *et al*., 1997). hCNT1 is found in intestine, kidney, liver, placenta, and brain (Huang *et al*., 1994; Young *et al.* 2013).

hCNT1 mediates pyrimidine nucleoside transport in a Na^+- and voltage-dependent manner (Ritzel *et al*., 1997; Smith *et al*., 2004) (Figure 1-1). In addition, hCNT1 also mediates transport of the purine nucleoside adenosine, but at rates much lower than pyrimidine nucleosides (Ritzel *et al*., 1997; Smith *et al*., 2004). Produced in *Xenopus laevis* oocytes, nucleoside transport mediated by hCNT1 is saturable and conforms to Michaelis-Menten kinetics with an apparent K_m value of 32 μM for uridine at a membrane potential of -50 mV (Smith *et al*., 2004). Unlike some other members of the CNT family (*e.g.* hCNT3), hCNT1 does not use the H^+ electrochemical gradient for transport (Smith *et al.,* 2004). The relationship between nucleoside flux and Na^+ concentration is hyperbolic, with an apparent K_{50} of 11 mM for Na^+ at a membrane potential of -30 mV, and a calculated Hill coefficient consistent with a 1:1 Na^+:nucleoside coupling ratio (Ritzel *et al*., 1997; Smith *et al*., 2004, 2007). Electrophysiological charge/flux ratio studies determined directly that the Na^+:nucleoside coupling ratio is 1:1 (Smith *et al*., 2004, 2007). Kinetic studies suggest an ordered binding mechanism in which Na^+ binds to the transporter first, increasing the affinity for nucleoside, which then binds second (Smith *et al*., 2004).

hCNT2 (SLC28A2)

The human gene locus for hCNT2 is 15q15 (Ritzel *et al*., 1998). This nucleoside transporter has been detected in a wide range of human tissues such as heart, liver, kidney, brain, placenta, pancreas, skeletal muscle, colon, and the small intestine (Ritzel *et al*., 1998). hCNT2 consists of 658 residues and is 72 % identical in amino acid sequence to hCNT1 (Ritzel *et al*., 1998). hCNT2 transports purine nucleosides and uridine in a Na^+- and voltage-dependent manner (Ritzel *et al*., 1997; Smith *et al*., 2007; Young *et al*., 2013) (Figure 1-1). The apparent K_m for uridine calculated by radioisotope flux studies in *Xenopus* oocytes is 40 μM (Ritzel *et al*., 1998). hCNT2 Na^+ concentration dependence curves are hyperbolic, with an apparent K_{50} of 16 mM for Na^+ at a membrane potential of -30 mV, and a Hill coefficient consistent with an apparent

Na^+:nucleoside coupling stoichiometry of 1:1 (Smith *et al*., 2007). Electrophysiological charge/flux ratio studies determined directly that the Na^+:nucleoside coupling ratio was 1:1 (Smith *et al*., 2004, 2007).

hCNT3 (SLC28A3)

The gene encoding hCNT3 is located at position q22.2 on chromosome 9 (Ritzel *et al*., 2001). hCNT3 has a broader tissue distribution than both hCNT1 and hCNT2; tissues containing hCNT3 transcripts include trachea, pancreas, bone marrow, mammary gland, liver, prostate and regions of the intestine, brain and heart (Ritzel *et al.,* 2001). hCNT3 is 691 amino acids in length and is 48 % and 47 % identical in amino acid sequence to hCNT1 and hCNT2, respectively (Ritzel *et al.,* 2001).

hCNT3 mediates the Na^+-dependent uptake of a broad range of both pyrimidine and purine nucleosides (Ritzel *et al*., 2001; Smith *et al*., 2005) (Figure 1-1). Pyrimidine and purine nucleosides are transported with similar kinetic efficiencies, with K_m values determined from radioisotope flux studies in the range of 15 to 53 μM for all nucleosides tested (Ritzel *et al*., 2001). Similar to hCNT1 and hCNT2, transport mediated by hCNT3 is voltage-dependent (Smith*et al*., 2004, 2007). Unlike hCNT1/2, however, the relationship between uridine uptake and Na^+ concentration is sigmoidal, with an apparent K_{50} of 4.7 mM for Na^+ at a membrane potential of -30 mV (Smith *et al*., 2007). The Hill coefficient is consistent with an apparent Na^+:nucleoside coupling stoichiometry of 2:1 (Smith *et al*., 2007). Electrophysiological charge/flux ratio studies are in agreement with the Hill coefficient, and determined directly that the Na^+:nucleoside coupling ratio is 2:1 (Smith *et al*., 2004, 2007). In addition to Na^+, and different from hCNT1/2, hCNT3 can also use the electrochemical gradient of H^+ to drive nucleoside uptake into cells (Smith *et al*., 2005, 2007). Unlike Na^+, the relationship between uridine uptake and external pH (in the absence of Na^+) is hyperbolic, with a Hill coefficient consistent with a H^+:nucleoside coupling stoichiometry of 1:1 (Smith *et al*., 2005). Apparent K_{50} values for H^+ and Na^+ differed by four orders of magnitude (480 nM and 4.7 mM, respectively) (Smith *et al*., 2005). Electrophysiological charge/flux ratio studies confirmed directly that the H^+:nucleoside coupling ratio is indeed 1:1 (Smith *et al*., 2005, 2007).

Transport in the presence of H^+ and in the absence of Na^+ has a marked effect on the permeant selectivity of hCNT3. In the presence of Na^+, all nucleosides tested were transported with similar efficiencies (Smith *et al*., 2005). In the presence of H^+ only, the selectivity profile of hCNT3 is as follows: uridine>> thymidine> adenosine> cytidine> inosine> guanosine (Smith *et al*., 2005). This difference in permeant selectivity between Na^+- and H^+-coupled hCNT3 is also seen with therapeutic nucleosides. hCNT3 mediates the Na^+-dependent uptake of the anti-cancer drug gemcitabine and the antiviral drugs AZT and ddC (Smith *et al*., 2005). H^+-coupled hCNT3 transports gemcitabine but not AZT and ddC (Smith *et al*., 2005). These findings suggest that Na^+- and H^+-coupled hCNT3 have different conformations of the nucleoside binding pocket and/or the translocation pore (Smith *et al.,* 2005).

The Na^+:H^+:nucleoside stoichiometry of hCNT3 in the presence of both Na^+ and H^+ is 1:1:1. Under these conditions, hCNT3 retains a higher affinity for H^+ over Na^+ and a broad permeant selectivity for both pyrimidine and purine nucleosides (Smith *et al*., 2005). These observations led to the proposal that one of the two cation-binding sites of hCNT3 accepts both Na^+ and H^+, while the second is Na^+-specific.

hCNT Membrane Topology

Using hydropathy analysis and multiple sequence alignments, human CNTs were initially predicted to contain 13 putative transmembrane domains (TMs) with a cytoplasmic N-terminus and an extracellular C-terminus (Hamilton *et al*., 2001). Computer algorithms also identified 2 additional weakly predicted TMs (Hamilton *et al*., 2001). Chimeric studies involving hCNT1/2, hCNT1/3 and hCNT1/hfCNT (a broadly selective CNT from the Pacific hagfish *Eptatretus stouti* with a Na^+:nucleoside coupling ratio of 2:1) have shown that the functional domains responsible for CNT nucleoside binding and cation coupling reside within TMs 7 - 13 of the protein (Loewen *et al*., 1999; Yao *et al*., 2002b; Smith *et al*., 2005). In comparison, NupC, a H^+-coupled CNT family member from *Escherichia coli,* lacks TMs 1 - 3, but otherwise shares a similar membrane topology (Loewen *et al*., 2004). It has been shown that TMs 1 - 3 are not required for Na^+-dependent uridine transport activity in hCNTs (Hamilton *et al*., 2001).

In the absence of a crystal structure for hCNT3, valuable information was obtained on the protein's membrane topology by substituted cysteine accessibility method (SCAM) analysis

using the impermeable thiol reactive reagent *p*-chloromercuribenzene sulfonate (PCMBS) (Sluogski *et al*., 2009). SCAM analysis was performed on the TM 11 - 13 region of hCNT3, including bridging extramembranous loops (Slugoski *et al*., 2009). The results identified residues of functional importance and predicted a new revised 15 TM topology for the CNTs with previously unidentified discontinuous helices that might potentially play a role in ion recognition, binding and translocation (Slugoski *et al*., 2009). Recently, Johnson *et al*. (2012) solved the crystal structure of a bacterial nucleoside transporter (vcCNT) that displays high sequence homology to hCNT3. This provided important insights into the possible 3D structure and predicted membrane topology of hCNT3, leading to a revised hCNT3 topology as will be discussed later in this thesis (Chapter 3).

vcCNT

Members of the CNT nucleoside transporter family are found in a wide range of both eukaryotes and prokaryotes (Young *et al*., 2013). The nucleoside transporter vcCNT from *Vibrio cholera* possesses a remarkably high amino acid sequence homology (39 %) to hCNT3 (Figure 1-2) and, like human CNTs, is Na^+ dependent (likely one or possibly two Na^+ ions). The recent crystal structure of vcCNT solved by Johnson *et al*. (2012) reveals, for the first time, the molecular 3D structure of a CNT protein (Figure 1-3). The structure was solved at a resolution of 2.4 Å with a single bound Na^+ ion and uridine molecule, revealing the potential locations of both the Na^+ and nucleoside binding sites (Johnson *et al*., 2012). Functional studies of vcCNT were limited to demonstrating that uridine uptake mediated by the protein is indeed Na^+-dependent, but further functional studies have not been undertaken (Johnson *et al*., 2012).

The vcCNT crystal structure shows a membrane topology consisting of 8 TMs, including discontinuous helices, hairpin loops, and interfacial helices (Johnson *et al*., 2012) (Figure 1-3C). The crystal structure also reveals a trimeric configuration, in which each monomer is believed to act independently from the other monomers (Johnson *et al*., 2012) (Figure 1-3A, B). The 8 TM monomer topology contains several unique features including two re-entrant helix-turn-helix hairpins (HP1 and HP2) and 3 interfacial helices (1H1, 1H2, and 1H3). HP1 and HP2 have opposite orientations in the membrane (Figure 1-3C). 1H1 and 1H3 run parallel to the extracellular face of the membrane and 1H2 runs parallel to the intracellular face of the

membrane (Johnson *et al*., 2012). vcCNT has extracellular N- and C-termini (Johnson *et al*., 2012).

Each monomer can be divided into two subdomains: a scaffold domain (TM1, TM2, 1H1, EH, TM3, and TM6) which is important for maintaining trimerization and transporter architecture, and a transport domain composed of two structural regions with a 2 fold-pseudo symmetry separated by TM6 (Johnson *et al*., 2012) (Figure 1-3C, D). The first subdomain comprises IH2, HP1, TM4a/b, and TM5 while the second subdomain comprises IH3, HP2, TM7a/b and TM8 (Figure 1-3C). The tips of HP1 and HP2 and the unwound parts of discontinuous helices TMs 4 and 7 are located at the centre of the transport domain equidistant from the two membrane surfaces (Johnson *et al*., 2012).

The vcCNT crystal structure shows the location of the single nucleoside binding site (Johnson *et al*., 2012) (Figure 1-4). As shown in Fig. 1-4C, polar or charged amino acids within HP1 (Q154, T155, and E156) and TM4b (V188) are predicted to interact with the uracil base of uridine, while HP2 (E332) and TM7 (N368 and S371) are predicted to interact with the ribose moiety of uridine. The side chains of amino acids of HP1 interact either directly (Q154) or indirectly (T155 and E156) through a water molecule with the uracil base (Johnson *et al*., 2012) (Figure 1-4C). V188 from TM4b interacts with the uracil base through van der Waals interactions (Johnson *et al*., 2012). The side chains of amino acids of HP2 and TM7b interact directly (E332 (HP2), N368 (TM7b), S371 (TM7b)) or indirectly with the ribose through a water molecule (N368 (TM7)) (Johnson *et al*., 2012).

The single Na^+-binding site predicted by the crystal structure of vcCNT is located between HP1 and the unwound region of TM4 (Johnson *et al*., 2012) (Figure 1-4D). The crystal structure demonstrates that the Na^+ ion is octahedrally coordinated by 3 backbone carbonyls and 2 side-chain hydroxyls contributed by amino acid residues N149, V152, S183, and I184. Since key amino acid residues involved in the binding of the nucleoside base are also located on HP1 and TM4b, it is hypothesized that the binding of Na^+ moves HP1 closer to TM4, enabling the complete formation of the nucleoside binding site, and thus increasing binding affinity for the nucleoside (Johnson *et al*., 2012) (Figure 1-4E).

A recent study by Feng *et al*. (2013) used molecular dynamics simulations of the vcCNT structure to model transport of uridine in the presence of various Na^+ gradients. These studies showed Na^+ to be required for transport of uridine but, in contrast to the vcCNT crystal structure,

predicted that 2 Na^+ ions are necessary for uridine to pass from its binding site through the entrance formed by TMs 6 and 7 and into the intracellular side of the membrane (Feng *et al*., 2013; Johnson *et al*., 2012). In this thesis, however, a kinetic analysis of vcCNT ispresented which is consistent with only a single binding site for Na^+ (Appendix I).

As described in this thesis, sequence alignments between the hCNTs (hCNT1, hCNT2, and hCNT3) and vcCNT and homology 3D modelling have identified each of the potential amino acids involved in coordinating the primary hCNT Na^+-binding site (*i.e*., theNa^+-binding site common to all hCNT family members). A discussion of these residues and the functional consequences of their mutation will be presented in subsequent chapters of this thesis.

Electrophysiology

Electrophysiology has evolved tremendously over the years. Previously a simple method for detecting neural activity of excitable tissues, it is now a robust tool for studying electrogenic (*i.e*., current generating) transport processes at a molecular level (Grewer *et al*., 2013). Initially, the transport properties of recombinant CNT proteins were studied using radioisotope flux assays in *Xenopus* oocytes. Initial molecular cloning and functional studies of hCNT1/2/3 were performed in this way (Ritzel *et al*., 1997, 1998, 2001). Functional studies of these proteins have subsequently been furthered by use of electrophysiological techniques (Smith *et al*., 2004, 2005, 2007). Electrophysiology is advantageous because it is highly sensitive, has a high time resolution, and allows accurate control of the membrane potential while measuring currents produced by voltage-dependent processes (Grewer *et al*., 2013). Electrophysiology also allows the study of all events involving the movement of charge, including electrogenic substrate transport (known as steady-state currents) and charge movements involved in the transport process (known as presteady-state currents). There are several recording techniques used to measure electrical signals of proteins; the most commonly used technique and the technique used in this thesis is the two-microelectrode voltage clamp.

Two-Microelectrode Voltage Clamp

The two-microelectrode voltage clamp technique is frequently used to study whole cell

currents through ion channels, electrogenic transporters, or ion pumps produced in the plasma membrane of *Xenopus* oocytes. This technique allows control of the membrane potential (voltage clamping) while measuring currents flowing through proteins. One intracellular microelectrode (voltage electrode) monitors the actual intracellular potential of the oocyte, while an amplifier compares the resting potential recorded by the voltage electrode to the desired potential (clamping/command potential). A second intracellular microelectrode (current electrode) injects current into the oocyte to minimize this difference (Axon Guide, 2008). The *Xenopus* oocyte is an ideal cell model to use in conjunction with the two-microelectrode voltage clamp because its characteristics make it possible to generate stable recordings over long periods of time (Grewer *et al*., 2013).

Depending on the design and objective of the experiment, two types of currents can be measured using the two-microelectrode voltage clamp: steady-state and presteady-state currents. Steady-state currents are measures of electrogenic permeant transport and are observed following activation of a transporter with a permeant (and coupling ion). Steady-state currents are used to measure parameters such as K_m or K_{50} values for interaction of transporters with, respectively, permeants or ions (measures of apparent affinity), voltage-dependence of transport, coupling ratio (permeant:ion coupling ratio), and permeant or ion specificity. Presteady-state currents are transient currents which reflect charge movements of voltage-dependent processes in transporters. They are observed following ion binding to and dissociation from a transporter and reflect conformational changes of the transporter within the membrane. Presteady-state currents are observed following a step change in the membrane potential in permeant-free medium in the presence or absence of a coupling ion (Grewer *et al*., 2013). Presteady-state currents allow examination of partial reactions in the transport cycle and calculation of parameters such as the number of functional proteins expressed in an oocyte plasma membrane, the effective fraction of the membrane field experienced by the movable charge, the turnover number of the transporter, and rate constants for individual steps in the translocation cycle.

Thesis Objectives

The research presented in this thesis focuses primarily on one member of the human CNT family - human concentrative nucleoside transporter 3 (human CNT3; hCNT3). hCNT3 contains

two Na^+-binding sites, one of which can also accept H^+ (Smith *et al.*, 2005, 2007). hCNT1 and hCNT2, in comparison, are only able to transport a single Na^+ ion and are Na^+-specific (Smith *et al*., 2007). Some other members of the CNT family of proteins, such as NupC from *Escherichia coli,* function exclusively as H^+:nucleoside symporters (Loewen *et al*., 2004). It is therefore hypothesized that the cation-binding site in hCNT3 corresponding to that seen in vcCNT is the hCNT3 cation-binding site that accepts both Na^+ and H^+. This cation-binding site is therefore the primary cation-binding site found in all CNT family members; it accepts either Na^+ alone (vcCNT, hCNT1, and hCNT2), H^+ alone (NupC), or both Na^+ and H^+ (hCNT3). The crystal structure of vcCNT has provided a powerful framework with which to characterize the primaryNa^+-binding site in human CNTs. Multiple sequence alignments and 3D homology modelingusing the crystal structure of vcCNT as a template allowed us to predict the residues in humanCNTs that correspond to those in vcCNT implicated in Na^+-binding. This thesis focuses on fourresidues of hCNT3 (N336, V339, T370, and I371), corresponding to those in vcCNT (N149, V152, S183, and I184), predicted to be responsible for coordinating the primary cation-binding site. Using the two-microelectrode voltage clamp, in combination with heterologous expression in *Xenopus* oocytes, I have compared the cation-coupling characteristics of hCNT3 wild-type (hCNT3-WT) with four hCNT3 mutants (N336C, V339C, T370C, and I371C) (Chapter 3). It is hypothesized that mutation of these residues will lead to changes in hCNT3 cation-binding affinity and, perhaps, cation-selectivity, and thus elucidate the structural basis of hCNT3 cation-binding.

As well, to further understand the Na^+-binding site of this and other CNTfamily members, residues N336 and T370 of hCNT3 were subject to further mutation (N336A, N336S and N336T and T370G and T370S) (Chapter 4). The choice of amino acids to which these residue positions were mutated was determined by possible correlations with cation specificity seen in different CNT family members.

This thesis also includes parallel studies of hCNT1, a Na^+-dependent, H^+-independent nucleoside transporter with a single cation-binding site (1:1 Na^+:nucleoside coupling ratio) (Smith *et al*., 2004) (Chapter 5). It is hypothesized that since hCNT1 has only a single Na^+-binding site, mutation of amino acids coordinating this site will result in marked impairment orloss of function, providing evidence that this is indeed the Na^+-binding site common to all CNT family members. Focusing on two of the residue positions studied in hCNT3 (N336 and T370),

the corresponding residues in hCNT1 (N315 and T349) were mutated to N315S, N315T, N315A, T349C, T349G, and T349S and the functional consequences determined.

Finally, this thesis also contains, for the first time, the functional characterization of vcCNT produced in *Xenopus laevis* oocytes using radioisotope flux analysis (Appendix I). Residue N149, which is important in coordinating the Na^+-binding site in vcCNT, was also mutated (N149S, N149T, and N149A) and the effect on function was examined.

The general discussion of this thesis in Chapter 6 draws these various findings together to provide insight and a fundamental understanding of the molecular mechanism(s) by which human and other CNTs interact with Na^+ and H^+ during nucleoside and nucleoside drug translocation.

References

Acimovic, Y. and Coe, I.R. Molecular Evolution of the Equilibrative Nucleoside Transporter Family: Identification of Novel Family Members in Prokaryotes and Eukaryotes. 2002. *Mol. Biol. Evol.* 12:2199-2210.

Baldwin, S.A., Mackey, J.R., Cass, C.E., and Young, J.D. 1999. Nucleoside transporters: molecular biology and implications for therapeutic development. *Mol. Med. Today.* 5:216-224.

Baldwin, S.A., Beal, P.R., Yao, S.Y., King, A.E., Cass, C.E., and Young, J.D. 2004. The equilibrative nucleoside transporter family, SLC29. *Pflügers Arch.* 447:735-743.

Baldwin, S.A., Yao, S.Y., Hyde, R.J., Ng, A.M., Foppolo, S., Barnes, K., Ritzel, M.W., Cass, C.E., and Young, J.D. 2005. Functional characterization of novel human and mouse equilibrative nucleoside transporters (hENT3 and mENT3) located in intracellular membranes. *J. Biol. Chem.* 280:15880-15887.

Barnes, K., Dobrzynski, H, Foppolo, S., Beal, P.R., Ismat, F., Scullion, E.R., Sun, L., Tellez, J., Ritzel, M.W.L., Claycomb, W.C., Cass, C.E., Young, J.D., Billeter-Clark, R., Boyett, M.R., and Baldwin, S.A. 2006. Distribution and functional characterization of equilibrative nucleoside transporter-4, a novel cardiac adenosine transporter activated at acidic pH. *Circ. Res.* 272:28423-28430.

Cass, C.E., Young, J.D., and Baldwin, S.A. 1998. Recent advances in the molecular biology of nucleoside transporters of mammalian cells. *Biochem. Cell Biol.* 76:761-770.

Coe, I.R., Griffiths, M., Young, J.D., Baldwin, S.A., and Cass, C.E. 1997. Assignment of the human equilibrative nucleoside transporter (hENT1) to 6p21.1-p21.2. *Genomics* 45:459-460.

Damaraju, V.L., Sambasivarao, D., Young, J.D., Baldwin, S.A., Mackey, J., Sawyer, M.B., and Cass, C.E. 2003. Nucleoside anticancer drugs: the role of nucleoside transporters in resistance to cancer chemotherapy. *Oncogene.* 22:7524-7536.

Damaraju, V.L., Sawyer, M.B., Mackey, J.R., Young, J.D., and Cass, C.E. 2009. Human nucleoside transporters: biomarkers for response to nucleoside drugs. *Nucleosides Nucleotides Nucleic Acids*. 28:450-463.

Engel, K., Zhou, M., and Wang, J. 2004. Identification and characterization of a novel monoamine transporter in the human brain. *Mol. Pharmacol*. 68:1397-1407.

Feng, Z., Hou, T., and Li, Y. 2013. Transport of nucleosides in the vcCNT facilitated by sodium gradients from molecular dynamics simulations. *Mol. Biosyst.* 9:2142-2153.

Griffiths, M., Beaumont, N., Yao, S. Y. M., Sundaram, M., Boumah, C. E., Davies, A., Kwong, F. Y. P., Coe, I., Cass, C. E., Young, J. D., and Baldwin, S. A. 1997a. Cloning of a human nucleoside transporter implicated in the cellular uptake of adenosine and chemotherapeutic drugs. *Nat. Med*. 3:89-93.

Griffiths, M., Yao S.Y., Abidi, F., Phillips, S.E., Cass, C.E., Young, J.D., and Baldwin, S.A. 1997b. Molecular cloning and characterization of a nitrobenzylthioinosine-insensitive (*ei*) equilibrative nucleoside transporter from human placenta. *Biochem. J*. 328:739-743.

Grewer, C., Gameiro, A., Mager, T., and Fendler, K. 2013. Electrophysiological characterization of membrane transport proteins *Annu. Rev. Biophys*. 42:95-120.

Hamilton, S. R., Yao, S. Y. M., Ingram, J. C., Hadden, D. A., Ritzel, M. W. L., Gallagher, M. P., Henderson, P. J. F., Cass, C. E., Young, J. D., and Baldwin, S. A. 2001. Subcellular distribution and membrane topology of the mammalian concentrative Na^+-nucleoside cotransporter rCNT1. *J. Biol. Chem*. 276:27981-27988.

Huang, Q., Yao, S.Y., Ritzel, M.W., Paterson, A.R., Cass, C.E., and Young, J.D. 1994. Cloning and functional expression of a complementary DNA encoding a mammalian nucleoside transport protein. *J. Biol Chem*. 269:17757-17760.

Hyde, R.J., Carol, C.E., James, J.D., and Baldwin, S.A. 2001. The ENT family of eukaryotic nucleoside and nucleobase transporters: recent identification of novel isoforms. *Mol. Membr. Biol.* 18:53-63.

Johnson, Z.L., Cheong, C., and Lee, S. Crystal structure of a concentrative nucleoside transporter from *Vibrio cholerae* at 2.4 Å. *Nature* 483:489-493.

Jordheim, L.P., Durantel, D., Zoulim, F., Dumontet, C. 2013. Advances in the development of nucleoside and nucleotide analogues for cancer and viral diseases. *Nat. Rev. Drug Discov*. 12: 447-464.

King, A.E., Ackley, M.A., Cass, C.E., Young, J.D., and Baldwin, S.A. 2006. Nucleoside transporters: from scavengers to novel therapeutic targets. *Trends Pharmacol. Sci*. 27:416-425.

Kiss, A., Farah, K., Kim, J., Garriock, R.J., Drysdale, T.A., and Hammond, J.R. 2000. Molecular cloning and functional characterization of inhibitor-sensitive (mENT1) and inhibitor-resistant (mENT2) equilibrative nucleoside transporters from mouse brain. *Biochem. J.* 352:363-372.

Larrayoz, I.M., Casado, F.J., Pastor-Anglada, M., and Lostao, M.P. 2004. Electrophysiological characterization of the human Na^+/nucleoside cotransporter 1 (hCNT1) and role of adenosine on hCNT1 function. *J. Biol. Chem.* 279:8999-9007.

Loewen, S.K., Yao, S.Y.M., Slugoski, M.D., Mohabir, N.N., Turner, R.J., Mackey, J.R., Weiner, J.H., Gallagher, M.P., Henderson, P.J.F., Baldwin, S.A., Cass, C.E., and Young, J.D. 2004. Transport of physiological nucleosides and anti-viral and anti-neoplastic nucleoside drugs by recombinant Escherichia coli nucleoside-H(+) cotransporter (NupC) produced in *Xenopus laevis* oocytes. *Mol. Membr. Biol.* 21:1-10.

Loffler, M., Morote-Garcia, J.C., Eltzschig SA, Coe, I.R., and Eltzschig, H.K. 2007. Physiological roles of vascular nucleoside transporters. *Arteriolscler. Thromb. Vasc. Biol*. 27:1004-1013.

Mackey, J.R., Baldwin, S.A., Young, J.D. and Cass, C.E. Nucleoside transport and its significance for anticancer drug resistance. 1998. *Drug Resist. Updat.* 1:310-324.

McIntosh, V.J., and Lasely, R.D. 2012. Adenosine receptor-mediated cardioprotection: are all 4 subtypes required or redundant? *J. Cardiovasc. Pharmacol. Ther.* 17:21-33.

Molecular Devices. Axon Guide for Electrophysiology & Biophysics Laboratory Techniques. 2008. Page 14.

Parkinson, F.E., Damaraju, V.L., Graham, K., Yao, S.Y.M., Baldwin, S.A., Cass, C.E., and Young, J.D. 2011. Molecular biology of nucleoside transporters and their distributions and functions in the brain. *Curr. Top. Med. Chem.* 11: 948-972.

Pastor-Anglada, M., Cano-Soldado, P., Molina-Arcas, M., Lostao, M.P., Larráyoz, I., Martinez-Picado, J., and Casado, F.J. 2005. Cell entry and export of nucleoside analogues. *Virus Res.* 107:151-164.

Pisoni, R.L., and Thoene, J.G. 1989. Detection and characterization of a nucleoside transport system in human fibroblast lysosomes. *J. Biol. Chem.* 264:4850-4856.

Podgorska, M., Kocbuch, K., and Pawelczyk, T. 2005. Recent advances in studies on biochemical and structural properties of equilibrative and concentrative nucleoside transporters. *Acta Biochim. Pol.* 52:749-758.

Ritzel, M.W.L., Ng, A.M.L., Yao, S.Y.M., Graham, K., Loewen, S.K., Smith, K.M., Ritzel, R.G., Mowles, D.A., Carpenter, P., Chen, X.Z., Karpinski, E., Hyde, R.J., Baldwin, S.A., Cass, C.E. and Young, J.D. 2001. Molecular identification and characterization of novel human and mouse concentrative Na^+ nucleoside cotransporter proteins (hCNT3 and mCNT3) broadly selective for purine and pyrimidine nucleosides (system *cib*). *J. Biol. Chem.* 276:2914-2927.

Ritzel, M.W.L., Yao, S.Y.M., Huang, M.-Y., Elliott, J.F., Cass, C.E., and Young, J.D. 1997. Molecular cloning and functional expression of cDNAs encoding a human Na^+-nucleoside cotransporter (hCNT1). *Am. J. Physiol.*272:C707-C714.

Ritzel, M.W., Yao, S.Y., Ng, A.M., Mackey, J.R., Cass, C.E., and Young, J.D. 1998. Molecular cloning, functional expression and chromosomal localization of a cDNA encoding a human Na^+/nucleoside cotransporter (hCNT2) selective for purine nucleosides and uridine. *Mol.Membr. Biol.* 15:203-211.

Slugoski, M. D., Ng, A. M. L., Yao, S. Y. M., Lin, C. C., Mulinta, R., Cass, C. E., Baldwin, S. A., and Young, J. D. 2009. Substituted Cysteine Accessibility Method Analysis of Human Concentrative Nucleoside Transporter hCNT3 Reveals a Novel Discontinuous Region of Functional Importance within the CNT Family Motif (G/A)XKX$_3$NEFVA(Y/M/F). *J. Biol.Chem*. 284:17281-17292.

Smith, K.M., Ng, A.M., Yao, S.Y., Labedz, K.A., Knauss, E.E., Wiebe, L.I., Cass, C.E., Baldwin, S.A., Chen, X.Z., Karpinski, E., and Young, J.D. 2004. Electrophysiological characterization of a recombinant human Na^+-coupled nucleoside transporter (hCNT1) produced in *Xenopus* oocytes. *J. Physiol.* 558:807-823.

Smith, K.M., Slugoski, M.D., Cass, C.E., Baldwin, S.A., Karpinski, E., and Young, J.D. 2007. Cation coupling properties of human concentrative nucleoside transporters hCNT1, hCNT2 and hCNT3. *Mol. Membr. Biol.* 24:53-64.

Smith, K.M., Slugoski, M.D., Loewen, S.K., Ng, A.M., Yao, S.Y., Chen, X.Z., Karpinski, E., Cass, C.E., Baldwin, S.A. and Young, J.D. 2005. The broadly selective human Na^+/nucleoside cotransporter (hCNT3) exhibits novel cation-coupled nucleoside transport characteristics. *J. Biol. Chem.* 280:25436-25449.

Spratlin, L., and Mackey, J.R. 2010. Human equilibrative nucleoside transporter 1 (hENT1) in pancreatic adenocarcinoma: towards individualized treatment decisions. *Cancers* 2:2044-2054.

Visser, F., Vickers, M.F., Ng, A.L., Baldwin, S.A., Young, J.D., and Cass, C.E. 2002. Mutation of residue 33 of human equilibrative nucleoside transporters 1 and 2 alters sensitivity to inhibition of transport by dilazep and dipyridamole. *J. Biol. Chem.* 277:395-401.

Wang, C., Lin, W., Playa, H., Sun, S., Cameron, K., and Buolamwini, J. K. 2013. Dipyridamole analogs as pharmacological inhibitors of equilibrative nucleoside transporters. Identification of novel potent and selective inhibitors of the adenosine transporter function of human equilibrative nucleoside transporter 4 (hENT4). *Biochem. Pharmacol.*86:1531-1540.

Ward, J.L., Sherail, A., Mo, Z.-P. and Tse, C.-M. 2000. Kinetic and pharmacological properties of clones human equilibrative nucleoside transporters, ENT1 and ENT2, stably expressed in nucleoside transporter-deficient PK 15 cells. ENT2 exhibits a low affinity for guanosine and cytidine but a high affinity for inosine. *J. Biol. Chem.* 275:8375-8381.

Yao, S.Y.M., Ng, A.M.L., Cass, C.E., Baldwin S.A., and Young J.D. 2011. Nucleobase transport by human equilibrative nucleoside transporter 1 (hENT1). *J. Biol. Chem.* 286:32552-32562.

Yao, S.Y., Ng, A.M., Vickers, M.F., Sundaram, M,, Cass, C.E,, Baldwin, S.A., and YoungJD. 2002a. Functional and molecular characterization of nucleobase transport by recombinant human and rat equilibrative nucleoside transporters 1 and 2. Chimeric constructs reveal a role for the ENT2 helix 5-6 region in nucleobase translocation. *J. Biol. Chem*. 277:24938-24948.

Yao, S.Y., Ng, A.M., Slugoski, M.D., Smith, K.M., Mulinta, R., Karpinski, E., Cass, C.E., Baldwin, S.A., Young, J.D. 2007. Conserved glutamate residues are critically involved in Na^+/nucleoside cotransport by human concentrative nucleoside transporter 1 (hCNT1). *J. Biol. Chem.* 282:30607-30617.

Yao, S.Y., Ng, A.M., Loewen, S.K., Cass, C.E., Baldwin, S.A., and Young, J.D. 2002b. An ancient prevertebrate Na^+-nucleoside cotransporter (hfCNT) from the Pacific hagfish (*Eptatretus stouti*). *Am. J. Physiol. Cell Physiol.* 283:C155-168.

Young, J.D., Yao, S.Y.M., Baldwin, J.M., Cass, C.E., and Baldwin, S.A. 2013. The human concentrative and equilibrative nucleoside transporter families, SLC28 and SLC29. *Mol. Aspects Med.* 34:529-547.

Young, J.D., Yao, S.Y.M., Sun, L., Cass, C.E., and Baldwin, S.A. 2008. Human equilibrative nucleoside transporter (ENT) family of nucleoside and nucleobase transporter proteins. *Xenobiotica* 38:995-1021.

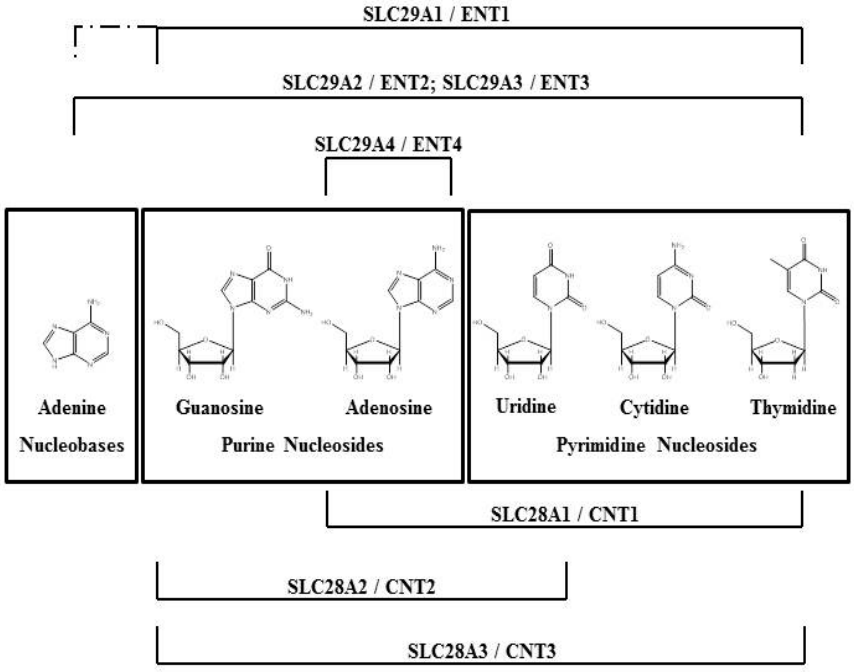

Figure 1-1: Permeant selectivities of human ENT and CNT nucleoside transporter proteins. (Young *et al*., 2013).

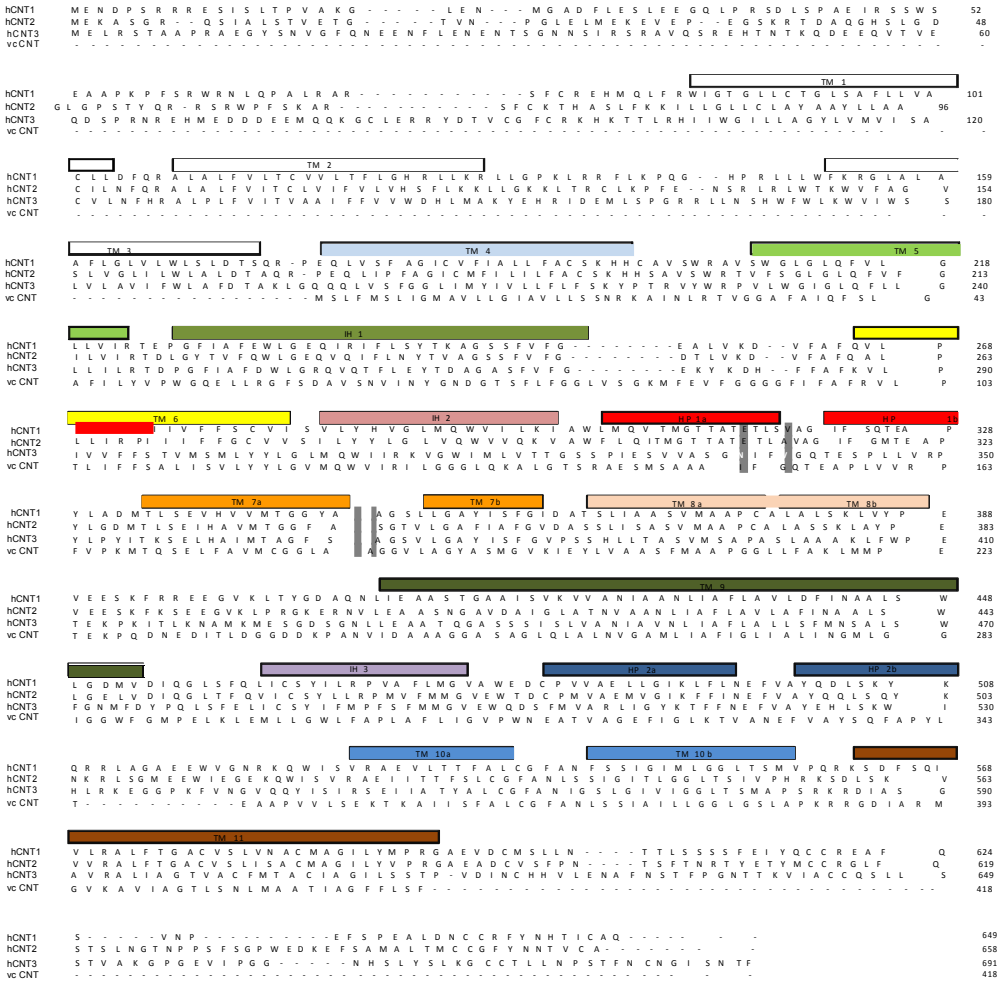

Figure 1-2: Sequence alignment of hCNTs and vcCNT. Sequence alignment of hCNT1 (U62968), hCNT2 (NP_004203.2), hCNT3 (AF305210), and vcCNT (NP_231982.1) was performed using Bio-edit software. Bars representing helices use the same color scheme as in Figure 3-1. Residues predicted to be involved in the Na^+-binding site in hCNT3, and its corresponding residues in hCNT1 and hCNT2, are highlighted in *grey*.

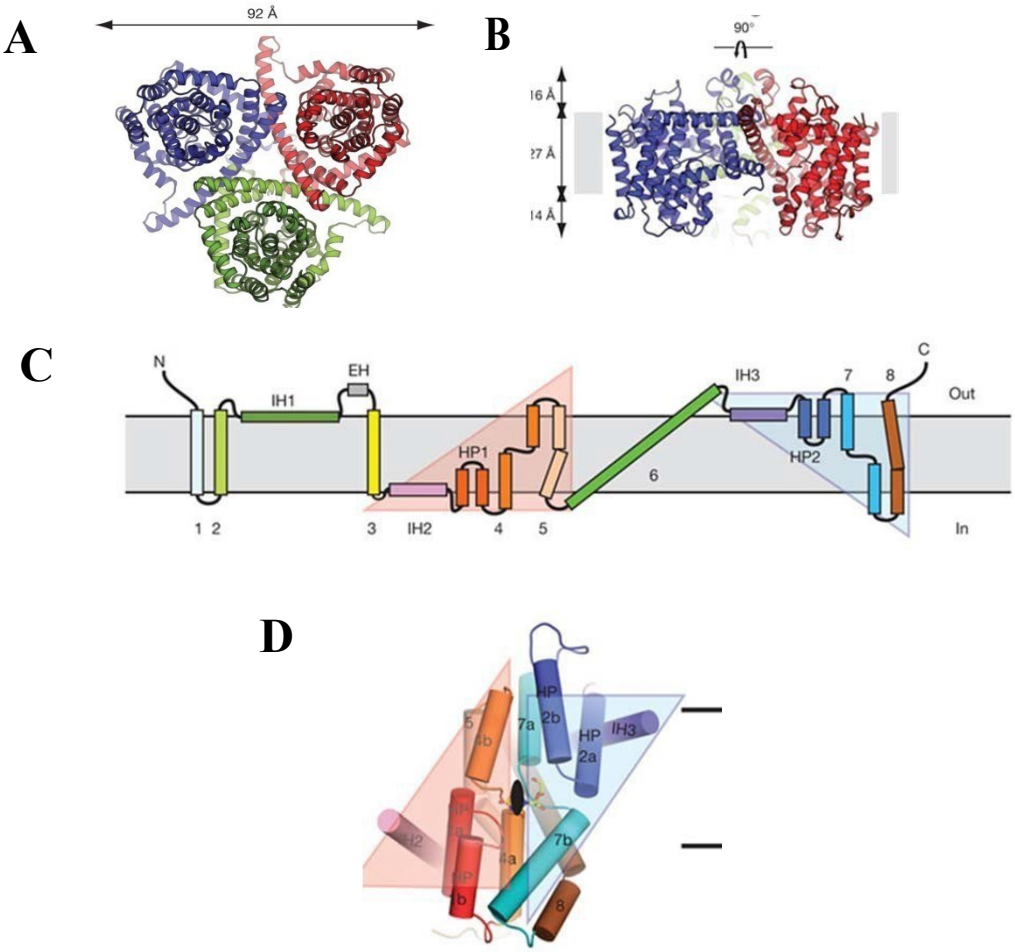

Figure 1-3: Crystal structure of vcCNT at 2.4 Å. The crystal structure of vcCNT shows a homo-trimeric transporter with dimensions of 92 Å on each side of the triangular shaped protein and 57 Å in height, forming an inverted triangular basin with its mouth facing the cytoplasm. Each protomer is coloured *red*, *green*, or *blue*. **A.** The trimer viewed from the cytoplasm. **B.** The trimer viewed from the side. **C.** The topology of vcCNT based on the crystal structure is shown, including 3 interfacial helices (IH-1- IH-3) and two helix-turn-helix re-entrant hairpin loops (HP1 and HP2). The scaffold domain consists of TMs1-3, TM6, IH1, and EH (extracellular helices) while the transporter domain consists of two subdomains of transmembrane regions: Subdomain 1 (IH2, HP1, TM4, and TM5) and Subdomain 2 (IH3, HP2, TM7, and TM8). The vcCNT N- and C-termini are extracellular. **D**. The two-fold pseudo-symmetry of the transporter is shown; the subdomains are overlaid in *pink* and *cyan* triangles (Johnson *et al*., 2012).

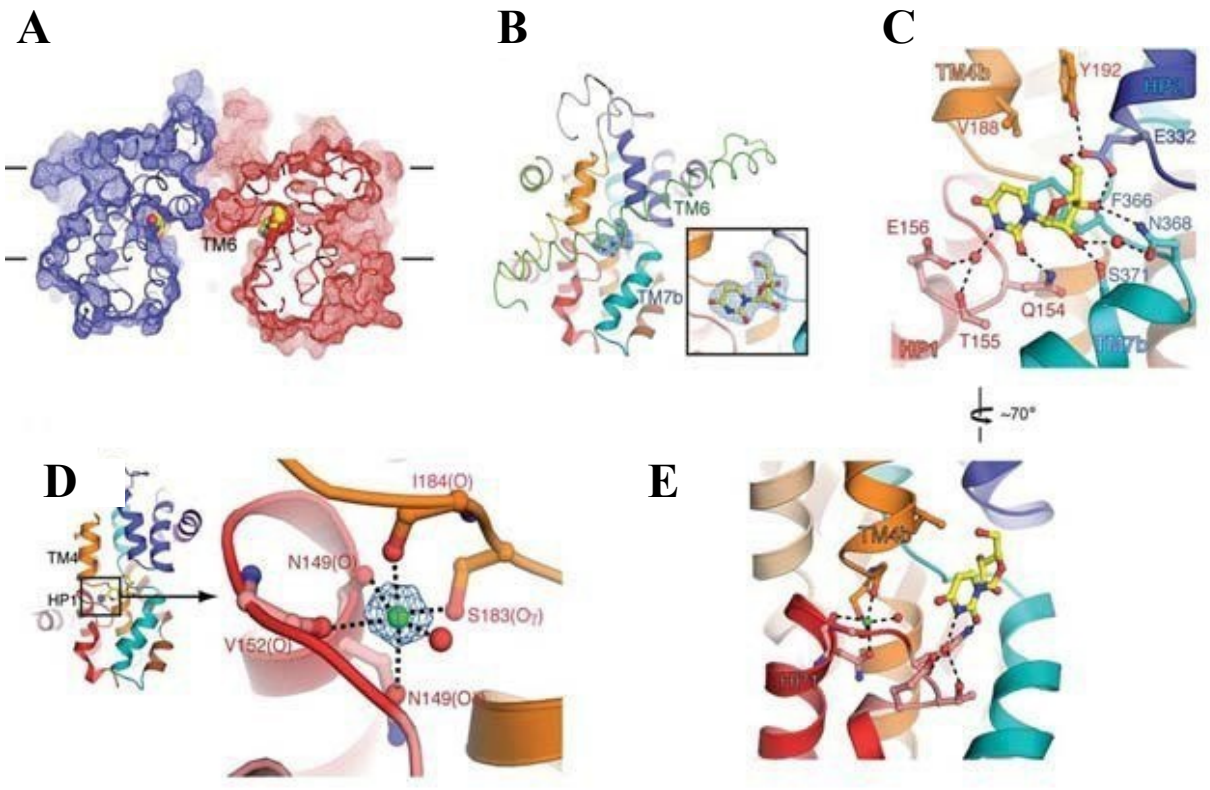

Figure 1-4: The vcCNT nucleoside- and Na^+-binding sites. **A.** View of vcCNT parallel to the membrane. The location of the membrane bilayer is denoted by horizontal lines. Uridine isshown as spheres. **B.** View of the center of the vcCNT trimer. The scaffold domain is shown inribbon representation and the transport domain is shown by cartoon representation. **C.** Thenucleoside binding site of vcCNT. Hydrogen bonds are denoted with dashed lines and watermolecules are shown as *red* spheres **D.** The Na^+-binding site of vcCNT. Coordination of the Na^+ ion is depicted as dashed lines. **E.** The vcCNT nucleoside- and Na^+-binding site are shown in close proximity (Johnson *et al.*,2012).

Chapter 2:

Materials and Methods

Xenopus laevis Oocyte Expression System

The *Xenopus laevis* oocyte heterologous expression system was the primary system utilized to clone and functionally characterize both human and other eukaryotic ENT and CNT proteins (Yao *et al*., 2002; Smith *et al.*, 2004). It is also the expression system used in all of the studies described in this thesis. Fully grown (stage V and VI*) Xenopus laevis* oocytes are large cells, about 1 mm in diameter, with a very large nucleus, and physiologically arrested at the diplotene stage of the first meiotic prophase of cell division (Stühmer *et al.*, 1995). The cells remain at this stage of development for long periods of time, if simply placed in an isotonic saline solution with a nutrient source and recommended antibiotics (Lui, 2006; Wang *et al*., 1997). This characteristic allows for simple control of experimental conditions; the large size of the cells facilitates easy electrophysiological manipulation (Lui, 2006).

One of the key advantages of using the *Xenopus* oocyte heterologous expression system is the lack of detectable endogenous nucleoside transport activity in the oocyte plasma membrane (Yao *et al*., 2002). This feature provides a powerful experimental tool to first produce and then functionally characterize recombinant nucleoside transport proteins in the absence of other competing transport activities with potentially overlapping permeant selectivities (Yao *et al*., 2002). Oocytes have a high capacity to synthesize proteins (200 - 400 ng of protein per day per oocyte) (Lui, 2006). Thus, they can robustly translate injected exogenous mRNA, as well as correctly perform post translational modifications and insert the transporter protein into the cell plasma membrane (Taglialatela *et al.,* 1992; Wang *et al.,* 1997; Bezanilla and Stefani, 1998; Yao *et al*., 2000).

Synthetic mRNA encoding the protein of interest is injected into the cytoplasm of the oocyte. The level of protein production can be varied by altering the concentration and/or volume of mRNA injected (Stühmer *et al.,* 1995). One potential disadvantage of producing human proteins in an amphibian cell is the possibility of functional differences compared with expression in a human or other mammalian cellular environment (Wang *et al.,* 1997; Lui, 2006). Generally, however, this system has proven to accurately reflect the functional phenotypes of the heterologous transporters it produces (Taglialatela *et al*., 1992; Yao *et al*., 2000). It has even proved possible to produce and functionally characterize bacterial transporter proteins in *Xenopus* oocytes (Loewen *et al*., 2004; Appendix I of this thesis).

Molecular Biology

Site-Directed Mutagenesis

The molecular cloning of hCNT1 and hCNT3 has previously been described (Ritzel *et al*., 1997; 2001). vcCNT cDNA was provided by our collaborators at the University of Leeds. hCNT1, hCNT3, or vcCNT cDNA in the *Xenopus* expression vector pGEM-HE provided the template for the construction of the mutants. Residues were individually converted into the desired amino acid using the QuickChange™ site-directed mutagenesis kit (Stratagene) according to the manufacturer's directions. The mutations for hCNT1 were hCNT1-N315A, hCNT1-N315S, hCNT1-N315T, hCNT1-T349C, hCNT1-T349G, and hCNT1-T349S. The mutations for hCNT3 were hCNT3-N336C, hCNT3-V339C, hCNT3-T370C, and hCNT3-I371C., hCNT3-N336T, hCNT3-N336S, hCNT3-N336A, hCNT3-T370G andhCNT3-T370S. The mutations for vcCNT were vcCNT-N149S, vcCNT-N149T, and vcCNT-N149A. Constructs were sequenced in both directions to confirm that the anticipated mutation had been introduced correctly. Plasmid DNA was linearized with *NheI* and transcribed with T7 polymerase using the mMESSAGE mMACHINE™ (Ambion) *in vitro* transcription system. Remaining template was removed by digestion with RNase-free DNase I.

Modelling of hCNTs

FATCAT (Flexible structure AlignmenT by Chaining Aligned fragment pairs allowing Twists) software aligns and compares two structures statistically (Yue and Goidzik, 2003). FATCAT was used to predict the 3D structure and membrane topology of hCNT3-WT based upon the crystal structure of vcCNT.

Oocyte Preparation

Stage V-VI oocytes were isolated by collagenase treatment (2 mg/ml for 2 h) of ovarian lobes from female *Xenopus laevis* (Biological Sciences Vivarium, University of Alberta) that had been anaesthetized by immersion in 0.3 % (w/v) tricaine methanesulphonate (pH 7.4). Frogs were humanely euthanized following collection of oocytes in compliance with guidelines approved by the Canadian Council on Animal Care. The remaining follicular layers were

removed by phosphate treatment (100 mM K_2PO_4) and manual defolliculation. Twenty-four hours after defolliculation, oocytes were injected (Inject + Matic System) with either 10 nl of water containing 10 ng of capped RNA transcripts or with 10 nl of water alone. Oocytes were incubated for 4 days following injection at 18 °C in modified Barth's solution (88 mM NaCl, 1 mM KCl, 0.33 mM $Ca(NO_3)_2$, 0.41 mM $CaCl_2$, 0.82 mM $MgSO_4$, 2.4 mM $NaHCO_3$, 10 mM Hepes, 2.5 mM Na^+ pyruvate, 0.05 mg/ml penicillin, and 0.1 mg/ml gentamycin sulfate, pH 7.5) prior to the assay of nucleoside transport activity.

Transport Media

In experiments investigating the Na^+ dependence of nucleoside transport, Na^+ concentrations ranged from 0 - 100 mM. Experiments were performed at a pH of 7.5 (vcCNT) or 8.5 (hCNT1/hCNT3). The Na^+-containing transport medium was composed of 100 mM NaCl, 2 mM KCl, 1 mM $CaCl_2$, 1 mM $MgCl_2$ and 10 mM HEPES. For solutions which had a Na^+ concentration < 100 mM, Na^+ in the transport medium was replaced by equimolar choline chloride (ChCl).

In experiments examining the H^+-dependence of transport, Na^+-free choline-containing transport medium was used at pH values ranging from 5.0 to 8.5. Na^+-free transport medium was composed of 100 mM ChCl, 2 mM KCl, 1 mM $CaCl_2$, 1 mM $MgCl_2$ and 10 mM HEPES (for pH values > 6.5) or 10 mM 2-(N-morpholino)ethanesulfonic acid (MES) (for pH values ≤ 6.5). The pH 8.5 or pH 5.0 media represent H^+-reduced or H^+-enriched conditions, respectively.

Electrophysiology

Electrophysiology experiments were conducted at room temperature (20 °C) using the whole-cell, two-electrode voltage clamp technique (GeneClamp 500B, Molecular Devices Corp., USA) as previously described (Smith *et al.,* 2004). The GeneClamp 500B was interfaced to a dedicated IBM-compatible computer *via* a Digidata 1322A A/D converter and controlled by Axoscope software (version 9.0, Molecular Devices Corp., USA).

Thin-wall, fiber-filled borosilicate glass capillaries were used as electrodes and filled with 3M KCl. The electrodes had resistances ranging from 0.5 to 2.5 MΩ (megaohms). Oocytes were then placed in the bath, and penetrated with the microelectrodes. The resting membrane potential was measured over a 5 - 10 min period prior to the start of the experiment. Oocytes

displaying an unstable membrane potential or a potential less than -30 mV were rejected, as well as oocytes with a blotchy appearance or that otherwise appeared unhealthy.

Unless otherwise indicated, the holding potential (V_h) of the oocytes was -50 mV in the required transport medium. The signal currents were filtered at 2 kHz (four-pole Bessel filter) at a sampling interval of 50 ms.

Na^+-concentration dependence curves were generated by challenging oocytes with solutions of varying Na^+ concentration, and H^+-dependence curves were generated by challenging oocytes with 100 mM ChCl solutions of varying pH. The uridine concentration was either 20 μM (hCNT3) or 100 μM (hCNT1). A uridine concentration of 100 μM was used for hCNT1 because of lower levels of functional expression compared to hCNT3. For H^+-concentration dependence experiments, a uridine concentration of 100 μM was also used for hCNT3, since hCNT3 H^+-dependent fluxes are lower than those in the presence of Na^+. Measurements which required Na^+-free solutions were preceded by 5 to 10 min of pre-incubation in Na^+-free solution (100 mM ChCl; pH 8.5). No currents were produced in control water-injected oocytes under any of the conditions tested.

Radioisotope Flux Measurements

Radioisotope Flux Measurements for hCNT1

Radioisotope flux studies for hCNT1 were performed at room temperature (20 ˚C) employing the same transport media used in electrophysiological experiments. Groups of 6 oocytes in 200 μl of transport medium (100 mM NaCl; pH 8.5) containing 10 μM of ^{3}H-uridine (1 μCi/ml) were incubated for a pre-determined time interval (1-min or 1-hr) to measure the uptake of uridine in oocytes producing wild-type hCNT1 (hCNT1-WT), hCNT1-T349G, hCNT1-T349C or hCNT1-T349S. Fluxes of 1-hr were used to assess relative activities of transporters under different conditions; fluxes of 1-min were used to determine initial rates of transport (influx). Following incubation, extracellular radioactivity was removed by five rapid washes with ice-cold ChCl transport medium (pH 8.5), and the oocytes were then transferred to individual scintillation vials where they were dissolved in 5% (w/v) sodium dodecyl sulfate (SDS). ScintiSafe Econo 2 Cocktail (Fisher Scientific) (2.5 ml) was added to each scintillation

vial, and the uptake of uridine quantified by measuring oocyte-associated radioactivity using a PerkinElmer (Tri-Carb 2910 TR) liquid scintillation analyzer. Values are presented as means ± SEM for 4 - 6 oocytes, and compared to uridine uptake by control water-injected oocytes.

Radioisotope Flux Measurements for vcCNT

Radioisotope flux measurements for vcCNT were performed at 20 °C using solutions similar to those used in electrophysiology experiments. The pH of the Na^+-containing transport medium (100 mM NaCl) was 7.5, and the pH of the Na^+-free transport medium (100 mM ChCl) was either 7.5 or 5.5 (Na^+-free or H^+-enriched experiments, respectively). Flux measurements were performed on groups of 10 - 12 oocytes in 200 µl transport medium containing different concentrations of ^{3}H-nucleosides (1 µCi/ml) for a pre-determined time interval of 10 min. Functional activity of vcCNT was lower than for hCNT1 and a 10 min incubation period was required to determine initial rates of transport (influx). Oocytes were processed as described for hCNT1. Values are presented as means ± SEM of 10 - 12 oocytes, and corrected for basal non-mediated uptake in control water-injected oocytes.

Kinetic Parameters

Kinetic parameters calculated from electrophysiological (hCNT1 and hCNT3) and radioisotope flux (vcCNT) experiments were determined by least squares fits to the Hill equation, $I = I_{max}[X]^n/(K_{50}^n + [X]^n)$ or $V = V_{max}[X]^n/(K_{50}^n + [X]^n)$, respectively, where I_{max} is the predicted current maximum, I is the nucleoside-induced current, V_{max} is the predicted flux maximum, V is the nucleoside-induced flux, K_{50} is the half-saturation constant for Na^+ or H^+ activation, X is Na^+ or H^+, and n is the Hill coefficient (Sigmaplot 2000 software version 13.0, Jandel Scientific Software, San Rafael, CA).

The Hill coefficient was used to predict the cation:nucleoside coupling ratio of the transporter. Based upon previous studies (Smith *et al*., 2007), a Hill coefficient less than 1 indicates a coupling ratio of 1:1, whereas a Hill coefficient greater than 1 indicates a coupling ratio of at least 2:1.

vcCNT uridine kinetic parameters, the value at which the flux is 50% of maximum (K_m) and predicted flux maximum (V_{max}), were determined by least squares fits to the Michaelis-Menten equation $V = V_{max}[S]/(K_m + [S])$, where V is the nucleoside-induced flux and S is the uridine concentration (SigmaPlot 2000 software version 13.0, Jandel Scientific Software, San Rafael, CA).

GraphPad Prism software (San Diego, CA) was used to determine thestatistical significance of the data obtained from radioisotope flux assays for vcCNT. For comparisons between two treatments, a paired t-test was performed, and for comparisons between multiple treatments, a one-way ANOVA was used. Following ANOVA analysis, Tukey's HSD test was performed for further data analysis. Significance was established at $P < 0.05$.

Kinetic parameters (K_{50} for Na^+ or H^+ activation) obtained from electrophysiological experiments are presented as fits to data from individual oocytes normalized to the I_{max} value obtained for that oocyte, and are presented as values ± SE for single representative oocytes or as means ± SEM of 5 or more representative cells. Hill coefficients (n) are presented as values ± SE for single representative oocytes. I_{max} values for hCNT3 are presented from single representative oocytes, and for hCNT1 as means ± SEM of 4 - 6 oocytes. The data from vcCNT radioisotope flux assays was averaged from 10 - 12 oocytes, and kinetic parameters (K_{50}, K_m, and V_{max}) are presented as values ± SE.

References

Bezanilla, F. and Stefani, E. 1998. Gating currents. *Methods Enzymol*. 293:331-352.

Loewen, S.K., Yao, S.Y., Slugoski, M.D., Mohabir, N.N., Turner, R.J., Mackey, J.R., Weiner, J.H., Gallagher, M.P., Henderson, P.J., Baldwin, S.A., Cass, C.E., and Young, J.D. 2004. Transport of physiological nucleosides and anti-viral and anti-neoplastic nucleoside drugs by recombinant *Escherichia coli* nucleoside-H(+) cotransporter (NupC) produced in *Xenopus laevis* oocytes. *Mol Membr. Biol*21:1-10.

Liu, X.J. 2006. *Xenopus* Protocols: Cell Biology and Signal Transduction. Totowa, N.J: Humana Press. Papke, R.L., and Smith-Maxwell, C. 2009. High throughput electrophysiology with *Xenopus* oocytes. *Comb. Chem. High Throughput Screen.* 12:38-50.

Ritzel, M.W., Yao, S.Y., Ng, A.M., Mackey, J.R., Cass, C.E., Young, J.D. 1998. Molecular cloning, functional expression and chromosomal localization of a cDNA encoding a human Na^+/nucleoside cotransporter (hCNT2) selective for purine nucleosides and uridine. *Mol.Membr. Biol.* 15:203-211.

Ritzel, M.W.L, Ng, A.M.L., Yao, S.Y.M., Graham, K., Loewen, S.K., Smith, K.M., Ritzel, R.G., Mowles, D.A., Carpenter, P., Chen, X.Z., Karpinski, E., Hyde, R.J., Baldwin, S.A., Cass, C.E., and Young, J.D. Molecular identification and characterization of novel human and mouse concentrative Na^+ nucleoside cotransporter proteins (hCNT3 and mCNT3) broadly selective for purine and pyrimidine nucleosides (system *cib*). *J. Biol. Chem*. 276:2914-2927.

Ritzel, M.W.L., Yao, S.Y.M., Huang, M.Y., Elliott, J.F., Cass, C.E., and Young, J.D. 1997. Molecular cloning and functional expression of cDNAs encoding a human Na^+-nucleoside cotransporter (hCNT1). *Am. J. Physiol.*272:C707-C714.

Smith, K.M., Ng, A.M., Yao, S.Y., Labedz, K.A., Knaus, E.E., Wiebe, L.I., Cass, C.E., Baldwin, S.A., Chen, X.Z., Karpinski, E., and Young, J.D, 2004. Electrophysiological characterization of a recombinant human Na^+-coupled nucleoside transporter (hCNT1) produced in *Xenopus* oocytes. *J. Physiol. (Lond)* 558:807-823.

Smith, K.M., Slugoski, M.D., Cass, C.E., Baldwin, S.A., Karpinski, E., and Young, J.D. 2007.

Cation coupling properties of human concentrative nucleoside transporters hCNT1, hCNT2 and hCNT3. *Mol. Membr. Biol.* 24:53-64.

Stühmer, W. and Parekh, A. 1995. Electrophysiological Recordings from *Xenopus* Oocytes. In Single Channel Recording. Sakmann, B., and Neher, E. Plenum Press, New York; pages 341-358.

Taglialatela, M. Toro, T., and Stefani, E. 1992. Novel voltage clamp to record small, fast currents from ion channels expressed in *Xenopus* oocytes. *Biophys. J.* 61:78-82.

Wang, J., Schaner, M.E., Thomassen, S., Su, S., Piquette-Miller, M., and Giacomini, K.M. 1997. Functional and molecular characteristics of Na^+- dependent nucleoside transporters. *Pharm. Res.* 14: 1524-1532.

Weiss, J.N. 1997. The Hill equation revisited: uses and misuses. *FASEB J.* 11:835-841.

Yao, S.Y., Cass, C.E., and Young, J.D. 2000. The *Xenopus* oocyte expression system for the cDNA cloning and characterization of plasma membrane transport proteins. In Membrane Transport. A Practical Approach. (Baldwin, S. A., ed.) Oxford: Oxford University Press; pages 47-78.

Yao, S.Y., Ng, A.M., Vickers, M.F., Sundaram, M., Cass, C.E., Baldwin, S.A., and Young J.D. 2002. Functional and molecular characterization of nucleobase transport by recombinant human and rat equilibrative nucleoside transporters 1 and 2. Chimeric constructs reveal a role for the ENT2 helix 5-6 region in nucleobase translocation. *J. Biol. Chem.* 277:24938-24948.

Yue, Y. and Godzik, A. 2003. Flexible structure alignment by chaining aligned fragment pairs allowing twists. *Bioinformatics*. 19:246-255.

Chapter 3:

Site-Directed Mutagenesis and Electrophysiological Characterization of Amino Acid Residues (N336, V339, T370, and I371) Involved in the Na^+/H^+-Binding Site of Human Concentrative Nucleoside Transporter 3 (hCNT3) Produced in *Xenopus laevis* Oocytes

Introduction

Chapter 1 describes the predicted membrane topology and 3D structure of vcCNT. In contrast to the previously predicted 15 TM model for hCNT3 based on SCAM analysis of the transport domain (Slugoski *et al*., 2009), the vcCNT crystal structure (Johnson *et al.,* 2012) predicts an 11 TM model for hCNTs (S.A. Baldwin, personal communication). Similar to vcCNT (Figure 3-1A), the newly predicted structure of hCNT3 (Figure 3-1B) can be subdivided into an outer or "scaffold" domain comprising TM4, TM5, IH1, TM6, and TM9, which surrounds an inner or "transport" domain. The transport domain can itself be divided into two structural subdomains that are related by a two-fold pseudo-symmetry (S.A. Baldwin, personal communication; Johnson *et al.,* 2012). The first subdomain includes IH2, HP1, TM7, and TM8 while the second subdomain includes IH3, HP2, TM10, and TM11 (Figure 3-1B). Residues contributing to uridine binding are from both subdomains, in particular at the tips of HP1 and HP2 and in the unwound regions of TM7 and TM10 (S.A. Baldwin, personal communication).The newly predicted membrane topology of hCNT3, as well as the regions suggested to interactwith uridine, are consistent with previous SCAM analyses of the transporter (Slugoski *et al*.,2009; Mulinta *et al.,* unpublished observations). In particular, the patterns of PCMBS inhibition seen bySCAM analysis provided functional evidence for extended structures resembling thediscontinuousmembrane helices (Mulinta e*t al*., unpublished observations). Residues that werePCMBS-sensitivewere located exofacially in the membrane, specifically at the linking regions of HP1, TM7, theupper helix of TM8, and the linking regions of TM9, IH3, HP2, and TM10. The location of these residues allows them to be accessible to the extracellular medium, andhence accessible to PCMBS. Residues that were PCMBS-sensitive, but protected by uridine, are also consistent withthe proposed location of the permeant binding site (Mulinta e*t al*.,unpublished observations).

As described in Chapter 1, the crystal structure of vcCNT has a single Na^+-binding site that is predicted to be the primary cation-binding site common to all CNTs (Johnson *et al*., 2012). Previous SCAM studies of hCNT3 implicated HP1, TM7, HP2, and TM10 in cation-binding, with regions in HP1 and TM7 corresponding to the vcCNT Na^+-binding site (Mulinta *et al*., unpublished observations).

Based upon the crystal structure of vcCNT, we have identified four residues that may play a key role in forming the primary cation-binding site in hCNT3. The residues in vcCNT implicated in forming the octahedral Na^+-binding site are N149, V152, S183, and I184, and the corresponding residues in hCNT3 are N336, V339, T370, and I371 (Figure 3-2). In this Chapter, each of these residues in hCNT3 was mutated to cysteine (to facilitate future cysteine-directed labeling studies), and the effects on cation (Na^+ and H^+) interactions examined by steady-state electrophysiology following production in *Xenopus* oocytes. The results provide evidence that these residues do indeed play a role in the primary cation-binding site of hCNT3.

Results

As depicted in Figure 3-2, four residues (N336, V339, T370, and I371) are predicted to coordinate the primary Na^+-binding site of hCNT3. These residues are located between HP1 and the unwound region of TM4 (Figures 3-1, 3-2).

Na^+-Activation Kinetics of hCNT3-WT and Mutants

Na^+-activation kinetics of hCNT3-WT - A plot of current as a function of increasing external Na^+ concentration (0 - 100 mM; pH 8.5) was performed at a uridine concentration of 20 μM and a holding potential of -50 mV (Figure 3-3A). A sigmoidal relationship was revealed with a Hill coefficient of 1.6 ± 0.1. This indicates that the Na^+:uridine stoichiometry is 2:1, and is similar to previously published findings (Smith *et al*., 2005, 2007). The K_{50} value for Na^+ was 1.7 ± 0.2 mM, also in agreement with previous studies (Smith *et al.,* 2005). Kinetic parameters are presented together with those of hCNT3 mutants in Table 3-1.

Na^+-activation kinetics of hCNT3-N336C - hCNT3 residue N336 (Figure 3-2B) corresponding to N149 in vcCNT (Figure 3-2A) was mutated to cysteine. The dependence of hCNT3-N336C mediated Na^+ currents on the external concentration of Na^+ (0 - 100 mM NaCl; pH 8.5) was examined at a uridine concentration of 20 μM and a holding potential of -50 mV (Figure 3-3B). A plot of current in response to increasing concentrations of Na^+ revealed a sigmoidal relationship with a Hill coefficient of 1.5 ± 0.1. Similar to hCNT3-WT, these results suggest a Na^+:uridine stoichiometry of 2:1 (Figure 3-3A; Table 3-1). However, the K_{50} value for Na^+ was 26.5 ± 8.9 mM, a value substantially greater than that observed for hCNT3-WT (1.7 ± 0.2 mM), suggesting a marked decrease in the affinity of hCNT3-N336C for Na^+. We also observed an approximate 4-fold decrease in the maximum current generated (25 nA; 20 μM uridine, 100 mM NaCl, pH 8.5; single representative oocyte) compared to hCNT3-WT (100 nA; 20 μM uridine, 100 mM NaCl, pH 8.5; single representative oocyte) (Table 3-1).

Na^+-activation kinetics of hCNT3-V339C - hCNT3 residue V339 (Figure 3-2B) corresponding to V152 in vcCNT (Figure 3-2A) was mutated to cysteine. The dependence of hCNT3-V339C

mediated Na^+ currents on the external concentration of Na^+ (0 - 100 mM NaCl; pH 8.5) was examined at a uridine concentration of 20 μM and a holding potential of -50 mV (Figure 3-4B). A plot of current in response to increasing concentrations of Na^+ revealed a hyperbolic relationship with a Hill coefficient of 1.1 ± 0.1, suggesting a change in Na^+:uridine stoichiometry from 2:1 to 1:1, as compared to hCNT3-WT (Table 3-1). The K_{50} value for Na^+ was 8.8 ± 1.3 mM, greater than that observed for hCNT3-WT (1.7 ± 0.2 mM), also indicating a decrease in the affinity of hCNT3-N336C for Na^+. We additionally observed a small decrease in the maximum current (70 nA; 20 μM uridine, 100 mM NaCl, pH 8.5; single representative oocyte) compared to hCNT3-WT (100 nA; 20 μM uridine, 100 mM NaCl, pH 8.5; single representative oocyte) (Table 3-1).

Na^+-activation kinetics of hCNT3-T370C - hCNT3 residue T370 (Figure 3-2B) corresponding to S183 in vcCNT (Figure 3-2A) was mutated to cysteine. The dependence of hCNT3-T370C mediated Na^+ currents on the external concentration of Na^+ (0 - 100 mM NaCl; pH 8.5) was examined at a uridine concentration of 20 μM and a holding potential of -50 mV (Figure 3-5B). A plot of current in response to increasing concentrations of Na^+ revealed a sigmoidal relationship with a Hill coefficient of 1.5 ± 0.1, suggesting a Na^+:uridine stoichiometry of 2:1 similar to that of hCNT3-WT (Table 3-1). The K_{50} value for Na^+ was 17.8 ± 0.9 mM which was substantially greater than that observed for hCNT3-WT (1.7 ± 0.2 mM), suggesting a decrease in the affinity of hCNT3-T370C for Na^+. We likewise observed a 60% reduction in the maximum current (40 nA; 20 μM uridine, 100 mM NaCl, pH 8.5; single representative oocyte) compared to hCNT3-WT (100 nA; 20 μM uridine, 100 mM NaCl, pH 8.5; single representative oocyte) (Table 3-1).

Na^+-activation kinetics of hCNT3-I371C - hCNT3 residue I371 (Figure 3-2B) corresponding to I184 in vcCNT (Figure 3-2A) was mutated to cysteine. The dependence of hCNT3-I371C mediated Na^+ currents on the external concentration of Na^+ (0 - 100 mM NaCl; pH 8.5) was examined at a uridine concentration of 20 μM and a holding potential of -50 mV (Figure 3-6B). A plot of current in response to increasing concentrations of Na^+ revealed a hyperbolic relationship with a Hill coefficient of 1.1 ± 0.1, suggesting a decrease in Na^+:uridine stoichiometry from 2:1 to 1:1, as compared to hCNT3-WT (Table 3-1). The K_{50} value for Na^+

was 20.7 ± 3.0 mM, a value substantially greater than that observed for hCNT3-WT (1.7 ± 0.1 mM), suggesting a decrease in the affinity of hCNT3-N336C for Na^+. We also observed a 50% reduction in maximum current (50 nA; 20 μM uridine, 100 mM NaCl, pH 8.5; single representative oocyte) compared to that of hCNT3-WT (100 nA; 20 μM uridine, 100 mM NaCl, pH 8.5; single representative oocyte) (Table3-1).

H^+-Activation Kinetics of hCNT3-WT and Mutants

H^+-activation kinetics of hCNT3-WT - The dependence of hCNT3-mediated currents on the external concentration of H^+ was determined in 100 mM ChCl transport medium at external pH values ranging from 8.5 - 5.0 (Na^+-free medium) (Figure 3-7A). Currents were measured at a uridine concentration of 100 μM (V_h = -50 mV). A plot of current in response to increasing concentrations of H^+ (pH 8.5 - 5.0) revealed a hyperbolic relationship with a corresponding Hill coefficient for hCNT3-WT of 0.4 ± 0.1, suggesting that the H^+:uridine stoichiometry is 1:1, consistent with previous findings (Smith *et al.,* 2005). The K_{50} value of hCNT3-WT for H^+ was 480 ± 105 nM, demonstrating that H^+ binds with high affinity to hCNT3. This K_{50} value is also in agreement with previous findings (Smith *et al.*, 2005). Kinetic parameters are presented in comparison with those of hCNT3 mutants in Table 3-1.

H^+-activation kinetics of hCNT3-N336C - The dependence of hCNT3-N336C mediated currents on the external concentration of H^+ was determined in 100 mM ChCl transport medium at external pH values ranging from 8.5 - 5.0 (Na^+-free medium). Currents were measured at a uridine concentration of 100 μM (V_h = -50 mV), but were too low (2 - 5 nA; 100 μM uridine, 100 mM ChCl, pH 8.5 - 5.0) for accurate kinetic analysis, and much lower than those seen with hCNT3-WT (150 nA; 100 μMuridine, 100 mM ChCl, pH 8.5 - 5.0; single representative oocyte) generated under the same conditions (Table3-1).

H^+-activation kinetics of hCNT3-V339C - The dependence of hCNT3-V339C mediated currents on the external concentration of H^+ was determined in 100 mM ChCl transport medium at external pH values ranging from 8.5 - 5.0 (Na^+-free medium). Currents were measured at a uridine concentration of 100 μM (V_h = -50 mV) (Figure 3-7B). A plot of current as a function of

increasing external H^+ concentration was hyperbolic, with a Hill coefficient of 0.6 ± 0.1. This suggests a H^+:nucleoside coupling ratio of 1:1, similar to that observed with hCNT3-WT (Figure3-7A). The K_{50} value of hCNT3-V339C for H^+ was 294 ± 32 nM which was less than that for hCNT3-WT (480 ± 105 nM), suggesting an increase in the affinity of hCNT3-N336C for H^+.We observed a 50% reduction in the maximum current generated following the addition of 100 μMuridine in Na^+-free medium (100 mM ChCl) at pH 5.0 (70 nA; single representative oocyte) compared to that of hCNT3-WT under the same conditions (150 nA; 100 μM uridine, 100 mMChCl, pH 8.5 - 5.0; single representative oocyte) (Table 3-1).

H^+-activation kinetics of hCNT3-T370C - The dependence of hCNT3-T370C mediated currents on the external concentration of H^+ was determined in 100 mM ChCl transport medium at external pH values ranging from 8.5 - 5.0 (Na^+-free medium). Currents were measured at a uridine concentration of 100 μM (V_h = -50 mV) (Figure 3-8B). A plot of current as a function of increasing external H^+ concentration was hyperbolic, with a Hill coefficient of 0.7 ± 0.1. This suggests a H^+:nucleoside coupling ratio of 1:1, similar to that seen with hCNT3-WT (Figure 3-8A). The K_{50} value of hCNT3-T370C for H^+ was 150 ± 53 nM, which is less than that observed for hCNT3-WT (480 ± 105 nM), suggesting an increase in the affinity of hCNT3-T370C for H^+. The maximum current observed with hCNT3-T370C was 150 nA (100 μM uridine, 100 mM ChCl, pH 8.5 - 5.0; single representative oocyte), similar to that seen with hCNT3-WT (150 nA; single representative oocyte; 100 μM uridine, 100 mM ChCl, pH 8.5 - 5.0) (Table 3-1).

H^+-activation kinetics of hCNT3-I371C - The dependence of hCNT3-I371C mediated currents on the external concentration of H^+ was determined in 100 mM ChCl transport medium at external pH values ranging from 8.5 - 5.0 (Na^+-free medium). Currents were measured at a uridine concentration of 100 μM (V_h = -50 mV) (Figure 3-9B). The magnitude of the currents increased as the external concentration of H^+ increased, but currents did not saturate. A plot of current as a function of increasing external H^+ concentration (pH 8.5 - 5.0) revealed a linear relationship. Kinetic values for transport could therefore not be determined. These results suggest a dramatic decrease in the affinity of hCNT3-I371C for H^+. We also observed a significant decrease in the maximal current (17 nA; 100 μM uridine, 100 mM ChCl, pH 8.5 - 5.0; single representative

oocyte; Table 3-1) compared to hCNT3-WT (150 nA; 100 μMuridine, 100 mM ChCl, pH 8.5 - 5.0; single representative oocyte) (Table 3-1).

Discussion

The crystallization of vcCNT, a bacterial homologue of hCNTs, by Johnson *et al*. (2012) allowed the identification of residues potentially involved in cation and uridine binding in members of the hCNT family of proteins. The objective of the experiments described in this Chapter was to mutate those residues predicted to coordinate with Na^+ and H^+ within the primary cation-binding site of hCNT3, and examine the effects on function compared to wild-type hCNT3. Using site-directed mutagenesis, the four hCNT3 mutants, hCNT3-N336C, hCNT3-V339C, hCNT3-T370C, and hCNT3-I371C, were constructed and produced as recombinant proteins in the *Xenopus* oocyte heterologous expression system.

Properties of the hCNT3 mutants (hCNT3-N336C, hCNT3-V339C, hCNT3-T370C, and hCNT3-I371C) were determined in comparison to hCNT3-WT measured nucleoside- induced Na^+ or H^+ currents in Na^+-containing transport medium (NaCl; pH 8.5) or Na^+-depleted, H^+-enriched media (ChCl; pH 8.5 - 5.0), respectively. The four hCNT3 mutants displayed sufficientactivity to perform kinetic analyses in Na^+-containing media using electrophysiology. While the mutations to cysteine produced functional proteins, a reduction in the maximal current was observed for all mutants in Na^+-containing media, with the lowest currents observed withhCNT3-N336C. The four hCNT3 mutants showed varying decreases in Na^+-binding affinity ascompared to hCNT3-WT, indicating a loss of function of the Na^+-binding site. The greatestdecrease in Na^+-binding affinity was seen with hCNT3-N336C, which had an approximately 15-fold higher K_{50} value compared to hCNT3-WT. hCNT3-T370C and hCNT3-I371C showed similar decreases in Na^+-binding affinity, while that for hCNT3-V339C was less marked. hCNT3-T370C and hCNT3-N336C retained the 2:1 Na^+:nucleoside coupling ratio seen with hCNT3-WT. A significant finding however was that with both hCNT3-V339C and hCNT3-I371C, the Na^+:nucleoside coupling ratio changed from 2:1 to 1:1, providing further evidence that these residues perform a critical role in Na^+-binding.

hCNT3 is unique amongst hCNT familymembers in that it is able to couple nucleoside transport to both Na^+ and H^+ ions (Smith *et al*., 2005). All four mutants exhibited nucleoside-induced H^+ currents, but of varying magnitude. hCNT3-V339C and hCNT3-T370C both showed an increase in H^+-binding affinity (H^+ K_{50} values were lower than that of hCNT3-WT). Their H^+:nucleoside coupling ratios remained unchanged (H^+:nucleoside coupling ratio of 1:1)

compared to hCNT3-WT. Currents observed with hCNT3-I371C did not saturate, even at the highest external concentration of H^+ ions (pH 5.0); the H^+-binding affinity was therefore outside the physiological range (> 10 μM compared to 480 ± 105 nM for hCNT3-WT). Current magnitudes seen with hCNT3-N336C were too low to characterize kinetically. Since this mutant generated readily measurable Na^+ currents, we can attribute the low H^+ currents to an alteration in H^+-binding rather than reduced trafficking of the mutant protein to the plasma membrane.

Several observations suggest that the cation-binding site common to all CNT family members, and coordinated in hCNT3 by residues N336, V339, T370, and I371, binds not only Na^+ but H^+ ions as well. Mutation of each of these residues to cysteine not only had varying effects on Na^+ kinetic parameters (K_{50} and I_{max}) and the Na^+:nucleoside coupling ratio, but also had effects on H^+ kinetic parameters (K_{50} and I_{max}). The mutation of hCNT3-N336 to cysteine had a greater effect on H^+-driven transport than Na^+-driven transport; in Na^+-containing media a reduction in K_{50} was observed compared to hCNT3-WT, while the Hill coefficient remained unaltered at 2:1. H^+-driven transport was almost completely eliminated (maximal currents of 5 nA were observed in H^+-enriched media). Mutation of hCNT3-T370 to cysteine resulted in reduced Na^+- binding affinity, but enhanced H^+-binding affinity (Na^+ K_{50} of 17.8 ± 0.9 and H^+ K_{50} of 150 ± 53 nM). In addition, SCAM studies have shown that inhibition of T370C (in the cysteine-less hCNT3 protein) by PCMBS only occurs in Na^+-free, acidified medium and is uridine protectable (Mulinta *et al*., unpublished observations). Together, these results provide support for the hypothesis that the primary cation-binding site in CNTs can variously (i) bind Na^+ only (vcCNT, hCNT1, and hCNT2), (ii) bind H^+ only (NupC), or (iii) bind both Na^+ and H^+ (hCNT3). Further evidence that the residue positions studied in the present Chapter reside within and contribute to the cation-binding site common to CNT family members is presented in Chapter 5, in which mutation of corresponding residues in hCNT1 is examined. The properties of the four hCNT3 mutants also show that mutation of multiple residues affect H^+-binding, suggesting more than one residue is potentially involved in H^+-binding. The interaction of H^+ with hCNT3 therefore likely occurs through binding of a hydronium ion, which requires tetrahedral coordination (von Ballmoos and Dimroth, 2007; Davidson *et al*., 2011).

In summary, the data presented in this Chapter indicates that the four hCNT3 residues studied (N336, V339, T370, and I371) belong to a conserved primary cation-binding site that is shared throughout the CNT protein family. The data also suggest that this cation-binding site,

which is found between HP1 and the discontinuous region of TM7, not only coordinates with the Na^+ cation but is also capable of coordinating a H^+ in the form of a hydronium ion. The primary cation-binding site is found in close proximity to residues involved in binding of the base moiety of the nucleoside, providing a possible explanation of why the nucleoside selectivity profile varies for Na^+- and H^+-coupled hCNT3. Further site-directed mutagenesis studies will be required to locate the second Na^+-binding site of hCNT3 and the residues involved. Based upon the 2 fold-pseudo symmetry of the transporter, the most likely location for the second Na^+-binding site is between HP2 and the non-helical portion of TM10.

References

Baldwin, S.A. Personal communication.

Davidson, V. L. 2011. Ion–protein coordination: The many faces of a proton. *Nat. Chem.* 3:662-663.

Feng, Z., Hou, T., and Li, Y. 2013. Transport of nucleosides in the vcCNT facilitated by sodium gradients from molecular dynamics simulations. *Mol. Biosyst.* 9:2142-2153.

Johnson, Z. L., Cheong, C., and Lee, S. 2012. Crystal structure of a concentrative nucleoside transporter from *Vibrio cholera* at 2.4 Å. *Nature*. 483:489-493.

Mulinta, R., Slugoski, M.D., Ng, A.M.L., Yao, S.Y.M., Cass, C.E., Baldwin, S.A., and Young, J.D. Substituted cysteine accessibility method (SCAM) analysis of transport domain of human concentrative nucleoside transporter 3 (hCNT3) reveals features of structural and functional importance. *Unpublished observations*.

Slugoski, M. D., Ng, A. M. L., Yao, S. Y. M., Lin, C. C., Mulinta, R., Cass, C. E., Baldwin, S. A., and Young, J. D. 2009. Substituted Cysteine Accessibility Method Analysis of Human Concentrative Nucleoside Transporter hCNT3 Reveals a Novel Discontinuous Region of Functional Importance within the CNT Family Motif (G/A)XKX$_3$NEFVA(Y/M/F). *J. Biol.Chem*. 284:17281-17292.

Smith, K.M., Slugoski, M.D., Cass, C.E., Baldwin, S.A., Karpinski, E., and Young, J.D. 2007. Cation coupling properties of human concentrative nucleoside transporters hCNT1, hCNT2 and hCNT3. *Mol. Membr. Biol.* 24:53-64.

Smith, K.M., Slugoski, M.D., Loewen, S.K., Ng, A.M.L., Yao, S.Y.M., Chen, X., Karpinski, E., Cass, C.E., Baldwin, S.A., and Young, J.D. 2005. The broadly selective human Na^+/nucleoside cotransporter (hCNT3) exhibits novel cation-coupled nucleoside transport characteristics. *J. Biol. Chem.* 280:25436-25449.

Young, J.D., Yao, S.Y.M., Baldwin, J.M., Cass, C.E., and Baldwin, S.A. 2013. The human concentrative and equilibrative nucleoside transporter families, SLC28 and SLC29. *Mol. Aspects Med.* 34:529-547.

von Ballmoos,C. and Dimroth, P. 2007. Two distinct proton binding sites in the ATP synthase family. *Biochem.* 46:11800-11809.

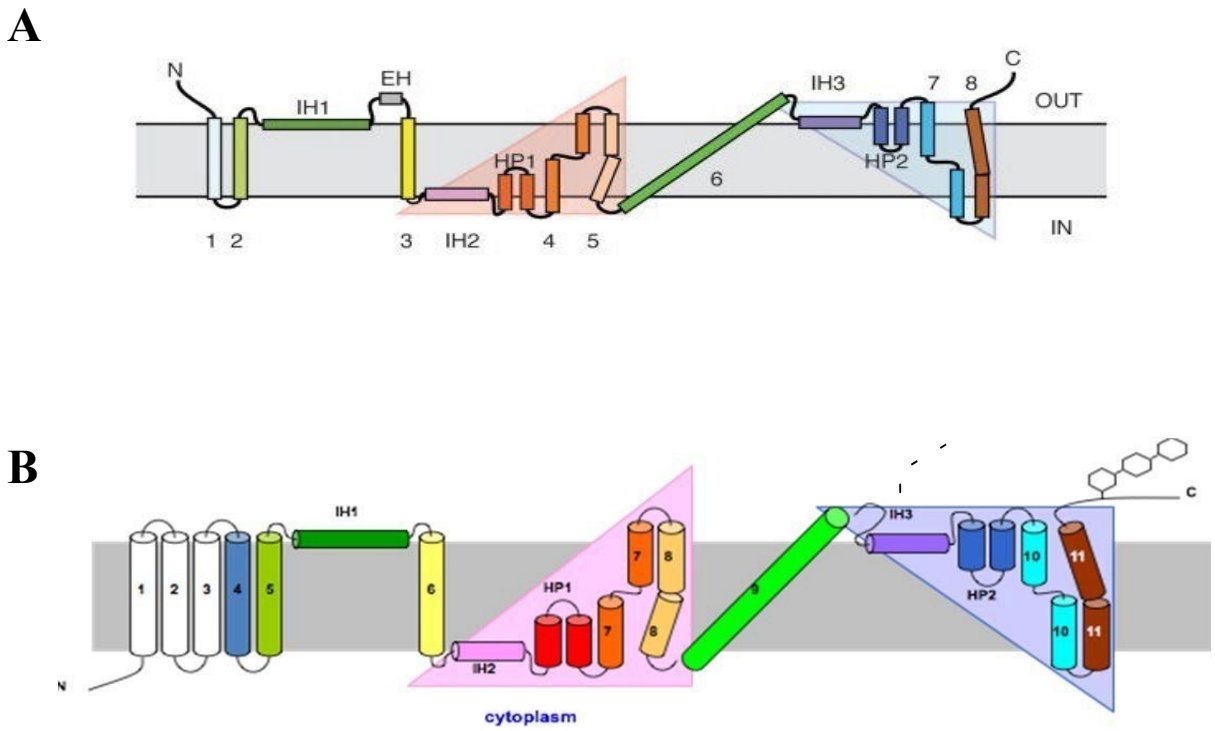

Figure 3-1: Topology of vcCNT and hCNT3. The group of helices under the *pink* triangular background is related to the group of helices under the *cyan* triangular background by a two-fold pseudo-symmetry with the symmetry axis parallel to the membrane (Johnson *et al*., 2012). **A.** Schematic representation of vcCNT topology showing TMs 1 - 8. **B.** Schematic representation of hCNT3 topology showing TMs 1 - 11. The scaffold domain includes: TM4, TM5, IH1, TM6, and TM9. The transport domain is further subdivided into two domains: Subdomain 1- IH2, HP1, TM7 and TM8; Subdomain 2- IH3, HP2, TM10 and TM11. hCNT3 has an intracellular N-terminus and an extracellular C-terminus. The first three TMs of hCNT3 are absent from vcCNT and do not contribute to transport.

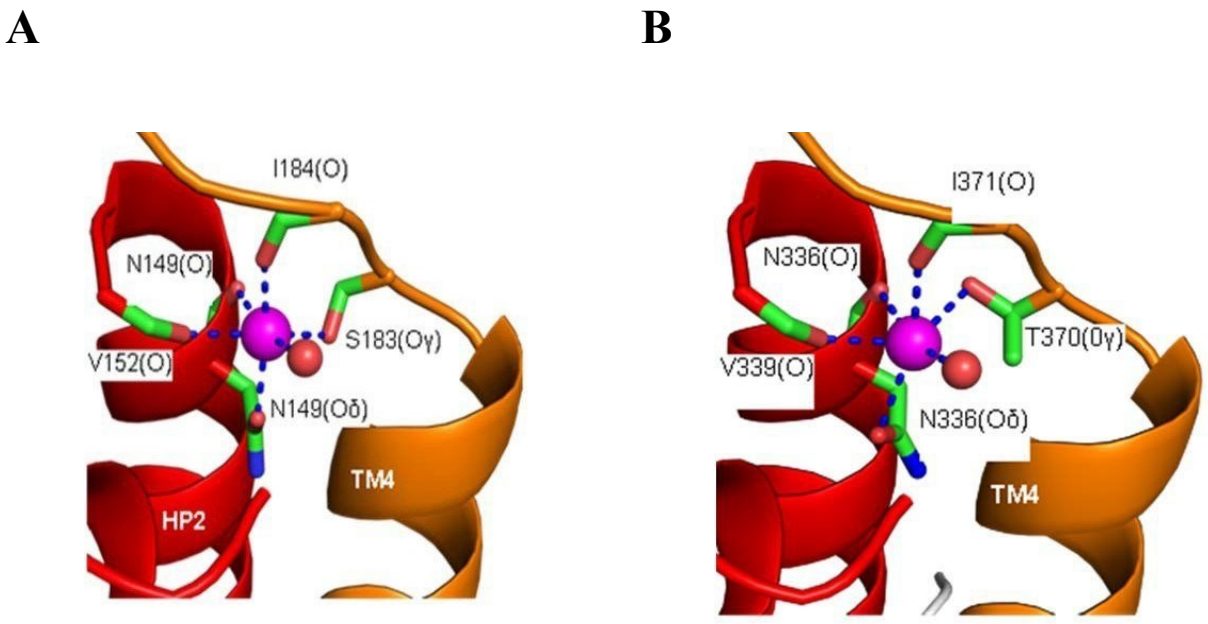

Figure 3-2: Modelled structure comparing the vcCNT and hCNT3 cation-binding sites. Coordination of an octahedral binding site, as predicted by the vcCNT crystal structure. The *magenta* sphere represents the cation. The *red* sphere is a water molecule. **A.** Structure of the vcCNT Na^+-binding site outlining key residues involved in the coordination of a Na^+ ion (N149, V152, I183, and I184). **B.** Structure of the hCNT3 Na^+-binding site outlining the putative corresponding key residues involved in the coordination of a Na^+ ion in this transporter (N336, V339, T370, and I371).

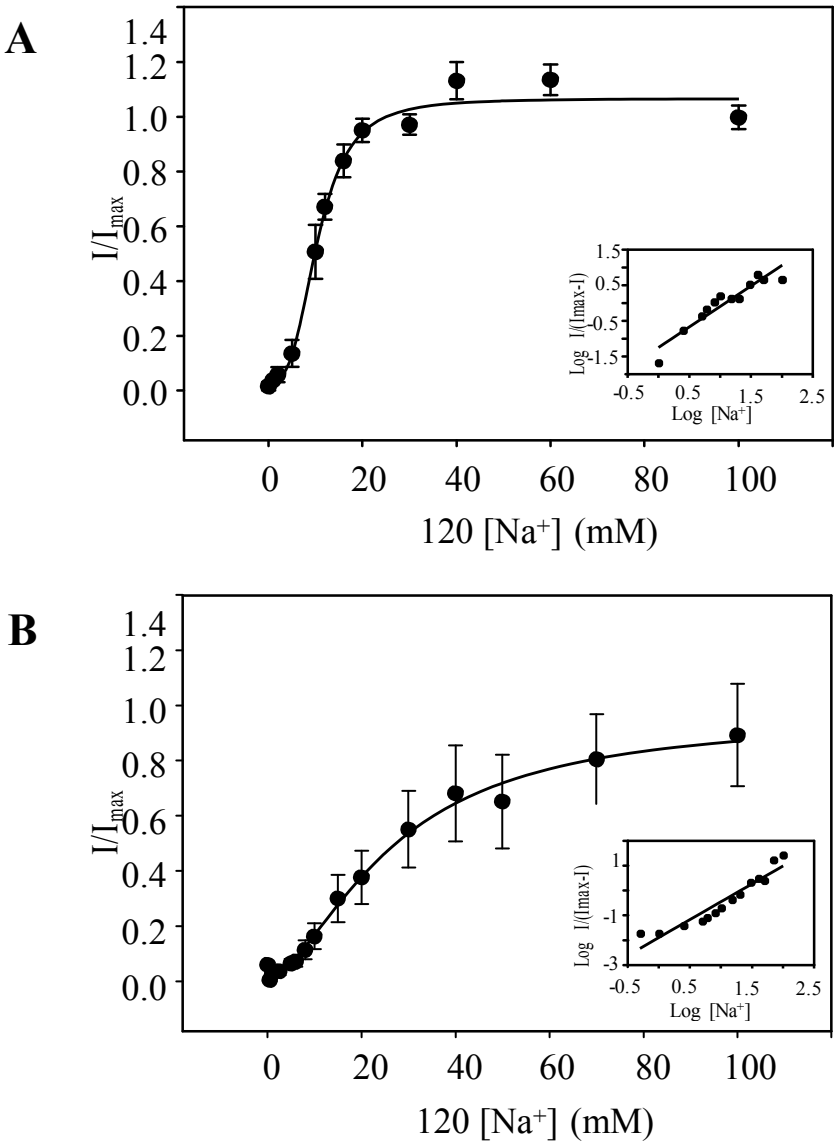

Figure 3-3: Na^+-activation of hCNT3-WT and hCNT3-N336C. A. Na^+-activation curve of hCNT3-WT producing oocytes measured in transport medium containing 0 - 100 mM NaCl (pH 8.5) at a uridine concentration of 20 µM (V_h= -50 mV). Currents were normalized to the fitted I_{max} for each oocyte and are presented as the average from 7 oocytes. The K_{50} was 1.7 ± 0.2 mM. The inset in **A** is a Hill plot of a representative oocyte with a Hill coefficient of 1.6 ± 0.1. **B.** Na^+-activation curve in hCNT3-N336C producing oocytes (n=7) under the same conditions as hCNT3-WT. The K_{50} was 26.5 ± 8.9 mM. The inset in **B** is a Hill plot of a representative oocyte with a Hill coefficient of 1.5 ± 0.1. Kinetic parameters are presented in **Table 3-I**. No currents were observed in control water-injected oocytes.

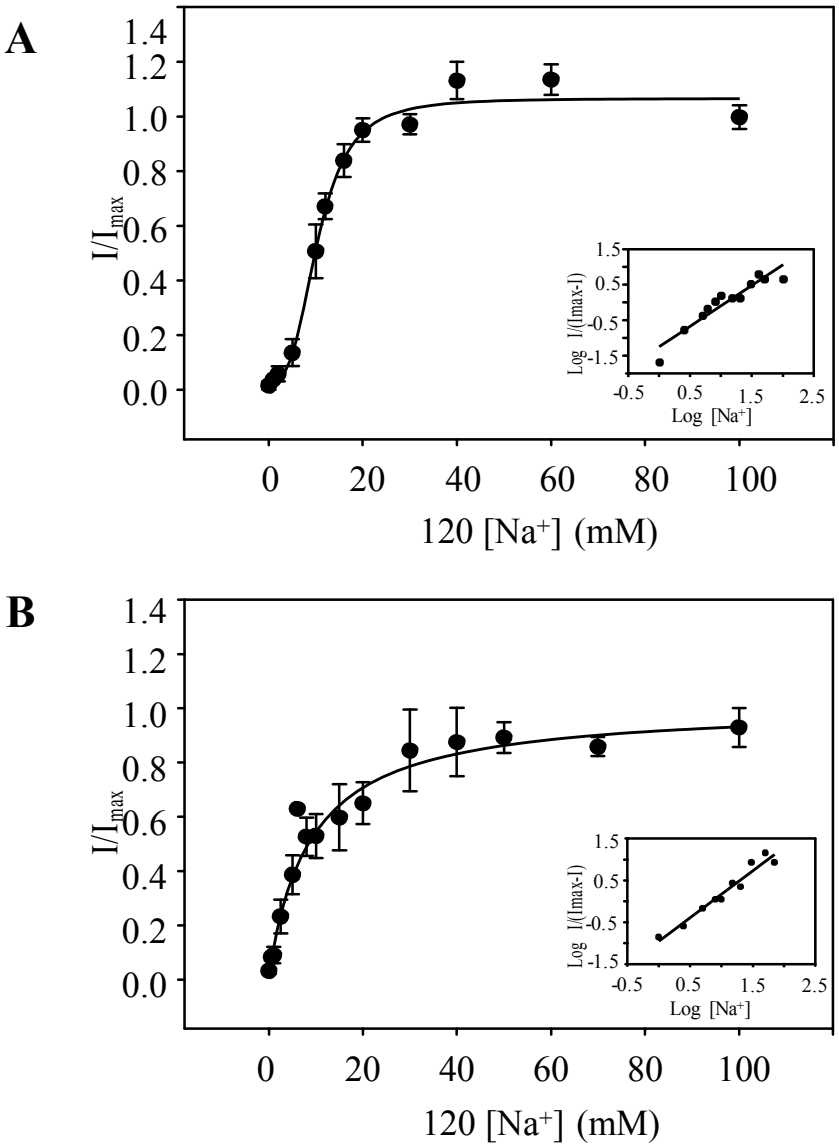

Figure 3-4: Na^+-activation of hCNT3-WT and hCNT3-V339C. A. Same data as Fig. 3-3A: Na^+-activation curve of hCNT3-WT producing oocytes measured in transport medium containing 0 - 100 mM NaCl (pH 8.5) at a uridine concentration of 20 µM (V_h= -50 mV). Currents were normalized to the fitted I_{max} for each oocyte and are presented as the average from 7 oocytes. The K_{50} was 1.7 ± 0.2 mM. The inset in **A** is a Hill plot of a representative oocyte with a Hill coefficient of 1.6 ± 0.1. **B.** Na^+-activation curve in hCNT3-V339C producing oocytes (n=7) under the same conditions as hCNT3-WT. The K_{50} was 8.8 ± 1.3 mM. The inset in **B** is a Hill plot of a representative oocyte with a Hill coefficient of 1.1 ± 0.1. Kinetic parameters are presented in **Table 3-I**. No currents were observed in control water-injected oocytes.

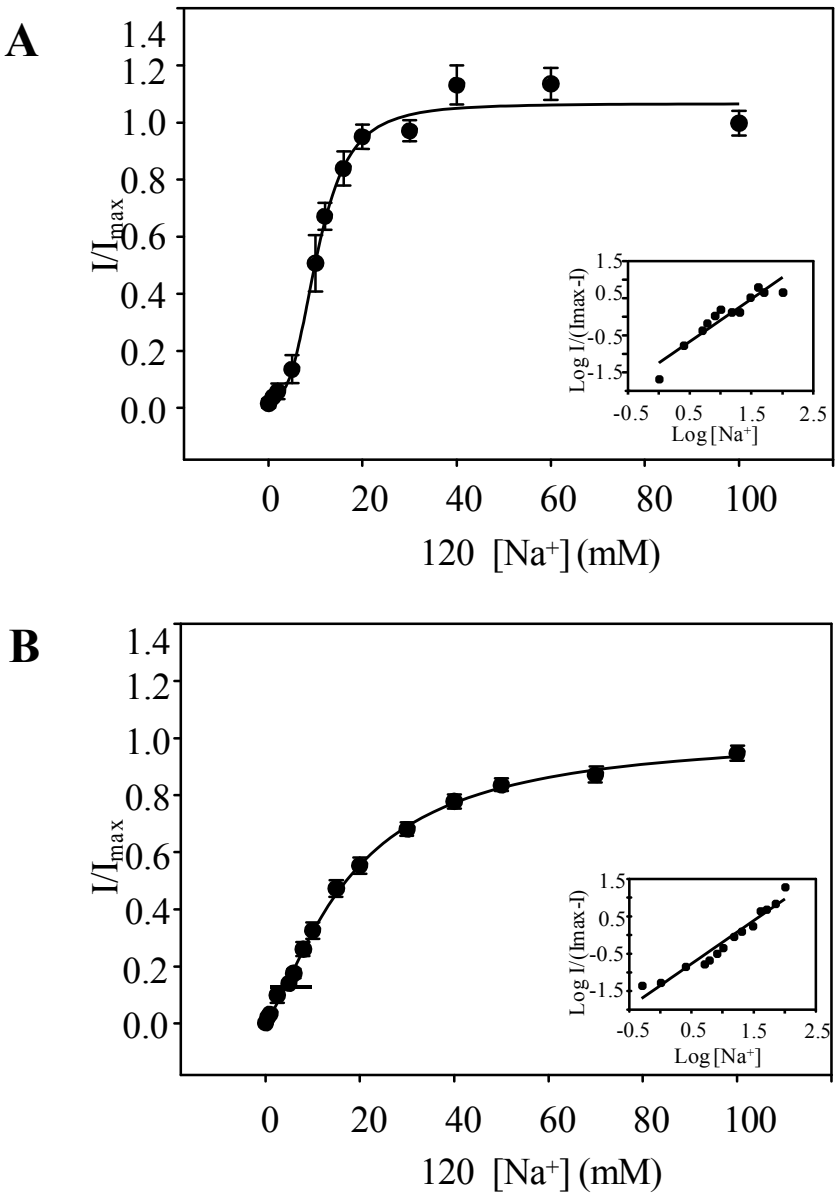

Figure 3-5: Na^+-activation of hCNT3-WT and hCNT3-T370C. A. Same data as Fig. 3-3A: Na^+-activation curve of hCNT3-WT producing oocytes measured in transport medium containing 0 - 100 mM NaCl (pH 8.5) at a uridine concentration of 20 µM (V_h= -50 mV). Currents were normalized to the fitted I_{max} for each oocyte and are presented as the average from 7 oocytes. The K_{50} was 1.7 ± 0.2 mM. The inset in **A** is a Hill plot of a representative oocyte with a Hill coefficient of 1.6 ± 0.1. **B.** Na^+-activation curve in hCNT3-T370C producing oocytes (n=7) under the same conditions as hCNT3-WT. The K_{50} was 17.8 ± 0.9 mM. The inset in **B** is a Hill plot of a representative oocyte with a Hill coefficient of 1.5 ± 0.1. Kinetic parameters are presented in **Table 3-I**. No currents were observed in control water-injected oocytes.

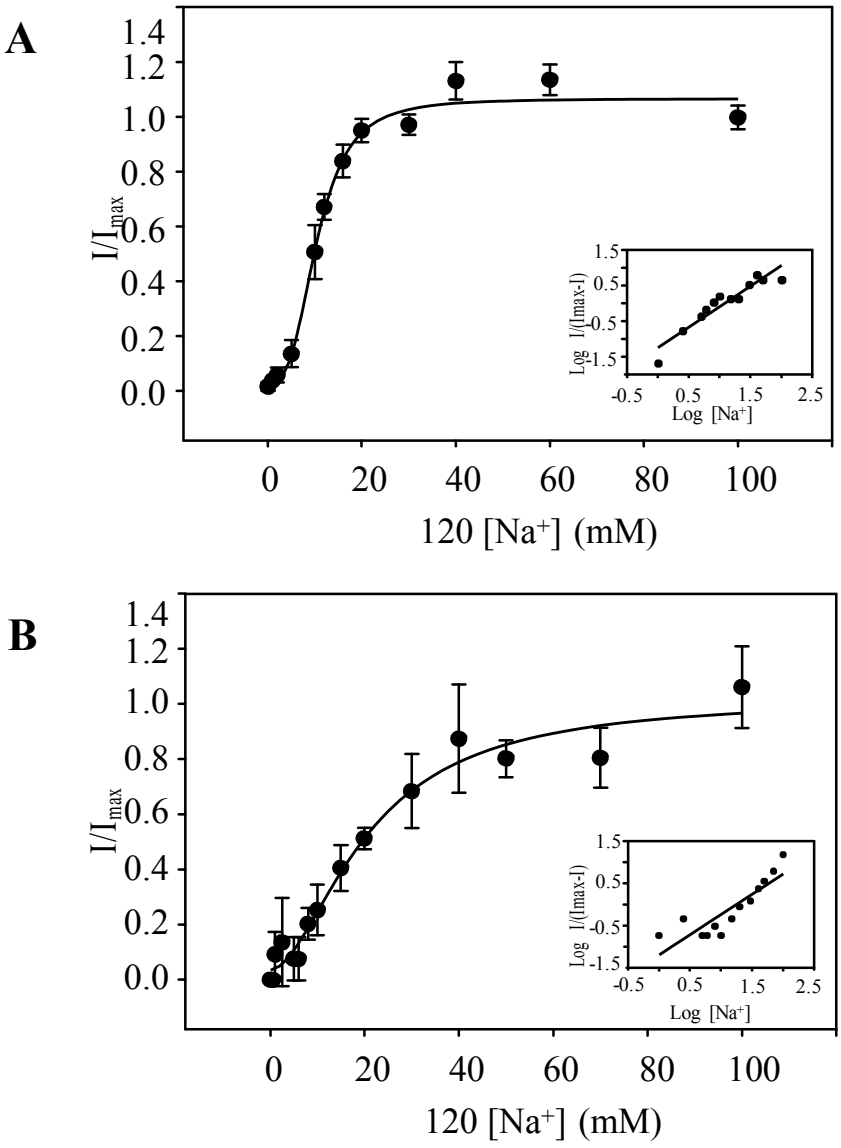

Figure 3-6: Na^+-activation of hCNT3-WT and hCNT3-I371C. A. Same data as Fig. 3-3A: Na^+-activation curve of hCNT3-WT producing oocytes measured in transport medium containing 0 - 100 mM NaCl (pH 8.5) at a uridine concentration of 20 µM (V_h= -50 mV). Currents were normalized to the fitted I_{max} for each oocyte and are presented as the average from 7 oocytes. The K_{50} was 1.7 ± 0.2 mM. The inset in **A** is a Hill plot of a representative oocyte with a Hill coefficient of 1.6 ± 0.1. **B.** Na^+-activation curve in hCNT3-I371C producing oocytes (n=7) under the same conditions as hCNT3-WT. The K_{50} was 20.7 ± 3.0 mM. The inset in **B** is a Hill plot of a representative oocyte with a Hill coefficient of 1.1 ± 0.1. Kinetic parameters are presented in **Table 3-I**. No currents were observed in control water-injected oocytes.

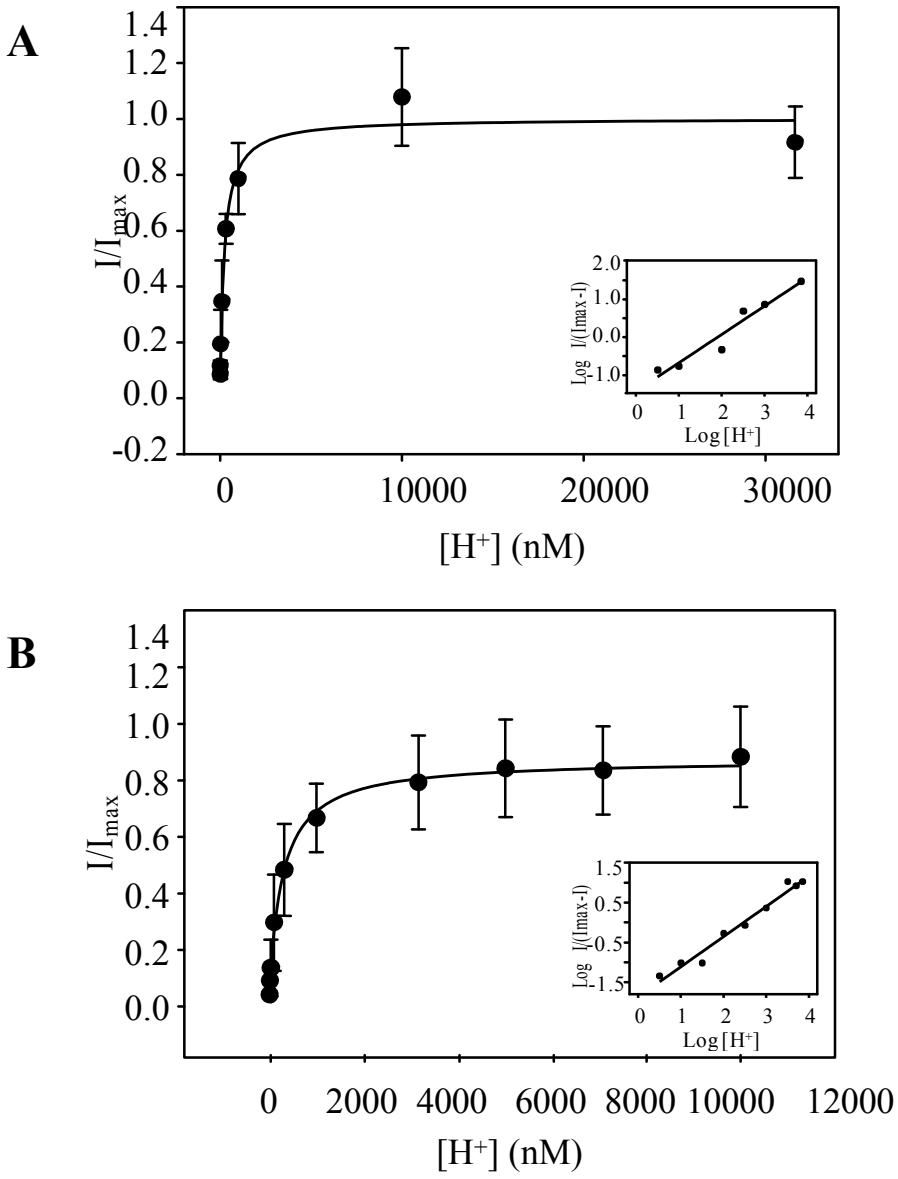

Figure 3-7: H^+-activation of hCNT3-WT and hCNT3-V339C. A. H^+-activation curve of hCNT3-WT producing oocytes measured in transport medium containing 100 mM ChCl (pH 8.5 - 5.0) at a uridine concentration of 100 μM (V_h= -50 mV). Currents were normalized to the fitted I_{max} for each oocyte and are presented as the average from 7 oocytes. The K_{50} was 480 ± 105 nM. The inset in **A** is a Hill plot of a representative oocyte with a Hill coefficient of 0.4 ± 0.1. **B.** H^+-activation curve in hCNT3-V339C producing oocytes (n=7) under the same conditions as hCNT3-WT. The K_{50} was 294 ± 32 nM. The inset in **B** is a Hill plot of a representative oocyte with a Hill coefficient of 0.6 ± 0.1. Kinetic parameters are presented in **Table 3-I**. No currents were observed in control water-injected oocytes.

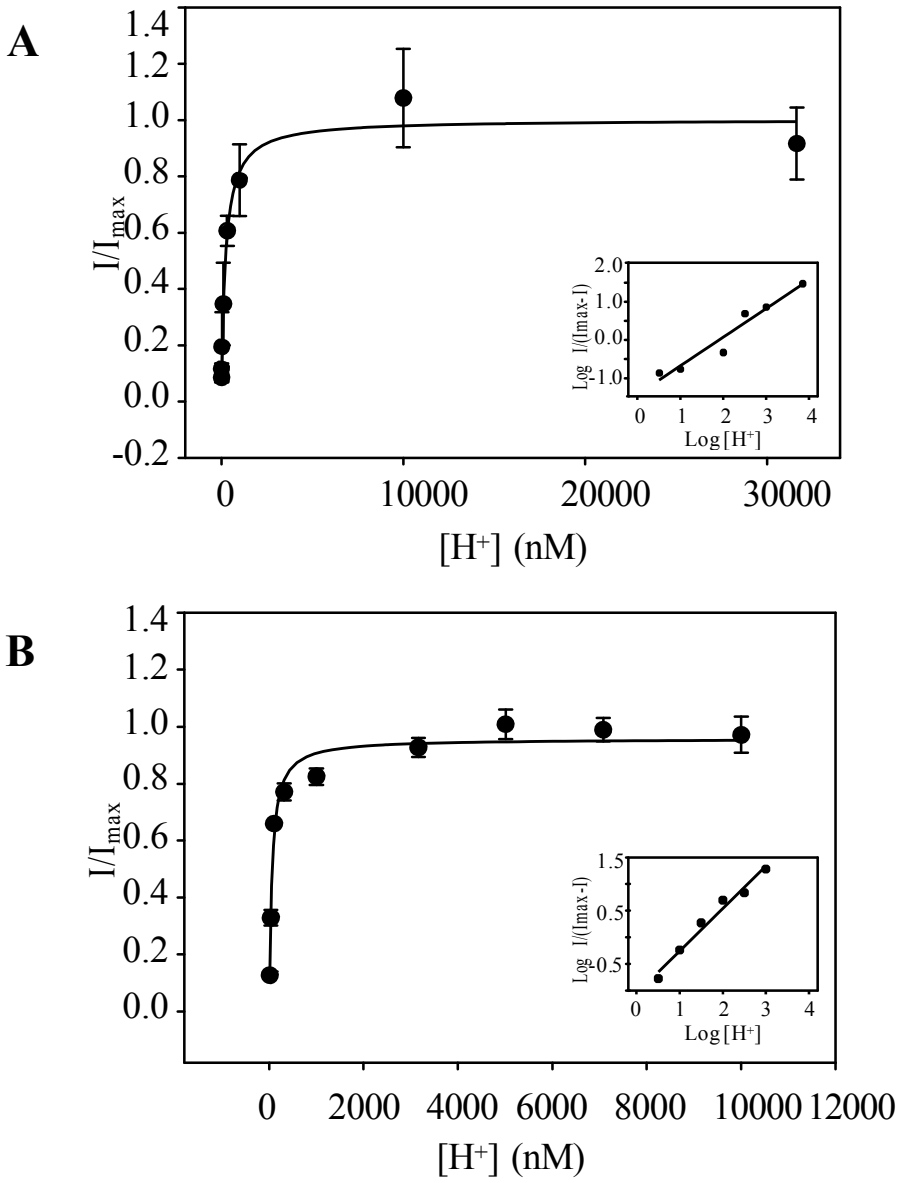

Figure 3-8: H^+-activation of hCNT3-WT and hCNT3-T370C. A. Same data as Fig. 3-7A: H^+-activation curve of hCNT3-WT producing oocytes measured in transport medium containing 100 mM ChCl (pH 8.5 - 5.0) at a uridine concentration of 100 µM (V_h= -50 mV). Currents were normalized to the fitted I_{max} for each oocyte and are presented as the average from 7 oocytes. The K_{50} was 480 ± 105 nM. The inset in **A** is a Hill plot of a representative oocyte with a Hill coefficient of 0.4 ± 0.1. **B.** H^+-activation curve in hCNT3-V339C producing oocytes (n=7) under the same conditions as hCNT3-WT. The K_{50} was 150 ± 53 nM. The inset in **B** is a Hill plot of a representative oocyte with a Hill coefficient of 0.7 ± 0.1. Kinetic parameters are presented in **Table 3-I**. No currents were observed in control water-injected oocytes.

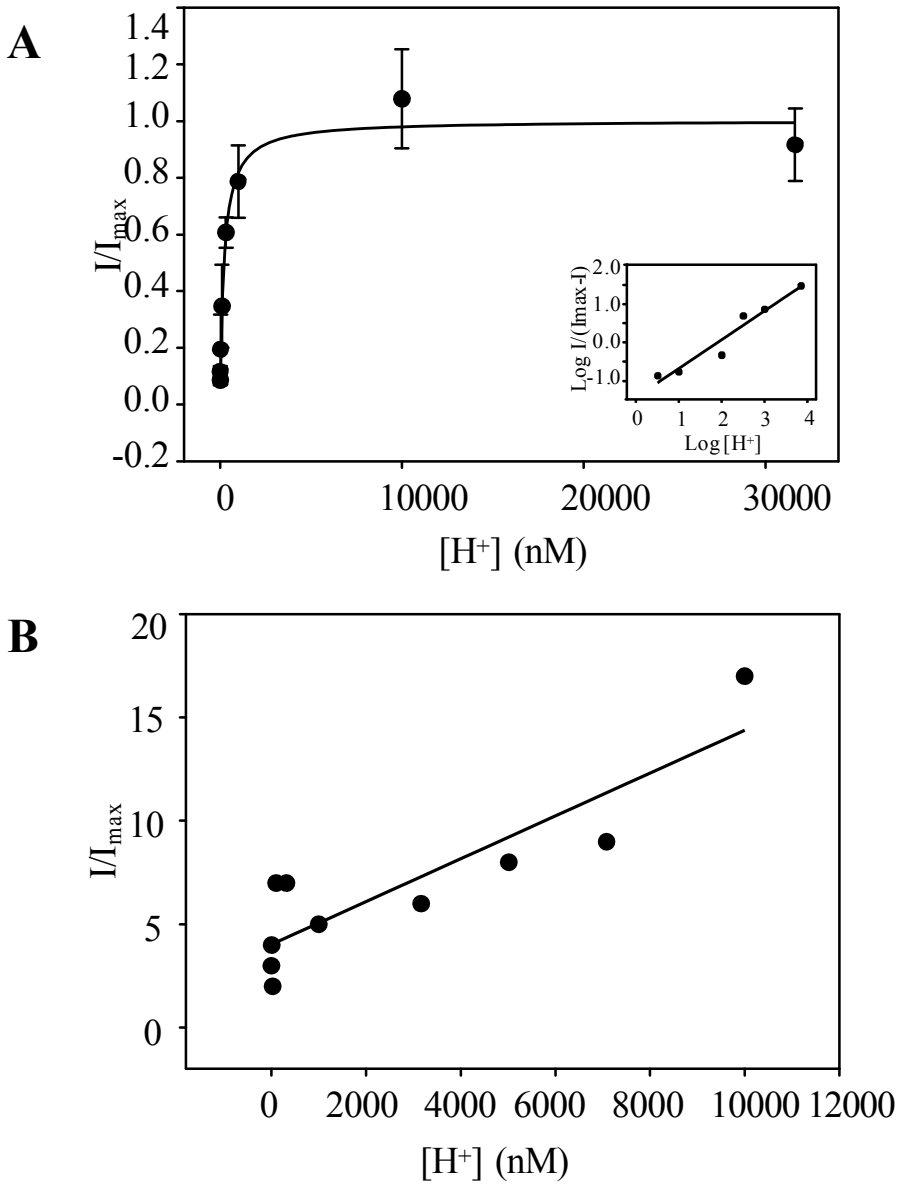

Figure 3-9: H^+-activation of hCNT3-WT and hCNT3-I371C. A. Same data as Fig. 3-7A: H^+-activation curve of hCNT3-WT producing oocytes measured in transport medium containing 100 mM ChCl (pH 8.5 - 5.0) at a uridine concentration of 100 μM (V_h= -50 mV). Currents were normalized to the fitted I_{max} for each oocyte and are presented as the average from 7 oocytes. The K_{50} was 480 ± 105 nM. The inset in **A** is a Hill plot of a representative oocyte with a Hill coefficient of 0.4 ± 0.1. **B.** H^+-activation curve in an hCNT3-I371C producing oocyte (n=1) under the same conditions as hCNT3-WT. Currents did not saturate. No currents were observed in control water-injected oocytes.

		hCNT3	N336C	V339C	T370C	I371C
Na^+	K_{50} (mM)	1.7 ± 0.2	26.5 ± 8.9	8.8 ± 1.3	17.8 ± 0.9	20.7 ± 3.0
	n_H	1.6 ± 0.1	1.5 ± 0.1	1.1 ± 0.1	1.5 ± 0.1	1.1 ± 0.1
	I_{max} (nA)	100	25	70	40	50
H^+	K_{50} (nM)	480 ± 105	n/d*	294 ± 32	150 ± 53	>10 µM
	n_H	0.4 ± 0.1	n/d*	0.6 ± 0.1	0.7 ± 0.1	n/d*
	I_{max} (nA)	150	5	70	150	17

Table 3-1: Na^+- and H^+-activation kinetic parameters of hCNT3-WT and mutants. Half-saturation constants (K_{50}) and Hill coefficients (n) for Na^+ were determined from Na^+ concentration response curves (0 - 100 mM NaCl; pH 8.5) measured at a uridine concentration of 20 µM. Half-saturation constants (K_{50}) and Hill coefficients (n) for H^+ were determined from H^+ concentration response curves (pH 8.5 - 5.0) measured in Na^+-free transport medium (100 mM ChCl) at a uridine concentration of 100 µM. K_{50} values for both Na^+ and H^+ were obtained from fits to data from individual oocytes normalized to the fitted I_{max} value obtained for that cell and are presented as means ± S.E.M. The hCNT3-I371C K_{50} for H^+ was calculated from a fitted estimate (± S.E.) for a single representative oocyte. The Hill coefficients (n) and I_{max} values for both Na^+ and H^+ are from a single representative oocyte. The membrane potential was -50 mV.

*n/d currents were too low to be characterized.

Chapter 4:

Further Site-Directed Mutagenesis and Electrophysiological Characterization of Amino Acid Residues (N336 and T370) Involved in the Na^+/H^+ Binding Site of Human Concentrative Nucleoside Transporter 3 (hCNT3) Produced in *Xenopus laevis* Oocytes

Introduction

Mutagenesis studies examining four hCNT3 residues (N336, V339, T370, and I371) found notable changes in hCNT3 Na^+:nucleoside coupling ratios and Na^+- and/or H^+-binding affinities (Chapter 3). The changes in Na^+- and H^+-binding characteristics seen by mutation of these residues suggested that this binding site not only coordinates Na^+, but H^+ as well, in the form of a hydronium ion. Two residues in particular, hCNT3-N336 and hCNT3-T370, exhibited marked changes in Na^+- and H^+-binding characteristics (Chapter 3) when converted to cysteine. Compared to wild-type, hCNT3-N336C showed a large decrease in Na^+-binding affinity, while retaining a 2:1 Na^+:nucleoside coupling ratio, and a loss of H^+-coupling. hCNT3-T370C also showed reduced Na^+-binding affinity and retention of a 2:1 Na^+:nucleoside coupling ratio, but enhanced H^+-binding affinity.

In this Chapter, these residue positions were subjected to additional amino acid substitutions to further explore the nature of their cation-binding interactions. The additional hCNT3-N336 and hCNT3-T370 mutations were selected based upon amino acid side chain structural considerations and sequence comparisons between different CNT family members (S.A. Baldwin, personal communication).

Of the known Na^+-dependent metazoan CNTs (108 sequences analyzed), 93 % have an asparagine at the corresponding position to N149 in vcCNT (*i.e.*, hCNT3-N336). In fungal transporters (68 sequences analyzed), which are generally H^+ symporters, this site is occupied by a serine or threonine. Prokaryotic CNTs (208 sequences analyzed) contain either an asparagine (63 %) or serine/threonine (23 %) at this site. From these findings, it was postulated that the presence of a serine or threonine residue at this position may be important for H^+-driven transport, and was the rationale behind generating the hCNT3 mutants hCNT3-N336S andhCNT3-N336T, which are predicted to lose Na^+-dependence and convert hCNT3 into an H^+- specific transporter. An hCNT3-N336A mutant was also generated to examine the importance of the asparagine residue itself in Na^+/H^+-coupling. Alanine, a small, nonpolar amino acid unable to form hydrogen bonds, is predicted to cause a loss or modification of both Na^+- and H^+- dependence at this position. The other residue, hCNT3-T370, was mutated to serine, since the majority of bacterial CNT familymembers contain a serine at the corresponding position. It is of importance to note that in vcCNT, a Na^+-dependent CNT family member, this position is

similarly occupied by a serine (S183). Other hCNT family members (*i.e.,* hCNT1/2), like hCNT3, also contain a threonine at this position. hCNT3-T370S is therefore predicted to have altered Na^+-binding as compared to hCNT3-WT and to be converted from a Na^+-driven to a H^+-driven transporter. The final mutation tested, hCNT3-T370G, is predicted to lose or have altered cation dependence, since glycine, like alanine, is a small, nonpolar amino acid. It is hypothesized, therefore, that mutation of hCNT3 residues N336 and T370 to the residues selected will lead to changes in hCNT3 cation-binding affinity and, perhaps, cation-selectivity, and thus unravel the structural foundation by which the side chains of these amino acids coordinate with Na^+ and H^+.

Results

Na^+-Activation Kinetics of hCNT3-WT and Mutants

Na^+-activation kinetics of hCNT3-WT - Measurements of current as a function of increasing external Na^+ concentration (0 - 100 mM; pH 8.5) were made at a uridine concentration of 20 μM and a holding potential of -50 mV (Figure 4-2A). A sigmoidal relationship was revealed with aHill coefficient of 1.6 ± 0.1, indicating that the Na^+:uridine stoichiometry is 2:1, similar topreviously published findings (Smith *et al*., 2005, 2007). The K_{50} value for Na^+ was 1.7 ± 0.2mM, in agreement with previous studies (Smith *et al.,* 2005). Kinetic parameters are presented incomparison with those of hCNT3 mutants in Table 4-1. These data are the same as presentedpreviously in Chapter 3 as Figures 3-3A, 3-4A, 3-5A, and 3-6A and in Table 3-1.

Na^+-activation kinetics of hCNT3-N336A, hCNT3-N336T, and hCNT3-N336S - hCNT3 residue N336 (Figure 4-1B), corresponding to N149 in vcCNT (Figure 4-1A), was mutated to alanine, threonine, or serine. The dependence of hCNT3-N336A-, hCNT3-N336T-, and hCNT3-N336S-mediated currents on the external concentration of Na^+ (0 - 100 mM NaCl; pH 8.5) was measured at a uridine concentration of 20 μMand a holding potential of -50 mV. We observed a marked decrease in the maximum currents generated by all three mutants (4 - 5 nA for all three mutants; 20 μM uridine, 100 mM NaCl, pH 8.5; single representative oocytes) compared to that of hCNT3-WT (100 nA; 20 μMuridine, 100 mM NaCl, pH 8.5; single representative oocyte) (Table 4-I). Kinetic parameters for Na^+ activation could not therefore be determined.

Na^+-activation kinetics of hCNT3-T370G - hCNT3 residue T370 (Figure 4-1B), corresponding to S183 in vcCNT (Figure 4-1A), was mutated to glycine, and the dependence ofhCNT3-T370G-mediated currents on the external concentration of Na^+ (0 - 100 mM NaCl; pH 8.5) wasdetermined at a uridine concentration of 20 μM and a holding potential of -50 mV (Figure 4-2B). A plot of current in response to increasing concentrations of Na^+ revealed a sigmoidal relationship with a Hill coefficient of 2.1 ± 0.1 (Table 4-1), suggesting that the Na^+:uridine stoichiometry is 2:1, similar to that seen with hCNT3-WT. The K_{50} value for Na^+ was 13.5 ± 1.3 mM, notably greater than that observed for hCNT3-WT (1.7 ± 0.2 mM), suggesting a significant

decrease in affinity of hCNT3-T370G for Na^+. We also observed an approximate 90% decrease in maximum current (8 nA; 20 μMuridine, 100 mM NaCl, pH 8.5; single representative oocyte) compared to that of hCNT3-WT (100 nA; 20 μMuridine, 100 mM NaCl, pH 8.5; single representative oocyte) (Table 4-1).

Na^+-activation kinetics of hCNT3-T370S - hCNT3 residue T370 (Figure 4-1B), corresponding to S183 in vcCNT (Figure 4-1A), was mutated to serine, and the dependence of hCNT3-T370S-mediated currents on the external concentration of Na^+ (0 - 100 mM NaCl; pH 8.5) was measured at uridine concentration of 20 μM and a holding potential of -50 mV. We observed a dramatic decrease in maximum current (4 nA; 20 μM uridine, 100 mM NaCl, pH 8.5; single representative oocyte) compared to that of hCNT3-WT (100 nA; 20 μM uridine, 100 mM NaCl, pH 8.5; single representative oocyte) (Table 4-1). Kinetic parameters for Na^+ activation could not therefore be determined.

H^+-Activation Kinetics of hCNT3-WT and Mutants

H^+-activation kinetics of hCNT3-WT - The dependence of hCNT3-mediated currents on the external concentration of H^+ was determined in 100 mM ChCl transport medium at external pH values ranging from 8.5 - 5.0 (Na^+-free medium) (Figure 4-3A). Currents were measured at a uridine concentration of 100 μM and a holding potential of -50 mV. A plot of current in response to an increasing concentration of H^+ (pH 8.5 - 5.0) revealed a hyperbolic relationship with a Hill coefficient of 0.4 ± 0.1, suggesting that the H^+:uridine stoichiometry is 1:1, consistent with previous findings (Smith *et al.,* 2005). The K_{50} value of hCNT3-WT for H^+ was 480 ± 105 nM, demonstrating that H^+ binds with high affinity to hCNT3. These findings are in agreement with previously published studies (Smith *et al.*, 2005). Kinetic parameters are presented in comparison with those of hCNT3 mutants in Table 4-1. These data are the same aspresented previously in Chapter 3 as Figures 3-7A, 3-8A, and 3-9A, and in Table 3-1.

H^+-activation kinetics of hCNT3-N336S - hCNT3 residue N336 (Figure 4-1B), corresponding to N149 in vcCNT (Figure 4-1A), was mutated to serine, and the dependence of hCNT3-N336S-mediated currents on the external concentration of H^+ determined in 100 mM ChCl transport

medium at external pH values ranging from 8.5 - 5.0 (Na^+-free medium), at a uridine concentration of 100 μM and a holding potential of -50 mV (Figure 4-3B). A plot of current in response to increasing concentrations of H^+ (pH 8.5 - 5.0) revealed a hyperbolic relationship with a Hill coefficient of 0.4 ± 0.1. This suggests that the H^+:uridine stoichiometry is 1:1, similar to that observed for hCNT3-WT. The K_{50} value of hCNT3-N336S for H^+ was 1200 ± 100 nM compared to 480 ± 105 nM for the wild-type transporter. This K_{50} value is significantly greater (p=0.0003) than that observed for hCNT3-WT, suggesting a decrease in affinity of hCNT3-N336S for H^+. We also observed a decrease in maximum current (10 nA; 100 μM uridine, 100 mM ChCl, pH 8.5 - 5.0; single representative oocyte) compared to hCNT3-WT (150 nA; 100 μM uridine, 100 mM ChCl, pH 8.5 - 5.0; single representative oocyte) (Table 4-1).

H^+-activation kinetics of hCNT3-N336A and hCNT3-N336T - hCNT3 residue N336 (Figure 4-1B), corresponding to N149 in vcCNT (Figure 4-1A), was mutated to alanine or threonine, and the dependence of hCNT3-N336A- and hCNT3-N336T-mediated currents on the external concentration of H^+ was determined in 100 mM ChCl transport medium at external pH values ranging from 8.5 - 5.0 (Na^+-free medium), at a uridine concentration of 100 μM and a holding potential of -50 mV. We observed a marked decrease in maximum currents for both mutants (5 and 5 nA for hCNT3-N336A and hCNT3-N336T, respectively; 100 μM uridine, 100 mM ChCl, pH 8.5 - 5.0; single representative oocytes) compared to that of hCNT3-WT (150 nA; 100 μM uridine, 100 mM ChCl, pH 8.5 - 5.0; single representative oocyte) (Table 4-I). Kinetic parameters for H^+ activation could not therefore be determined.

H^+-activation kinetics of hCNT3-T370G - hCNT3 residue T370 (Figure 4-1B), corresponding to S183 in vcCNT (Figure 4-1A), was mutated to glycine, and the dependence of hCNT3-T370G-mediated currents on the external concentration of H^+ was determined in 100 mM ChCl transport medium at external pH values ranging from 8.5 - 5.0 (Na^+-free medium), at a uridine concentration of 100 μM and a holding potential of -50 mV (Figure 4-4B). A plot of current in response to increasing concentrations of H^+ (pH 8.5 - 5.0) revealed a hyperbolic relationship with a Hill coefficient of 0.7 ± 0.1. Similar to hCNT3-WT, this suggests a H^+:uridine stoichiometry of 1:1. The K_{50} value of hCNT3-T370G for H^+ was 200 ± 31 nM, significantly less (p=0.0251) than that observed for hCNT3-WT (480 ± 105 nM), suggesting an increase in the affinity of hCNT3-

T370G for H^+. We also observed maximum currents (100 nA; 100 μM uridine, 100 mM ChCl, pH 8.5 - 5.0; single representative oocyte) of similar magnitude to those seen with hCNT3-WT (150 nA; 100 μM uridine, 100 mM ChCl, pH 8.5 - 5.0; single representative oocyte) (Table4-1).

H^+-activation kinetics of hCNT3-T370S - hCNT3 residue T370 (Figure 4-1B), corresponding to S183 in vcCNT (Figure 4-1A), was mutated to serine, and the dependence of hCNT3-T370S-mediated currents on the external concentration of H^+ was measured in 100 mM ChCl transport medium at external pH values ranging from 8.5 - 5.0 (Na^+-free medium), at a uridineconcentration of 100 μM and a holding potential of -50 mV (Figure 4-5B). A plot of current inresponse to increasing concentrations of H^+ (pH 8.5 - 5.0) revealed a hyperbolic relationship with a Hill coefficient of 0.9 ± 0.1. This suggests that H^+:uridine stoichiometry is 1:1, consistent withthat calculated for hCNT3-WT. The K_{50} value of hCNT3-T370S for H^+ was 298 ± 69 nM, which, while less than that observed for hCNT3-WT, is not significantly different (p=0.1731) from hCNT3-WT. We also observed maximum currents (80 nA; 100 μM uridine, 100 mM ChCl, pH 8.5 - 5.0; single representative oocyte) similar to that seen with hCNT3-WT (150 nA; 100 μM uridine, 100 mM ChCl, pH 8.5 - 5.0; single representative oocyte) (Table 4-1).

Discussion

Using site-directed mutagenesis, the five hCNT3 mutants, hCNT3-N336S, hCNT3-N336T, hCNT3-N336A, hCNT3-T370G, and hCNT3-T370S, were constructed and produced as recombinant proteins in the *Xenopus* oocytes heterologous expression system. Electrophysiological characterization of the mutants in comparison to hCNT3-WT measured nucleoside-induced Na^+ or H^+ currents and activation kinetics in Na^+-containing H^+-reduced transport media (NaCl; pH 8.5) or in Na^+-depleted, H^+-enriched media (ChCl; pH 8.5 - 5.0), respectively.

Mutation of hCNT3-N336 to serine, threonine, or alanine had dramatic effects on protein function. Mutants hCNT3-N336A, hCNT3-N336S, and hCNT3-N336T all displayed very low currents in both Na^+-containing, H^+-reduced and Na^+-depleted, H^+-enriched medium compared to those of hCNT3-WT. Currents were insufficient to accurately determine Na^+ and H^+ kinetic parameters for hCNT3-N336A and hCNT3-N336T. Currents seen with hCNT3-N336S were also significantly reduced in both Na^+-containing, H^+-reduced and Na^+-depleted, H^+-enriched medium; kinetic parameters for H^+ were, however, able to be characterized. hCNT3-N336S had a 2.5-fold higher K_{50} value for H^+ than hCNT3-WT, suggesting a significant decrease in the affinity of hCNT3-N336S for H^+, while the coupling ratio for H^+:nucleoside transport remained unaltered at 1:1.

Mutation of hCNT3-N336 to serine and threonine, therefore, did not convert hCNT3 from a Na^+-driven to an H^+-driven transporter as hypothesized. Both mutants neverthelessshowed a marked loss-of-function in Na^+-medium, confirming the importance of this residue position in Na^+-coupling. Loss of function was also apparent in Na^+-depleted, H^+-enrichedmedium, with only hCNT3-N336S able to generate sufficient current for kinetic analysis.hCNT3-N336A showed loss of both Na^+ and H^+ dependence. Taken together, these resultsreinforce the conclusion that this residue position resides within the primary cation-binding sitepresent in CNT family members and is capable of binding either Na^+ or H^+. A caveat to thisconclusion is that additional experiments to determine cell-surface expression are needed toexclude the possibility that mutation of thehCNT3-N336 residue impairs correct trafficking tothe plasma membrane, since mutation of thisresidue to serine, threonine, or alanine, like theprevious mutation to cysteine (Chapter 3), allcaused severe reductions in functions compared to

those of the wild-type protein. hCNT3-N336S did, however, exhibit sufficient H^+-coupled activity to demonstrate a significant loss in H^+-binding affinity.

Similar to mutations of residue position hCNT3-N336, mutation of hCNT3-T370 to glycine or serine produced dramatic loss-of-function in Na^+ medium, with mutation of hCNT3-T370 to glycine also causing an approximate 8-fold increase in the K_{50} value of the mutant for Na^+, indicating a large loss of affinity for Na^+. hCNT3-T370G did, however, retain a Na^+:nucleoside coupling ratio of 2:1. In marked contrast to mutation of N336, however, both hCNT3-T370G and hCNT3-T370S exhibited H^+ currents of similar magnitude to that seen with hCNT3-WT. Furthermore, the K_{50} values of both mutants for H^+ decreased approximately 50%, relative to those of the wild-type protein, indicating increased affinities for H^+ while maintaining a 1:1 H^+:nucleoside coupling ratio. Thus both mutations (hCNT3-T370G and hCNT3-T370S) converted the protein from a Na^+/ H^+-coupled transporter to a H^+-preferring transporter. Therefore, while mutation of hCNT3-T370 to glycine did not cause a total loss of cation dependence as predicted, hCNT3-T370S did have significant altered Na^+-binding characteristics. Since H^+-coupling was preserved, loss of Na^+-binding activity could not be attributed to loss of trafficking to the plasma membrane.

Chapter 5 further looks at the role of these residue positions in cation-binding by examining corresponding residues in another member of the CNT family of proteins - human concentrative nucleoside transporter 1 (hCNT1).

References

Baldwin, S.A. Personal communication.

Johnson, Z. L., Cheong, C., and Lee, S. 2012. Crystal structure of a concentrative nucleoside transporter from *Vibrio cholera* at 2.4 Å. *Nature*. 483:489-493.

Smith, K.M., Slugoski, M.D., Cass, C.E., Baldwin, S.A., Karpinski, E., and Young, J.D. 2007. Cation coupling properties of human concentrative nucleoside transporters hCNT1, hCNT2 and hCNT3. *Mol. Membr. Biol*. 24:53-64.

Smith, K.M., Slugoski, M.D., Loewen, S.K., Ng, A.M.L., Yao, S.Y.M., Chen, X., Karpinski, E., Cass, C.E., Baldwin, S.A., and Young, J.D. 2005. The broadly selective human Na^+/nucleoside cotransporter (hCNT3) exhibits novel cation-coupled nucleoside transport characteristics. *J. Biol. Chem*. 280:25436-25449.

Young, J.D., Yao, S.Y.M., Baldwin, J.M., Cass, C.E., and Baldwin, S.A. 2013. The human concentrative and equilibrative nucleoside transporter families, SLC28 and SLC29. *Mol. Aspects Med*. 34:529-547.

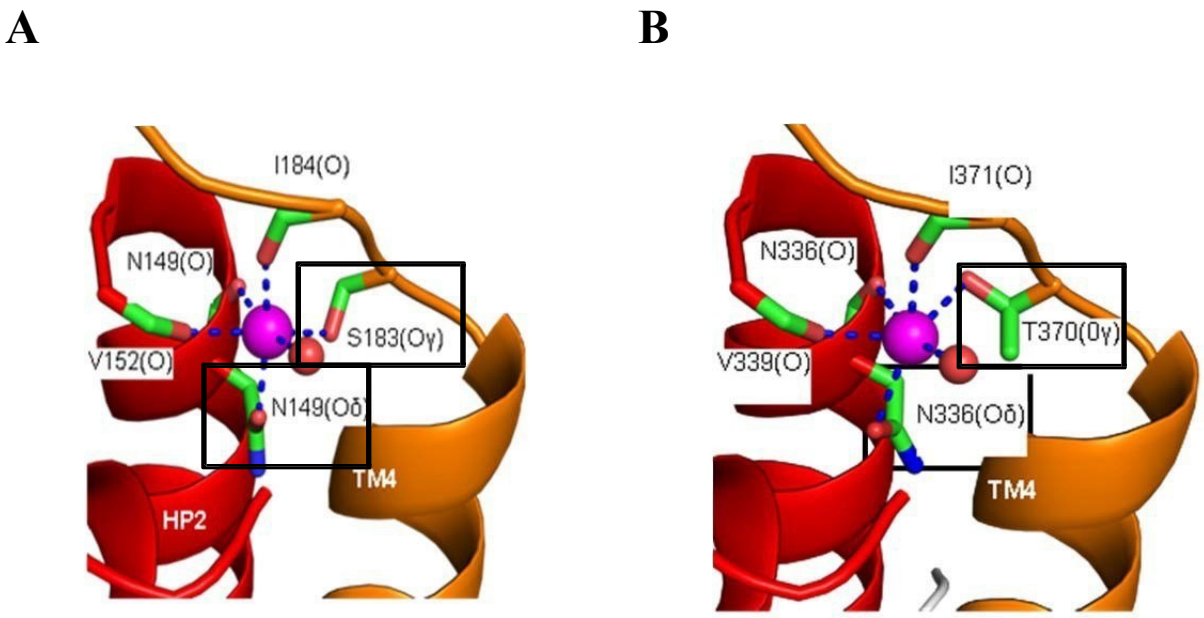

Figure 4-1: Modelled structure comparing the vcCNT and hCNT3 cation-binding sites. Coordination of an octahedral binding site as predicted by the vcCNT crystal structure. The *magenta* sphere represents the cation. The *red* sphere is a water molecule. **A**. Structure of the vcCNT cation-binding site highlighting residues N149 and S183. **B**. Structure of the hCNT3 cation-binding site highlighting corresponding residues N336 and T370 (Baldwin, personal communication).

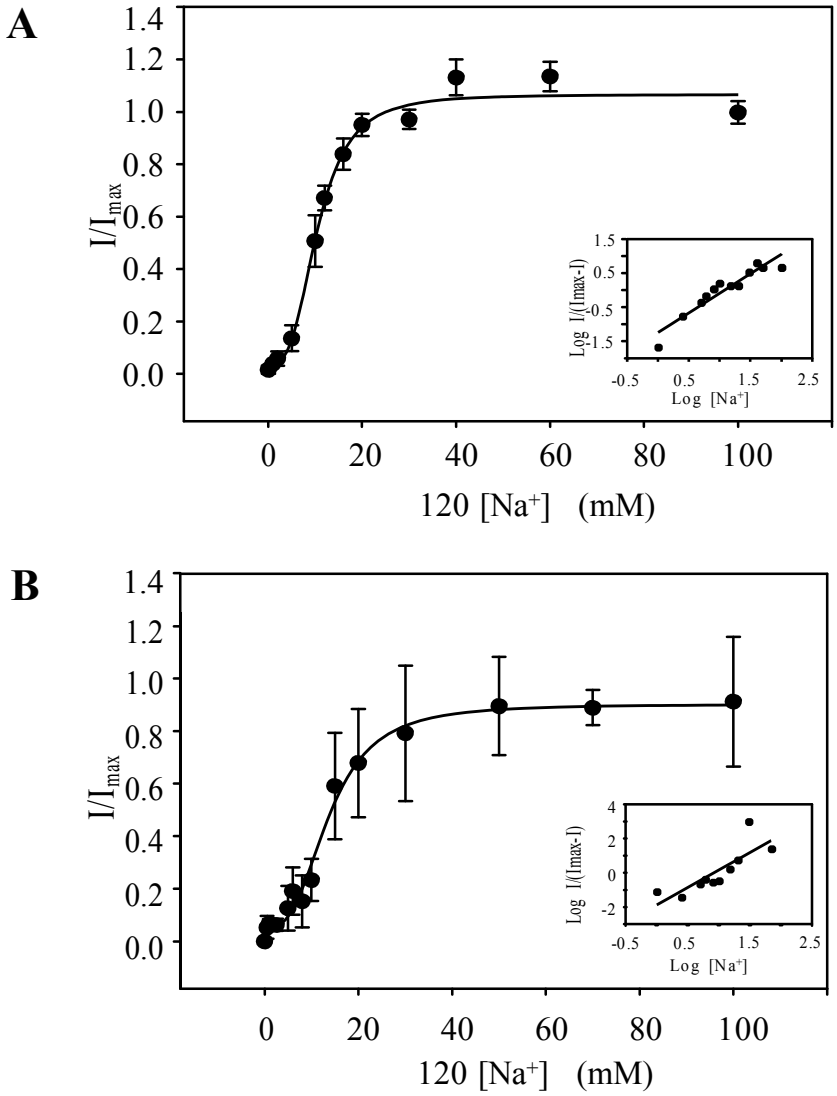

Figure 4-2: Na^+-activation of hCNT3-WT and hCNT3-T370G. A. Na^+-activation curve of hCNT3-WT producing oocytes measured in transport medium containing 0 - 100 mM NaCl (pH 8.5) at a uridine concentration of 20 μM (V_h= -50 mV). Currents were normalized to the fitted I_{max} for each oocyte and are presented as the average from 7 oocytes. The K_{50} was 1.7 ± 0.2 mM. The inset in **A** is a Hill plot of a representative oocyte with a Hill coefficient of 1.6 ± 0.1. **B.** Na^+-activation curve in hCNT3-T370G producing oocytes (n=7) under same conditions as hCNT3-WT. The K_{50} was 13.5 ± 1.3 mM. The inset in **B** is a Hill plot of a representative oocyte with a Hill coefficient of 2.1 ± 0.1. Kinetic parameters are presented in **Table 4-1**. No currents were observed in control water-injected oocytes. Figure 4-2A is the same hCNT3-WT experiment that is presented in Chapter 3.

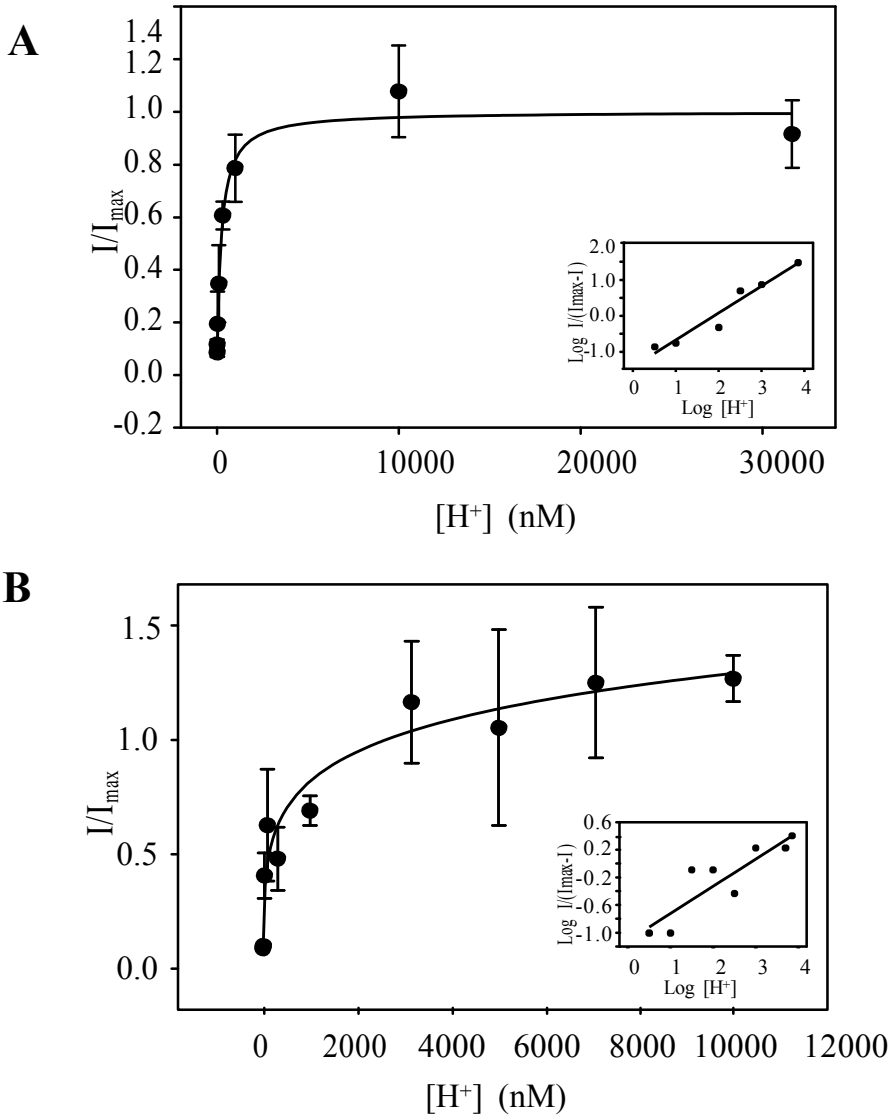

Figure 4-3: H^+-activation of hCNT3-WT and hCNT3-N336S. A. H^+-activation curve of hCNT3-WT producing oocytes measured in transport medium containing 100 mM ChCl (pH 8.5 - 5.0) at a uridine concentration of 100 µM (V_h= -50 mV). Currents were normalized to the fitted I_{max} for each oocyte and are presented as the average from 7 oocytes. The K_{50} was 480 ± 105 nM. The inset in **A** is a Hill plot of a representative oocyte with a Hill coefficient of 0.4 ± 0.1. **B.** H^+-activation curve in hCNT3-N336S producing oocytes (n=7) under the same conditions as hCNT3-WT. The K_{50} was 1200 ± 100 nM. The inset in **B** is a Hill plot of a representative oocyte with a Hill coefficient of 0.4 ± 0.1. Kinetic parameters are presented in **Table 4-1**. No currents were observed in control water-injected oocytes. Figure 4-3A is the same hCNT3-WT experiment presented in Chapter 3.

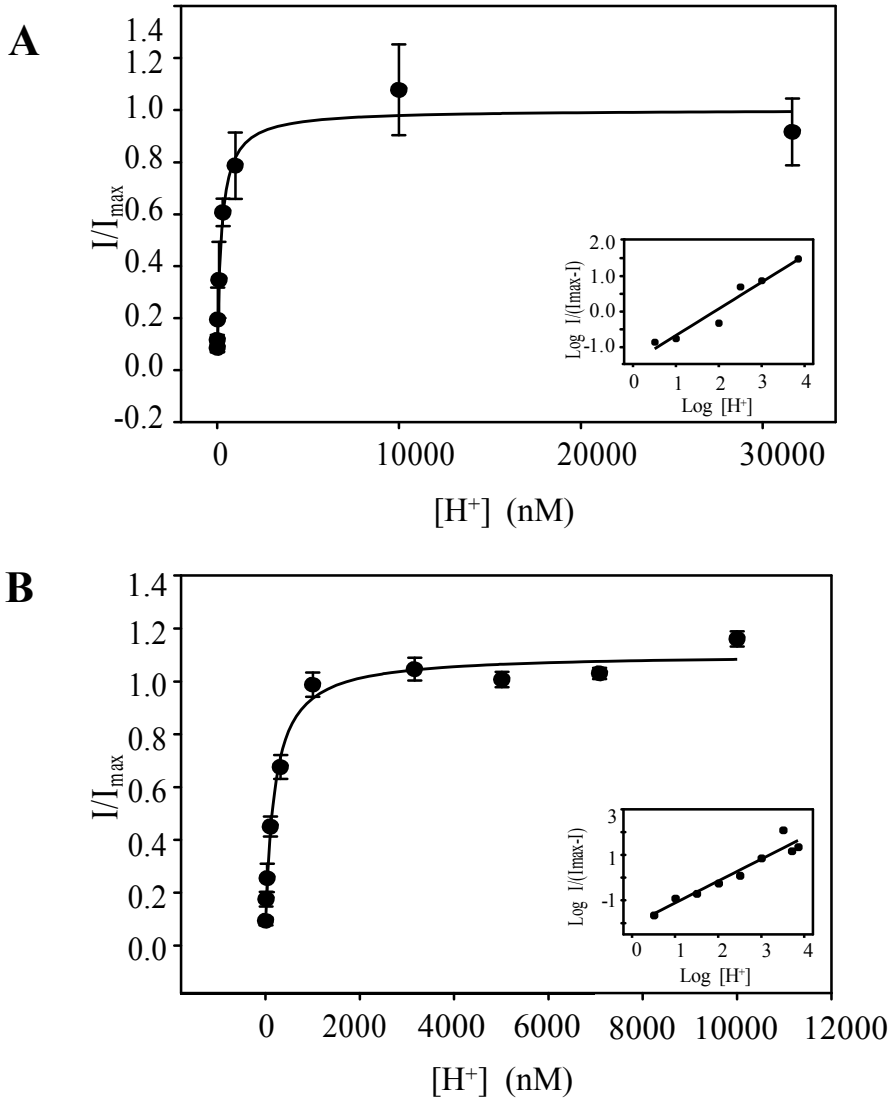

Figure 4-4: H^+-activation of hCNT3-WT and hCNT3-T370G. A. H^+-activation curve ofhCNT3-WT producing oocytes measured in transport medium containing 100 mM ChCl (pH 8.5 - 5.0) at a uridine concentration of 100 µM (V_h= -50 mV). Currents were normalized to the fitted I_{max} for each oocyte and are presented as the average from 7 oocytes. The K_{50} was 480 ± 105 nM. The inset in **A** is a Hill plot of a representative oocyte with a Hill coefficient of 0.4 ± 0.1. **B.** H^+-activation curve in hCNT3-T370G producing oocytes (n=7) under the same conditions as hCNT3-WT. The K_{50} was 200 ± 31 nM. The inset in **B** is a Hill plot of a representative oocyte with a Hill coefficient of 0.7 ± 0.1. Kinetic parameters are presented in **Table 4-1**. No currentswere observed in control water-injected oocytes. Figure 4-4A is the same hCNT3-WTexperiment presented in Chapter 3 and in Figure4-3A.

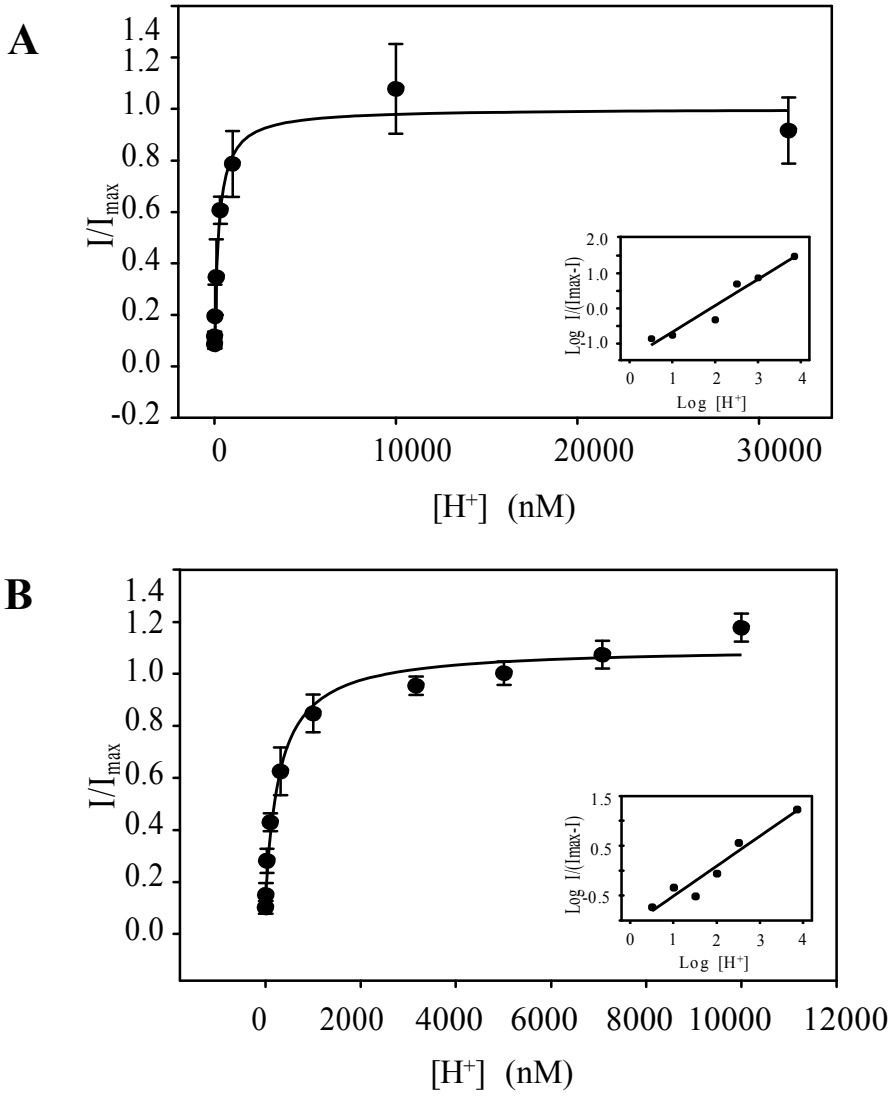

Figure 4-5: H^+-activation of hCNT3-WT and hCNT3-T370S. A. H^+-activation curve ofhCNT3-WT producing oocytes measured in transport medium containing 100 mM ChCl (pH 8.5 - 5.0) at a uridine concentration of 100 µM (V_h= -50 mV). Currents were normalized to the fitted I_{max} for each oocyte and are presented as the average from 7 oocytes. The K_{50} was 480 ± 105 nM. The inset in **A** is a Hill plot of a representative oocyte with a Hill coefficient of 0.4 ± 0.1. **B.** H^+-activation curve in hCNT3-T370S producing oocytes (n=7) under the same conditions as hCNT3-WT. The K_{50} was 298 ± 69 nM. The inset in **B** is a Hill plot of a representative oocyte with a Hill coefficient of 0.9 ± 0.1. Kinetic parameters are presented in **Table 4-1**. No currents were observed in control water-injected oocytes. Fig. 4-5A is the same hCNT3-WT experiment presented in Chapter 3 and in Figures 4-3A and 4-4A.

		hCNT3	N336T	N336S	N336A	T370G	T370S
Na^+	K_{50} (mM)	1.7 ± 0.2	n/d*	n/d*	n/d*	13.5 ± 1.3	n/d*
	n_H	1.6 ± 0.1	n/d*	n/d*	n/d*	2.1 ± 0.1	n/d*
	I_{max} (nA)	100	4	5	4	8	4
H^+	K_{50} (nM)	480 ± 105	n/d*	1200 ± 100	n/d*	200 ± 31	298 ± 69
	n_H	0.4 ± 0.1	n/d*	0.4 ± 0.1	n/d*	0.7 ± 0.1	0.9 ± 0.1
	I_{max} (nA)	150	5	10	5	100	80

Table 4-1: Na^+- and H^+-activation kinetics of hCNT3-WT and mutants. Half-saturation constants (K_{50}) and Hill coefficients (n) for Na^+ were determined from Na^+ concentration response curves (0 - 100 mM NaCl; pH 8.5) measured at a uridine concentration of 20 μM. Half-saturation constants (K_{50}) and Hill coefficients (n) for H^+ were determined from H^+ concentration response curves (pH 8.5 - 5.0) measured in Na^+-free transport medium (100 mM ChCl) at a uridine concentration of 100 μM. K_{50} values for both Na^+ and H^+ were obtained from fits to data from individual oocytes normalized to the fitted I_{max} value obtained for that cell and are presented as means ± S.E.M. The Hill coeffic ients (n) and I_{max} values for both Na^+ and H^+ are from a single representative oocyte. The membrane potential was -50 mV.

*n/d currents were too low to be characterized. Data for hCNT3-WT are the same as presented in Chapter 3.

Chapter 5:

Site-Directed Mutagenesis and Electrophysiological Characterization of Amino Acid Residues (N315 and T349) Involved in the Na^+-Binding Site of Human Concentrative Nucleoside Transporter 1 (hCNT1) Produced in *Xenopus laevis* Oocytes

Introduction

To further investigate the possibility of a universal cation-binding site shared between CNT family members, examination of residues in another key human CNT family member was undertaken. Human CNT1 (hCNT1) is a Na^+-dependent nucleoside transporter with a 1:1 Na^+:nucleoside coupling ratio (Smith *et al.,* 2004, 2007). Unlike hCNT3, hCNT1 is unable to utilize H^+ electrochemical gradients to drive nucleoside influx and is exclusively Na^+-coupled (Smith *et al.*, 2004, 2005, 2007).

Mutagenesis studies examining hCNT3 residues N336, V339, T370, and I371 (Chapters 3 and 4) found marked changes in Na^+- and H^+-binding characteristics, suggesting that these residues coordinate binding of not only Na^+ ions, but H^+ ions as well, the latter in the form of hydronium ions (S.A. Baldwin, personal communication). In the present Chapter, parallel studies were performed on hCNT1 to further examine the role of these residues in cation-binding. hCNT1 has only a single Na^+-specific cation-binding site (1:1 Na^+:nucleoside coupling ratio), so severe impairment of function would be anticipated as a result of mutation of residues contributing to that Na^+-binding site, providing additional evidence that this is the cation-binding site common to CNT family members.

Selection of the appropriate hCNT1 mutants to generate was based upon structural considerations as well as sequence alignments performed to determine the residues commonly located at the corresponding positions in various CNT family members (S.A. Baldwin, personal communication). Similar to the studies conducted with hCNT3-N336 (Chapter 4), hCNT1 residue N315 was mutated to serine, threonine or alanine. As stated previously, a serine or threonine at the residue position corresponding to N149 in vcCNT may be important for H^+-driven transport, and might possibly convert hCNT1 from a Na^+-driven transporter to an H^+-driven transporter. hCNT1-N315A was also generated to examine the importance of the asparagine residue itself in Na^+/H^+ coupling. hCNT1-T349 was mutated to cysteine and glycine, as preliminary studies on the corresponding mutations of hCNT3-T370 (hCNT3-T370C and hCNT3-T370G) showed reduced Na^+-binding affinity but enhanced H^+-binding affinity (Chapters 3 and 4). Mutation of hCNT3-T370 to serine caused a loss of Na^+-binding and an increase in the H^+-binding affinity (Chapter 4).

Using the two-microelectrode voltage clamp technique and radiotracer flux analysis, in combination with heterologous expression in *Xenopus* oocytes, the cation-binding characteristics of hCNT1-WT and six hCNT1 mutants (hCNT1-N315S, hCNT1-N315T, hCNT1-N315A, hCNT1-T349C, hCNT1-T349G, and hCNT1-T349S) were examined (Figure 5-1). It is predicted that these mutations will lead to changes in hCNT1 cation-binding affinity and, perhaps, alsocation-selectivity, thus revealing the key hCNT1 residues responsible for cation-dependentnucleoside transport activity, as well as shedding light on the cation-binding site common to allCNT family members

Results

Cation Specificity and Expression Levels of hCNT1-WT and Mutants

Cation-dependence of hCNT1-WT and mutants - Using site-directed mutagenesis, the asparagine residue at position 315 of hCNT1 was mutated to serine, threonine, or alanine and maximumcurrents were recorded in response to the addition of 100 μM uridine in 100 mM NaCl pH 8.5medium, 100 mM ChCl pH 8.5 medium or 100 mM ChCl pH 5.5 medium at a holding potential of -50 mV (Figure 5-2A; n= 4 - 6) to assess the mutants' functionality and cation-selectivity incomparison to hCNT1 wild-type (hCNT1-WT). While hCNT1-WT oocytes produced an average maximum current of 29 nA in 100 mM NaCl medium (pH 8.5), hCNT1-N315A and hCNT1-N315T demonstrated dramatic decreases in maximum currents to 6 and 5 nA, respectively.hCNT1-N315S, in contrast, exhibited functional activity similar to that of hCNT1-WT, withmaximum currents of 42 nA in 100 mM NaCl medium (pH 8.5). Similar to hCNT1-WT-producing oocytes, none of the hCNT1-N315 mutants showed observable currents in 100 mMChCl medium at pH 8.5 or pH 5.5.

The second residue of interest, threonine at position 349 of hCNT1, was mutated to cysteine, glycine, or serine. To compare functionality to hCNT1-WT, maximum currents were similarly recorded in response to the addition of 100 μM uridine at a holding potential of -50 mV in 100 mM NaCl pH 8.5 medium, 100 mM ChCl pH 8.5 medium or 100 mM ChCl pH 5.5 medium (Figure 5-2B; n= 4 - 6). hCNT1-T349S showed a slight decrease in current compared to that of hCNT1-WT (29 nA), with a mean maximum current of 21 nA. hCNT1-T349C and hCNT1-T349G, in contrast, did not generate detectable inward currents. Similar to hCNT1-WT, none of the hCNT1-N349 mutants generated detectable currents in 100 mM ChCl medium at pH 8.5 or pH 5.5.

Radioisotope flux analysis of hCNT1-WT and mutants - To confirm the lack of detectable functional activity of hCNT1-T349G and hCNT1-T349C, 1-min and 1-hr radiotracer flux assays were performed using ^{3}H-uridine in oocytes producing hCNT1-T349G, hCNT1-T349C, or hCNT1-T349S (Figure 5-3). Uptake of 10 μM uridine was measured in 100 mM NaCl transport medium at a pH of 8.5. Under initial rate conditions (1-min fluxes), oocytes producing hCNT1-

WT, hCNT1-T349G, hCNT1-T349C, or hCNT1-T349S all showed significant uptake of uridine (Figure 5-3). hCNT1-T349S exhibited a uridine flux similar to that of hCNT1-WT (5.9 ± 1.0 pmol/oocyte and 3.9 ± 0.5 pmol/oocyte for hCNT1-WT and hCNT1-T349S, respectively), while hCNT1-T349G and hCNT1-T349C showed significantly reduced uridine uptake compared to that of hCNT1-WT (1.3 ± 0.7 pmol/oocyte and 0.8 ± 0.2 pmol/oocyte for hCNT1-T349G and hCNT1-T349C, respectively). Uptake in control water-injected oocytes was 0.1 ± 0.1 pmol/oocyte. A longer flux interval of 1-hr was also measured to confirm and extend the 1-min transport data and confirm the different activity levels between the various hCNT1 constructs (Figure 5-3B). Following a 1-hr incubation, hCNT1-WT showed uridine uptake of 61.1 ± 10.5 pmol/oocyte, hCNT1-T349S showed a similar uridine flux (48.9 ± 9.8 pmol/oocyte), and both hCNT1-T349C and hCNT1-T349G showed lower but detectable fluxes (9.4 ±1.2 and 22.0 ± 3.4 pmol/oocyte, respectively). The control flux in water-injected oocytes was 1.4 ± 0.4 pmol/oocyte after 1-hr.

Na^+-Activation Kinetics of hCNT1-WT and Mutants

Na^+-activation kinetics of hCNT1-WT - Measurements of current as a function of increasing external Na^+ concentration (0 - 100 mM; pH 8.5) were made at a uridine concentration of 100 μM and a holding potential of -50 mV (Figure 5-4A). A hyperbolic relationship was revealed with a corresponding Hill coefficient for hCNT1-WT of 1.1 ± 0.2. This indicates that the apparent Na^+:uridine stoichiometry is 1:1, in agreement with previously published findings (Smith *et al*., 2004, 2007). The K_{50} value for Na^+ was 6.0 ± 0.2 mM, also in agreement with previous studies (Smith *et al.,* 2004). Kinetic parameters are presented in Table 5-1.

Na^+-activation kinetics of hCNT1-N315A and hCNT1-N315S - Measurements of current as a function of increasing external Na^+ concentration (0 - 100 mM; pH 8.5) were made at a uridine concentration of 100 μM and a holding potential of -50 mV for hCNT1-N315A and hCNT1-N315S (Figure 5-4C and D, respectively). hCNT1-N315A exhibited non-saturable Na^+ dependence, with a K_{50} value above the physiological range (> 100 mM) and a Hill coefficient that could not be determined (Figure 5-4C). hCNT1-N315S, while producing Na^+ currents of similar magnitude as those of hCNT1-WT, also exhibited non-saturable kinetics and a K_{50} value

that could not be determined (Figure 5-4D). These results suggested that these mutants have a very low Na^+-binding affinity.

Na^+-activation kinetics of hCNT1-N315T - hCNT1-N315T-generated currents as a function of increasing external Na^+ concentration (0 - 100 mM; pH 8.5) were measured at a uridine concentration of 100 µM and a holding potential of -50 mV. Currents were too low (< 5 nA) to determine Na^+-activation kinetics (data not shown).

Na^+-activation kinetics of hCNT1-T349S - Measurements of current as a function of increasing external Na^+ concentration (0 - 100 mM; pH 8.5) were made at a uridine concentration of 100 µM and a holding potential of -50 mV (Figure 5-4B). A hyperbolic relationship was revealed with a corresponding Hill coefficient for hCNT1-T349S of 1.0 ± 0.1. This indicates that the apparent Na^+:uridine stoichiometry is 1:1, similar to that of hCNT1-WT. The K_{50} value for Na^+ was 46.5 ± 14.7 mM, suggesting a marked decrease in the affinity of the mutant for Na^+ compared to hCNT1-WT. Kinetic parameters are presented in comparison with those of hCNT1-WT and other hCNT1 mutants in Table 5-1.

Na^+-activation kinetics of hCNT1-T349C and hCNT1-T349G - Neither hCNT1-T349C or hCNT1-T349G showed detectable current with a saturating concentration of uridine (100 µM) in 100 mM NaCl medium (pH 8.5). Na^+-activation curves could therefore not be generated.

Discussion

The recently solved crystal structure of the bacterial homologue vcCNT by Johnson *et al*. (2012) allowed us to mutate corresponding residues comprising the putative Na^+-binding site of hCNT1. For hCNT1 residues N315 and T349, three mutations were made in accordance with homologous residues in other CNT family members or with the goal of altering or eliminating functional activity by modifying the size and/or polarity of the residues. Using site-directed mutagenesis, hCNT1 mutants hCNT1-N315A, hCNT1-N315S, hCNT1-N315T, hCNT1-T349C, hCNT1-T349G, and hCNT1-T349S were constructed and produced in *Xenopus* oocytes to test for functional activity.

Mutation of hCNT1-N315 to alanine or threonine elicited very low Na^+ currents at the limit of detection, indicating reduced trafficking of the mutated proteins to the plasma membrane and/or reduced catalytic activity due to altered Na^+-binding. hCNT1-N315A, but not hCNT1-N315T, exhibited sufficient functional activity to permit analysis of Na^+-activation kinetics, the very high K_{50} value (> 100 mM) indicating that Na^+-binding activity was indeed impaired. hCNT1-N315S, in contrast, exhibited a maximum current greater than that of hCNT1-WT, but also had a very high K_{50} value (> 100 mM), again indicating that Na^+-binding was severely impaired. hCNT1-N315S and hCNT1-N315T, but not hCNT1-N315A, retained the potential to form hydrogen bonds with Na^+, but with different geometries compared to asparagine, the residue normally found at this position in hCNT1-WT.

For the second residue position studied, hCNT1-T349, mutation to cysteine or glycine elicited very low Na^+ currents at the limit of detection, again indicating reduced trafficking of the mutated proteins to the plasma membrane and/or reduced catalytic activity due to altered Na^+-binding. Mutation to serine, in contrast, resulted in currents similar to those of hCNT1-WT, but with an ~ 8-fold increase in K_{50} value for Na^+, consistent with involvement of this residue position in the hCNT1 Na^+-binding site. The more dramatic loss of current in mutants hCNT1-T349C and hCNT1-T349G compared to hCNT1-T349S can be attributed to the similarity of the amino acid functional groups of serine and threonine. While the electrophysiological studies suggest that hCNT1-T349C and hCNT1-T349G were non-functional, ^{3}H-uridine radioisotope flux analysis, a more sensitive technique, found both hCNT1-T349C and hCNT1-T349G to have low but detectable transport activity.

Of the three hCNT1 mutants with sufficient current to perform kinetic analysis, hCNT1-N315A, hCNT1-N315S, and hCNT1-T349S all showed marked decreases in Na^+-binding affinity, indicating loss of function of the Na^+-binding site. This decrease in Na^+-binding affinity supports the hypothesis that both of these residues are part of the Na^+-binding site of hCNT1. This is supported by evidence from mutation of the corresponding hCNT3 residues N336 and T370 (Chapters 3 and 4).

Unlike hCNT1, hCNT3 is coupled to both H^+ and Na^+ ions. Mutations of residues in hCNT3 corresponding to those involved in Na^+-binding in vcCNT not only produced changes in Na^+-binding affinity and Na^+:nucleoside coupling ratio, but changes in H^+-binding affinity as well (Chapters 3 and 4). These results therefore suggest that this binding site in hCNT3 not only binds Na^+ but H^+ as well. Residues in hCNT1 (N315 and N349) corresponding to hCNT3 residues N336 and T370, respectively, were mutated to serine and threonine, amino acids commonly found at this position in CNT family members which are H^+-coupled. It was hypothesized that this might convert hCNT1 from a Na^+-coupled transporter into a H^+-coupled transporter. None of these mutants, however, produced current in Na^+-depleted, H^+-enriched medium. These results, while failing to generate detectable H^+ currents, suggest that mutation of multiple residues may be required to confer H^+ coupling to hCNT1, particularly if H^+ binds inthe form of a hydronium ion.

In summary, the data presented in this and previous Chapters indicates that four residues in hCNT3 (N336, V339, T370, and I371) and two corresponding residues in hCNT1 (N315 and T349) belong to a conserved primary cation-binding site that is shared throughout the CNT protein family. Furthermore, the data suggest that this site, which is found between HP1 and the discontinuous region of TM7, not only coordinates with Na^+ but is also capable of coordinating H^+ in the form of a hydronium ion. The close proximity of this cation-binding site to the nucleoside binding site, as predicted by the vcCNT crystal structure, provides a potential structural basis for cation:permeant coupling in CNTs that will require crystal structures for additional conformational states within the transport cycle to fully resolve.

References

Baldwin, S.A. Personal communication.

Feng, Z., Hou, T., and Li, Y. 2013. Transport of nucleosides in the vcCNT facilitated by sodium gradients from molecular dynamics simulations. *Mol. Biosyst.* 9:2142-2153.

Johnson, Z.L., Cheong, C., and Lee, S. 2012. Crystal structure of a concentrative nucleoside transporter from *Vibrio cholera* at 2.4 Å. *Nature*.483:489-493.

Mulinta, R., Slugoski, M.D., Ng, A.M.L., Yao, S.Y.M., Cass, C.E., Baldwin, S.A., and Young, J.D. Substituted cysteine accessibility method (SCAM) analysis of transport domain of human concentrative nucleoside transporter 3 (hCNT3) reveals features of structural and functional importance. *Unpublishedobservations*.

Smith, K.M., Ng, A.M., Yao, S.Y., Labedz, K.A., Knaus, E.E., Wiebe, L.I., Cass, C.E., Baldwin, S.A., Chen, X.Z., Karpinski, E., and Young, J.D. 2004. Electrophysiological characterization of a recombinant human Na^+-coupled nucleoside transporter (hCNT1) produced in *Xenopus* oocytes. *J. Physiol.* 558:807-823.

Smith, K.M., Slugoski, M.D., Loewen, S.K., Ng, A.M.L., Yao, S.Y.M., Chen, X., Karpinski, E., Cass, C.E., Baldwin, S.A., Young, J.D. 2005. The broadly selective human Na^+/nucleoside cotransporter (hCNT3) exhibits novel cation-coupled nucleoside transport characteristics. *J. Biol. Chem*. 280:25436-25449.

Smith, K.M., Slugoski, M.D., Cass, C.E., Baldwin, S.A., Karpinski,E., and Young, J.D. 2007. Cation coupling properties of human concentrative nucleoside transporters hCNT1, hCNT2 and hCNT3. *Mol. Membr. Biol*. 24:53-64.

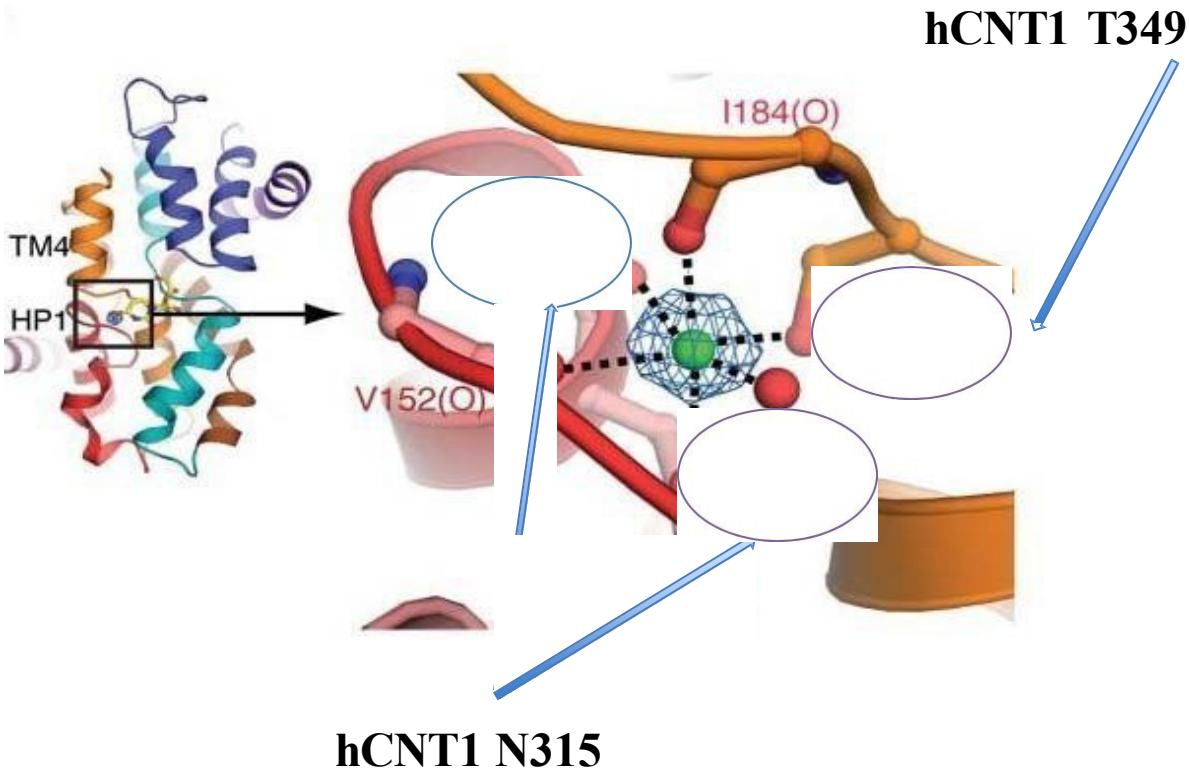

Figure 5-1: Modelled structure of the Na^+-binding site in vcCNT. The Na^+-binding site, located between HP1 and the unwound region of TM4 in vcCNT, is coordinated in an ideal octahedral coordination site with N149, V152, S183, and I184 and a water molecule (shown in *red*). Coordination of the Na^+ ion is shown as dashed lines. The hCNT1 residues N315 and T349 corresponding to vcCNT residues N149 and S183, respectively, are indicated.

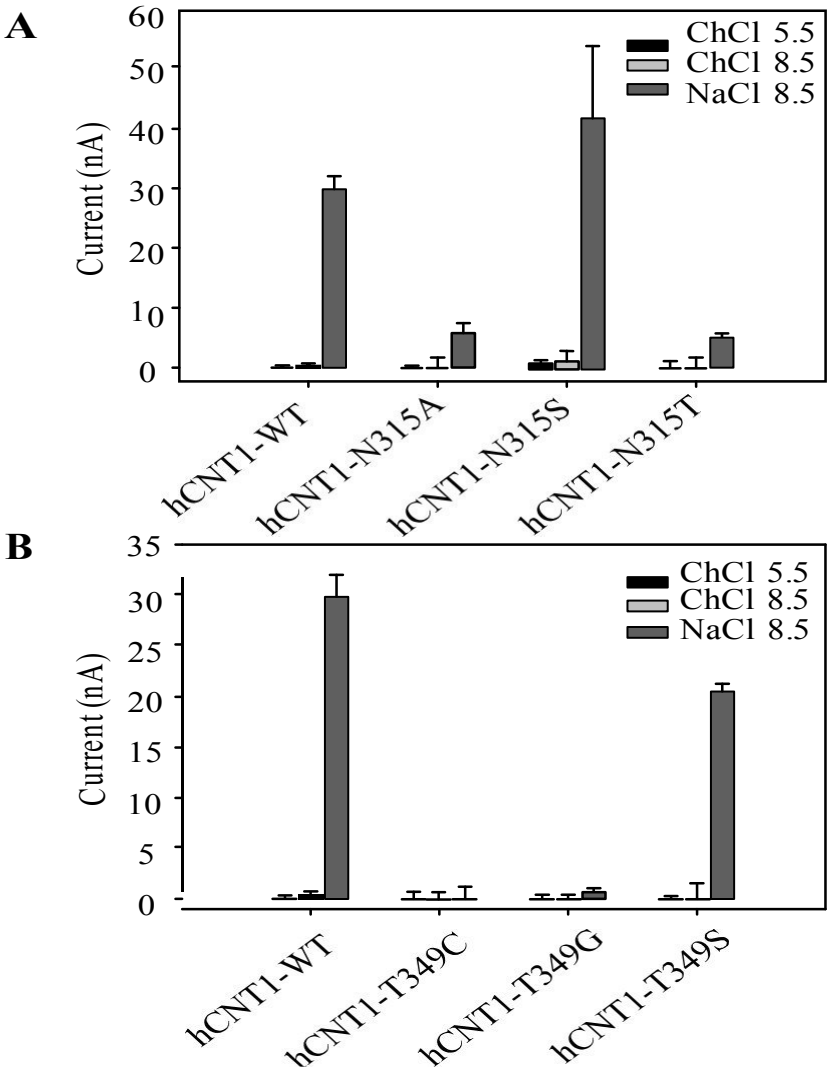

Figure 5-2: Maximum currents generated by hCNT1-WT and mutants. *Xenopus* oocytes were exposed to 100 μMuridine in either 100 mM NaCl pH 8.5 medium, 100 mM ChCl pH 8.5 medium or 100 mM ChCl pH 5.5 medium. **A.** Maximum currents of hCNT1-N315 mutants in comparison to those of hCNT1-WT. Currents were only present in Na^+-containing medium and were 29 ± 2 nA for hCNT1-WT and 42 ± 12, 6 ± 2, and 5 ± 1 nA for hCNT1-N315S, hCNT1-N315A and hCNT1-N315T, respectively. **B.** Maximum currents of hCNT1-T349 mutants in comparison to those of hCNT1-WT (the data in **A** and **B** are the same). Currents were only present in Na^+-containing medium. hCNT1-T349S was the only T349 mutant with observable current at 21 ± 1 nA, while both hCNT1-T349C and hCNT1-T349G showed no detectable inward current. Values are means ± SEM of 4 - 6 individual oocytes. No currents were observed in control water-injected oocytes.

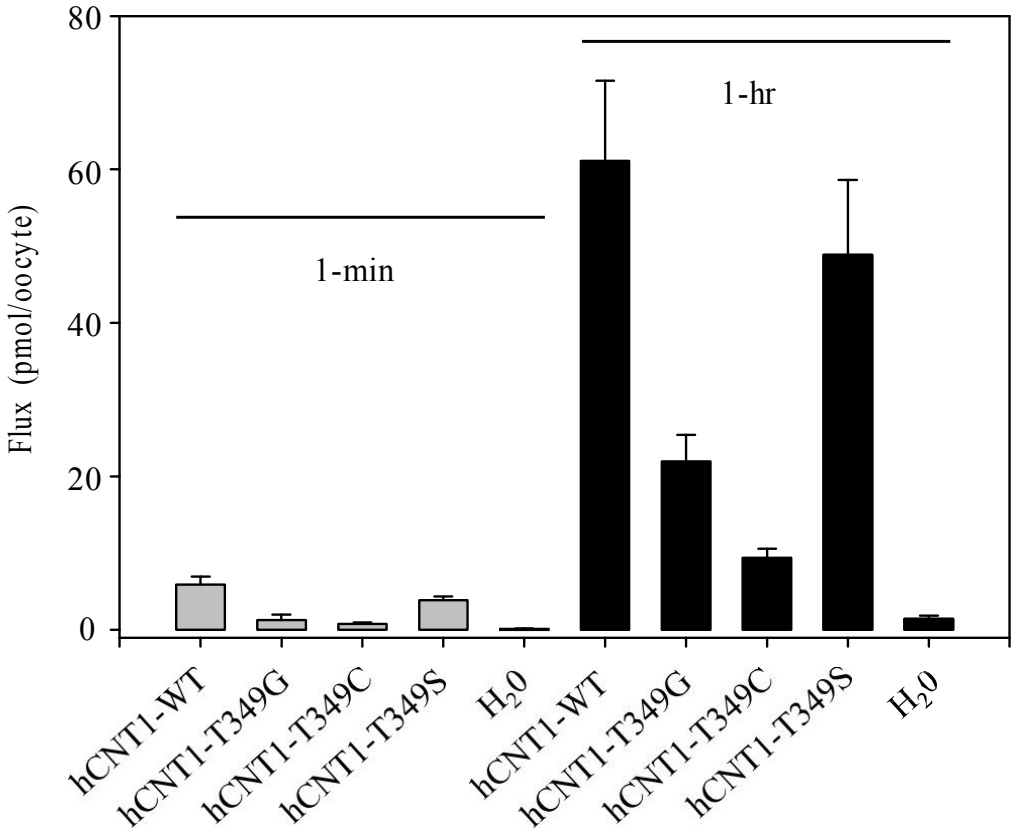

Figure 5-3: hCNT1-T349 mutants 1-min and 1-hr ^{3}H-uridine radioisotope fluxes. The 1-min flux values (*grey* fill) show minimal but statistically significant uridine influx for hCNT1-T349C (0.8 ± 0.2 pmol/oocyte) and hCNT1-T349G (1.3 ± 0.7 pmol/oocyte) in comparison to control water-injected oocytes (0.1 ± 0.1 pmol/oocyte). The flux for hCNT1-T349S (3.9 ± 0.5 pmol/oocyte) was not significantly different from hCNT1-WT (5.9 ± 1.0 pmol/oocyte). Uridinefluxes were also not significantly different between hCNT1-WT and hCNT1-T349S after 1-hr incubation (61.1 ± 10.5 pmol/oocyte and 48.9 ± 9.8 pmol/oocyte, respectively; *black*fill).

Uptake in control water-injected oocytes was 1.4 ± 0.4 pmol/oocyte. After 1-hr, uridine uptake by hCNT1-T349G and hCNT1-T349C was greater than water-injected oocytes, with fluxes of 22.0 ± 3.4 pmol/oocyte and 9.4 ± 1.2 pmol/oocyte, respectively. Values are means ± SEM of 10 - 12 individual oocytes.

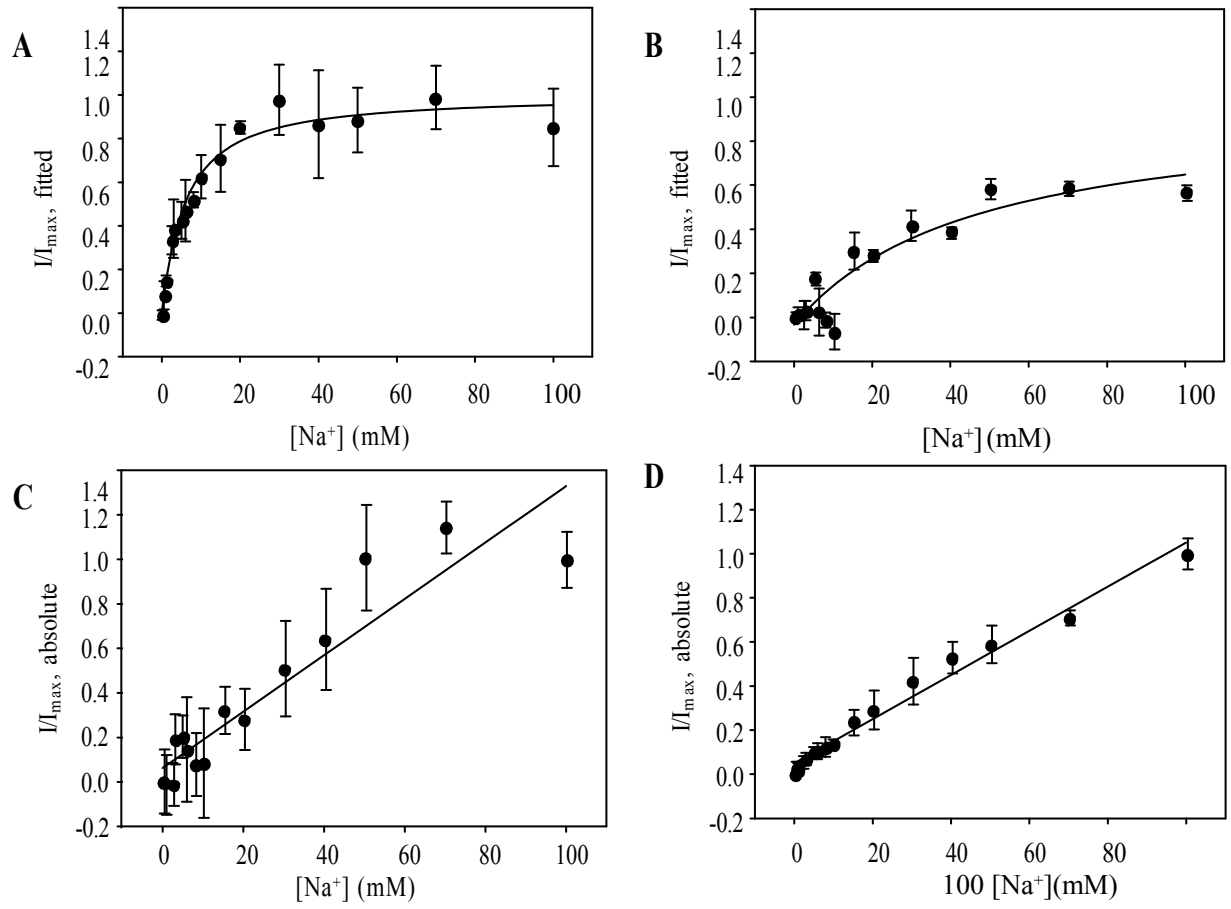

Figure 5-4: Na^+-activation of hCNT1-WT and mutants. A. Na^+-activation curve of hCNT1-WT-producing oocytes measured in transport medium containing 0 - 100 mM NaCl (pH 8.5) at a uridine concentration of 100 μM (V_h= -50 mV). The K_{50} was 6.0 ± 1.1 mM and the Hill coefficient was 1.1 ± 0.2. **B**. Na^+-activation curve of hCNT1-T349S-producing oocytes under the same conditions as hCNT1-WT. The K_{50} was 46.5 ± 14.7 mM and the Hill coefficient was 1.0 ± 0.1. **C** and **D** show the corresponding curves of hCNT1-N315A and hCNT1-N315S, respectively, under the same conditions as hCNT1-WT. Curves for hCNT1-N315A and hCNT1-N315S were non-saturable. Curves for hCNT1-WT and hCNT1-T349S were normalized to the fitted I_{max} for each oocte and presented as the means of 4 - 6 individual oocytes. Curves for hCNT1-N315A and hCNT1-N315S were normalized to the maximum current generated with 100 μMurdine in 100 mM NaCl (pH 8.5) medium and presented as the means of 4 - 6 individual oocytes. Kinetic parameters are presented in **Table 5-I**. No currents were observed in control water-injected oocytes.

		hCNT1	N315A	N315S	N315T	T349S	T349C	T349G
Na^+	K_{50} (mM)	6.0 ± 1.1	> 100	> 100	n/d*	46.5 ± 14.7	n/d*	n/d*
	n_H	1.1 ± 0.2	n/d*	n/d*	n/d*	1.0 ± 0.1	n/d*	n/d*
	I_{max} (nA)	29 ± 2	6 ± 2	42 ± 12	5 ± 1	21 ± 1	n/d*	n/d*

Table 5-1: Na^+-activation kinetics of hCNT1-WT and mutants. Half-saturation constants (K_{50}) and Hill coefficients (n) for Na^+ were determined from Na^+ concentration response curves (0 - 100 mM NaCl; pH 8.5) measured at a uridine concentration of 100 μM. hCNT1-WT and hCNT1-T349S K_{50} values and Hill coefficients (n) for Na^+ were obtained from fits to data from individual oocytes normalized to the fitted I_{max} value obtained for that cell and are presented as means ± S.E.M (n = 4 - 6 oocytes). The I_{max} values are mean currents generated with a saturating concentration of uridine (100 μM) and are presented as means ± SEM (n = 4 - 6 oocytes). The membrane potential was -50 mV.

*n/d currents were too low to be characterized.

Chapter 6:

General Discussion

Overview

In mammalian cells, two major structurally unrelated protein families mediate nucleoside transport processes: the equilibrative nucleoside transporter family (ENTs) and the concentrative nucleoside transporter family (CNTs). Four human ENT members (hENT1-4) and three human CNT members (hCNT1-3) have been cloned and functionally characterized (Young *et al*., 2013). CNTs mediate the active transport of nucleosides across cellular membranes, using the electrochemical gradient of the coupling cation. These transporters differ from each other in their nucleoside and cation selectivities, and their cation stoichiometries (Young *et al*., 2013). hCNT1/2 are strictly Na^+-coupled, whereas hCNT3 utilizes Na^+, H^+, and Li^+ electrochemical gradients to transport nucleosides across cellular membranes (Smith *et al.,* 2004, 2005, 2007). The cation:nucleoside coupling stoichiometry of hCNT3 is 2:1 in the presence of Na^+ and both Na^+ and H^+, but only 1:1 in the presence of H^+ alone, suggesting that hCNT3 possesses two Na^+-binding sites, only one of which is shared by H^+; the corresponding Na^+:nucleoside coupling stoichiometry of hCNT1/2 is 1:1 (Smith *et al*., 2004, 2005, 2007). CNTs are predominantly found in specialized cells such as intestine, kidney, and liver epithelia, where they play important roles in the secretion, distribution, and elimination of nucleosides and nucleoside drugs (Young *et al.,* 2013). The functional diversity that members of the CNT family exhibit provides unique opportunities to elucidate the structural and molecular mechanisms underlying cation-nucleoside membrane co-transport.

In the absence of a crystal structure, valuable information regarding a membrane protein's architecture can be obtained from mutagenesis studies and SCAM analysis using thiol reactive reagents such a *p*-chloromercuribenzne sulfonate (PCMBS). Previous studies generated a hCNT1/3 chimera, which implicated the C-terminal half of the protein as the functional domain responsible for cation coupling (Smith *et al*., 2005). Subsequent SCAM studies of hCNT3 led to the identification of novel discontinuous regions and key amino acid residues of functional significance, and the prediction of a 15 TM model (Slugoski *et al*., 2009; Mulinta *etal*., unpublished observations). The crystallization of vcCNT (Johnson *et al.,* 2012), however, led to new revelations regarding the CNT architecture and, as described in this thesis, a revised 11 TM homology model for hCNTs. The crystal structure revealed that four amino acid residues, V152, S183, N149, and I184, octahedrally coordinate the single Na^+-binding site in vcCNT (Johnson *et*

al., 2012). Multiple sequence alignments between members of the CNT family and 3D homology modelling based upon the crystal structure of vcCNT (Johnson *et al*., 2012) led to the identification of the corresponding residues of potential importance in coordination of human CNT cation-binding sites. In hCNT3, residues N336, V339, T370, and I371 were predicted to belong to a conserved primary cation-binding site shared throughout the CNT protein family that potentially binds both Na^+ ions and H^+ ions. Site-directed mutagenesis was used to generate hCNT3 mutants with the goal of altering cation-binding characteristics, including cation-(Na^+ and/or H^+) binding affinity, cation specificity, and cation:nucleoside coupling ratio, and thus test and elucidate the role of these residues in cation coordination. Parallel studies were also performed on hCNT1 to examine the role of its corresponding amino acids in cation binding. The structure-function studies of recombinant wild-type hCNT3 and mutants produced in *Xenopus laevis* oocytes and presented in Chapters 3 and 4 describe my contributions to our current understanding of the CNT molecular mechanisms underlying cation coupling in the hCNTs.

hCNT3 residues N336, V339, T370, and I371 are predicted to belong to a conserved primary cation-binding site shared throughout the CNT protein family. These hCNT3 residues were first mutated to cysteine (Chapter 3). hCNT3 mutants hCNT3-N336C, hCNT3-V339C, hCNT3-T370C, and hCNT3-I371C all displayed altered cation-binding characteristics. Each of the four hCNT3 mutants exhibited reductions in maximum currents and varying decreases in Na^+-binding affinities as compared to wild-type hCNT3, with the largest decrease in Na^+-binding affinity observed with the hCNT3-N336 mutant. The Na^+:nucleoside coupling ratio of hCNT3-V339C and hCNT3-I371C changed from 2:1 to 1:1. Mutation of hCNT3 residues N336, V339, T370, and I371 to cysteine not only had effects on Na^+-binding but H^+-binding as well. The mutation of hCNT3-N336 to cysteine had a greater effect on H^+-driven transport than Na^+-driven transport; H^+-driven transport was almost completely eliminated. hCNT3-T370C and hCNT3-V339C resulted in enhanced H^+-binding affinity, while retaining a 1:1 H^+:nucleoside coupling ratio. Currents generated by hCNT3-I371C in Na^+-depleted H^+-enriched medium were significantly reduced compared to hCNT3-WT and did not saturate, preventing the accurate determination of H^+-binding kinetics. That Na^+ and H^+-binding characteristics were altered following mutation of each residue individually to cysteine provides strong evidence that the cation-binding site coordinated by hCNT3 residues N336, V339, T370, and I371, and

homologous to residues N149, V152, S183, and I184 in vcCNT, not only binds Na^+ ions, but H^+ ions as well.

hCNT3 residues N336 and T370 underwent additional amino acid substitutions to further explore the nature of their cation-binding interactions (Chapter 4). These mutations were selected based upon amino acid side chain structural considerations and sequence comparisons between different CNT family members (S.A. Baldwin, personal communication). The mutations to serine or threonine were hypothesized to potentially convert the protein from a Na^+/H^+-driven to an exclusively H^+-driven cotransporter. Mutation of hCNT3-N336 to serine, threonine, or alanine had dramatic effects on protein function. Currents were reduced and insufficient to accurately determine Na^+- and H^+- activation kinetic parameters for hCNT3-N336A and hCNT3-N336T. Although currents seen with hCNT3-N336S were also reduced, it was possible to determine kinetic parameters for H^+. hCNT3-N336S displayed a significant decrease in the affinity of hCNT3-N336S for H^+, while the coupling ratio for H^+:nucleoside transport remained unaltered at 1:1. Mutation of hCNT3-T370 to glycine or serine produced dramatic loss-of-function in Na^+ medium, with mutation of hCNT3-T370 to glycine also causing a significant decrease in the affinity of the mutant for Na^+. hCNT3-T370G did, however, retain a Na^+:nucleoside coupling ratio of 2:1. hCNT3-T370G and hCNT3-T370S produced H^+ currents of similar magnitude to that seen with hCNT3-WT, with the affinity of both mutants for H^+ increasing while maintaining a 1:1 H^+:nucleoside coupling ratio.

Together, the results seen following mutation of hCNT3 residues N336, V339, T370, and I371 support the hypothesis that these residues contribute to the primary cation-binding site found in all CNT family members, and that this site in hCNT3 binds both Na^+ and H^+ ions. Although mutation of hCNT3-T370 to serine and hCNT3-N336 to serine or threonine did not completely eliminate Na^+-coupled transport, these mutations resulted in altered Na^+- and H^+-coupled transport and, in particular, significantly altered H^+-binding affinity, confirming the role of these residues in coordinating the Na^+/H^+-binding site.

hCNT1 residues N315 and T349, corresponding to hCNT3 residues N336 and T370, respectively, were also selected for analysis (Chapter 5). Since hCNT1 has only a single Na^+-specific cation-binding site (1:1 Na^+:nucleoside coupling ratio) (Smith *et al*., 2004), mutation of residues contributing to the Na^+-binding site were predicted to cause severe impairment of function, thus providing further evidence that this is the cation-binding site common to all CNT family members. The amino

acids to which these residues were mutated were again selected based upon amino acid side chain structural considerations and sequence comparisons between different CNT family members (S.A. Baldwin, personal communication). Mutation of hCNT1-N315 to alanine or threonine generated proteins with very low functional activity, preventing the determination of Na^+-binding kinetics. Although hCNT1-N315T exhibited significant functional activity, the affinity of the mutant for Na^+ was reduced as compared to wild-type hCNT1. The low functional activity of mutants hCNT1-T349C and hCNT1-T349G also prevented the determination of Na^+-activation kinetics. Mutation to serine, in comparison, resulted in a significantly reduced affinity for Na^+. The results seen with hCNT1-N315 and hCNT1-T349 are consistent with involvement of these residues in coordination of the Na^+-binding site. It was hypothesized that mutation of hCNT1-N315 to serine or threonine might convert hCNT1 from a Na^+-specific to a H^+-specific cotransporter based on sequence comparisons between CNT family members. Similarly, mutation of hCNT1-T349 to serine was also predicted to potentially convert hCNT1 from Na^+- to H^+-preferring, since mutation of hCNT3-T370 to serine caused a loss of Na^+ binding and an increase in the H^+-binding affinity. The hCNT1 mutants did not mediate H^+-driven nucleoside transport, likely because mutation of multiple residues may be required to confer H^+ coupling to hCNT1, particularly if H^+ binds in the form of a hydronium ion (Davidson *et al.,* 2011).

Future Directions

The structure-function studies of CNT family members presented in this thesis have advanced the current understanding of the molecular basis of hCNT-mediated nucleoside transport. In addition to identifying key residues involved in coordination of the primary cation-binding site, these studies revealed novel insights into the binding characteristics of this site, including its ability to bind both Na^+ ions and H^+ ions. There still remains, however, many unexplored areas of research with respect to the cation-binding sites in the CNT family of nucleoside transport proteins.

In addition to hCNTs, extending mutagenesis studies to other CNT family members will be beneficial. Different CNT family members exhibit different cation coupling characteristics. For example, hfCNT exhibits a 2:1 Na^+:nucleoside coupling ratio, but unlike hCNT3, is strictly Na^+-dependent (Yao *et al*., 2002). CNT family members that are exclusively H^+-dependent

include *C. albicans* CaCNT (1:1 H^+:nucleoside coupling ratio) (Loewen *et al*., 2005) and *E. coli* NupC (1:1 H^+:nucleoside coupling ratio) (Loewen *et al*., 2004). Mutagenesis studies of these CNT family members may provide further insights into cation coordination by amino acid residues comprising the primary cation-binding site, specifically, differences in the Na^+-binding site between hfCNT and hCNT3 that allow hCNT3, but not hfCNT, to bind both Na^+ ions and H^+ ions, and how H^+ ion binding is coordinated in hCNT3.

As many of the hCNT1/3 mutants resulted in significant changes in Na^+ (hCNT1/3) and/or H^+ (hCNT3) transport activity, it is of importance to determine their relative cell-surface expression through biotinylation studies to exclude the possibility that the mutation impaired correct protein folding and trafficking to the plasma membrane. An indication that the majority of the mutants were correctly processed to the cell surface, and that their reduced functional activity derived from impaired cation-coupling, is that each of the mutants studied showed changes in Na^+- and/or H^+-activation kinetics.

Based upon the two-fold pseudo symmetry of the vcCNT crystal structure, the second cation-binding site in hCNT3 is predicted to be located at the tip of HP2 and in the non-helical section of TM 10 (Figure 3-1B) (S.A. Baldwin, personal communication; Johnson *et al*., 2012). SCAM studies of hCNT3 have identified residues in which mutation to cysteine (in the cysteine-less hCNT3 protein) result in significant changes in the Na^+:H^+ uridine uptake ratios (Slugoski *et al*., 2009; Mulinta, unpublished observations). The majority of these residues are located in HP1and TM7 (primary cation-binding site), and HP2 and TM10 (postulated secondary cation-binding site) (Slugoski *et al*., 2009; Mulinta, unpublished observations). Mutagenesis studies within HP2 and TM10 may provide insights into the geometry and function of the second Na^+-binding site in hCNT3, and explain why hCNT3, unlike hCNT1/2, has a 2:1 Na^+:nucleoside coupling ratio.

From a pharmacological perspective, an understanding of the CNT mechanism and structure-function relationships will provide a foundation for the development of novel permeants and inhibitors, which will be of great value in the development of new chemotherapeutic compounds. The information gained from CNT structure-function studies will further benefit studies of other cation-dependent transporter proteins.

References

Baldwin, S.A. Personal communication.

Davidson, V.L. 2011. Ion-protein coordination: The many faces of a proton. *Nat. Chem.* 3:662-663.

Johnson, Z.L., Cheong, C., and Lee, S. 2012. Crystal structure of a concentrative nucleoside transporter from *Vibrio cholera* at 2.4 Å. *Nature*. 483:489-493.

Loewen, S.K., Ng, A.M.L., Mohabir, N.N., Baldwin, S.A., Cass, C.E., and Young, J.D. 2005. Functional characterization of a H^+/nucleoside co-transporter (CaCNT) from *Candida albicans*, a fungal member of the concentrative nucleoside transporter (CNT) family of membrane proteins. *Yeast* 20:661-675.

Loewen, S.K., Yao, S.Y.M., Slugoski, M.D., Mohabir, N.N., Turner, R.J., Mackey, J.R., Weiner, J.H., Gallagher, M.P., Henderson, P.J.F., Baldwin, S.A., Cass, C.E., and Young, J.D. 2004. Transport of physiological nucleosides and anti-viral and anti-neoplastic nucleoside drugs by recombinant Escherichia coli nucleoside-H(+) cotransporter (NupC) produced in *Xenopus laevis* oocytes. *Mol. Membr. Biol.* 21:1-10.

Mulinta, R., Slugoski, M.D., Ng, A.M.L., Yao, S.Y.M., Cass, C.E., Baldwin, S.A., and Young, J.D. Substituted cysteine accessibility method (SCAM) analysis of transport domain of human concentrative nucleoside transporter 3 (hCNT3) reveals features of structural and functional importance. Unpublished observations.

Ritzel, M.W.L., Ng, A.M.L., Yao, S.Y.M., Graham, K., Loewen, S.K., Smith, K.M., Ritzel, R.G., Mowles, D.A., Carpenter, P., Chen, X.Z., Karpinski, E., Hyde, R.J., Baldwin, S.A., Cass, C.E., and Young, J.D. 2001. Molecular identification and characterization of novel human and mouse concentrative Na^+ nucleoside cotransporter proteins (hCNT3 and mCNT3) broadly selective for purine and pyrimidine nucleosides (system *cib*). *J. Biol. Chem*. 276:2914-2927.

Ritzel, M.W.L., Yao, S.Y.M., Huang, M.-Y., Elliott, J.F., Cass, C.E., and Young, J.D. 1997. Molecular cloning and functional expression of cDNAs encoding a human Na^+-nucleoside cotransporter (hCNT1). *Am. J. Physiol.*272:C707-C714.

Ritzel, M.W., Yao, S.Y., Ng, A.M., Mackey, J.R., Cass, C.E., and Young, J.D. 1998. Molecular cloning, functional expression and chromosomal localization of a cDNA encoding a human Na^+/nucleoside cotransporter (hCNT2) selective for purine nucleosides and uridine. *Mol.Membr. Biol.* 15:203-211.

Slugoski, M. D., Ng, A. M. L., Yao, S. Y. M., Lin, C. C., Mulinta, R., Cass, C. E., Baldwin, S. A., and Young, J. D. 2009. Substituted Cysteine Accessibility Method Analysis of Human Concentrative Nucleoside Transporter hCNT3 Reveals a Novel Discontinuous Region of Functional Importance within the CNT Family Motif (G/A)XKX$_3$NEFVA(Y/M/F). *J. Biol.Chem*. 284:17281-17292.

Smith, K.M., Ng, A.M., Yao, S.Y., Labedz, K.A., Knauss, E.E., Wiebe, L.I., Cass, C.E., Baldwin, S.A., Chen, X.Z., Karpinski, E., and Young, J.D. 2004. Electrophysiological characterization of a recombinant human Na^+-coupled nucleoside transporter (hCNT1) produced in *Xenopus* oocytes. *J. Physiol.* 558:807-823.

Smith, K.M., Slugoski, M.D., Cass, C.E., Baldwin, S.A., Karpinski, E., and Young, J.D. 2007. Cation coupling properties of human concentrative nucleoside transporters hCNT1, hCNT2 and hCNT3. *Mol. Membr. Biol.* 24:53-64.

Smith, K.M., Slugoski, M.D., Loewen, S.K., Ng, A.M.L., Yao, S.Y.M., Chen, X., Karpinski, E., Cass, C.E., Baldwin, S.A., and Young, J.D. 2005. The broadly selective human Na^+/nucleoside cotransporter (hCNT3) exhibits novel cation-coupled nucleoside transport characteristics. *J. Biol. Chem*. 280: 25436-25449.

Yao, S.Y., Ng, A.M., Loewen, S.K., Cass, C.E., Baldwin, S.A., and Young, J.D. 2002. An ancient prevertebrate Na^+-nucleoside cotransporter (hfCNT) from the Pacific hagfish (*Eptatretus stouti*). *Am. J. Physiol. Cell Physiol.* 283:C155-168.

Young, J.D., Yao, S.Y.M., Baldwin, J.M., Cass, C.E., and Baldwin, S.A. 2013. The human concentrative and equilibrative nucleoside transporter families, SLC28 and SLC29. *Mol. Aspects Med.* 34:529-547.

Appendix I:

Functional characterization of vcCNT from *Vibrio cholera*

Introduction

The crystal structure of the *Vibrio cholerae* CNT (vcCNT) in complex with uridine and Na^+ was resolved at 2.4 Å (Johnson *et al*., 2012). This discovery revealed unique characteristics regarding vcCNT architecture, providing a better understanding of the mechanism of Na^+/nucleoside cotransport in the CNT family (Johnson *et al*., 2012). Preliminary functional studies of vcCNT have been limited to demonstrating that the transporter uses a Na^+ electrochemical gradient to drive nucleoside transport (Johnson *et al*., 2012; Feng *et al*., 2013). The crystal structure predicts 1 Na^+ ion to be involved in nucleoside translocation; in contrast, a molecular dynamics simulation study by Feng *et al*. (2013) predicts that 2 Na^+ ions are necessary for vcCNT-mediated nucleoside transport. Thus, the present study aimed to functionally characterize vcCNT and, in so doing, examine its cation-dependence, permeant selectivity, and Na^+ and uridine transport kinetics.

The single Na^+-binding site predicted by the crystal structure of vcCNT, located between HP1 and the unwound region of TM4, is coordinated by amino acids residues N149, V152, S183, and I184 (Johnson *et al*., 2012) (Figure A-1). Previous studies of residues hCNT3-N336 and the corresponding residue in hCNT1 (hCNT1-N315) demonstrated that mutations of these amino acids cause alterations in Na^+- and/or H^+-binding characteristics (Chapters 3 - 5). Functional changes resulting from mutation of the corresponding residue in vcCNT (vcCNT-N149) were investigated here in attempts to further elucidate the molecular mechanism(s) of cation-dependent nucleoside transport.

Using radioisotope flux analysis of ^{3}H-nucleoside uptake, in combination with heterologous expression in *Xenopus* oocytes, the functional characteristics of wild-type vcCNT (vcCNT-WT) and three vcCNT mutants (vcCNT-N149A, vcCNT- N149S, and vcCNT-N149T) were examined. It was predicated that these mutations would lead to changes in vcCNT function, thus shedding light on the cation-binding site common to all CNT family members

Results

Time course and cation dependence of uridine uptake - The time course of uridine uptake was examined to establish the conditions required to determine the initial rate of uridine transport. Figure A-2 presents the time course of vcCNT-mediated uptake of 1 μM ^{3}H-labelled uridine inboth Na^+-containing transport medium (100 mM NaCl; pH 7.5) and Na^+-depleted, H^+-enriched medium (100 mM ChCl; pH 5.5). vcCNT-mediated uridine uptake was compared with uridineuptake values for control water-injected oocytes in 100 mM NaCl pH 7.5 transport medium. Asthere are no endogenous nucleoside transporters in oocytes (Yao *et al*., 1996), data from thecontrol water-injected oocytes is thought to be representative of passive diffusion across theoocyte plasma membrane. vcCNT-mediated uridine uptake in Na^+-depleted, H^+- enriched medium (100 mM ChCl; pH 5.5) was similar to that of water-injected oocytes, suggesting that the presence of H^+ in the extracellular medium does not play a role in facilitating uridine uptake. Conversely, uridine uptake in Na^+-containing transport medium (100 mM NaCl; pH 7.5) wassubstantially greater than that of either the control water-injected oocytes in Na^+-containingmedium (100 mM NaCl; pH 7.5) or the vcCNT-producing oocytes in Na^+-depleted, H^+-enriched medium (100 mM ChCl; pH 5.5). Thus vcCNT was confirmed to be Na^+-dependent. A linear relationship between uridine uptake and time was observed for at least the first ten minutes in the vcCNT–producing oocytes in 100 mM NaCl pH 7.5 transport medium, suggesting that uridineuptake is proportional to time within this period. From these data, it was decided that subsequent radioisotope flux experiments would utilize Na^+-containing, H^+-depleted transport media (100mM NaCl; pH 7.5) and ten-minute uridine uptake/influx intervals to measure initial rates ofvcCNT-mediated uridine transport.

To further investigate and confirm the cation dependence of the transporter, vcCNT-mediated uptake of 1 μM ^{3}H-labelled uridine in the presence of Na^+ and/or H^+ (100 mM NaCl or 100 mM ChCl, pH 7.5 and 5.5) was examined (Figure A-3). Uridine uptake values for bothvcCNT-producing (*black bars*) and control water-injected oocytes (*white bars*) are shown. In the presence of Na^+ (100 mM NaCl; pH 7.5), uridine uptake (0.29 ± 0.03 pmol/oocyte.10min^{-1}) was 3-fold greater than that observed in water-injected oocytes (0.09 ± 0.01 pmol/oocyte.10min^{-1}),while in the presence of Na^+ and H^+ (100 mM NaCl; pH 5.5; 0.22 ± 0.05 pmol/oocyte.10min^{-1}), a 4-fold difference was observed; however, the mediated uridine uptake values for both the NaCl

pH 7.5 and 5.5 conditions were not significantly different, suggesting pH-independent uridine uptake. In the presence of H^+ (100 mM ChCl; pH 5.5; 0.07 ± 0.01 pmol/oocyte.10min^{-1}) or absence of Na^+ at low H^+ concentration (100 mM ChCl; pH 7.5; 0.10 ± 0.01 pmol/oocyte.10min^{-1}), there was no significant difference in uridine uptake between vcCNT-producing oocytes and control water-injected oocytes, confirming that vcCNT-mediated uridine uptake is Na^+-dependent.

Concentration dependence of uridine influx - To determine the optimal uridine concentration to use in subsequent experiments, and to better understand vcCNT uridine transport kinetics, the concentration dependence of vcCNT-mediated influx of ^{3}H-labelled uridine in Na^+-containing,H^+-depleted transport media (100 mM NaCl; pH 7.5) is presented in Figure A-4. Uridine influx in vcCNT-producing oocytes in comparison to water-injected controls is shown in Figure A-4**A**, while Figure A-4**B** depicts mediated uridine influx, defined as the difference in uridine influx between control water-injected oocytes and vcCNT-producing oocytes. The relationship between vcCNT-mediated uridine influx and uridine concentration was hyperbolic and consistent with simple Michaelis-Menten kinetics, with a uridine K_m value of 5.1 ± 1.0 μM and a V_{max} value of 2.4 ± 0.12 pmol/oocyte.10min^{-1}.

Nucleoside selectivity - Competition studies, which involve the simultaneous addition of two potential permeants to the transporter, one radiolabelled, were undertaken to determine the nucleoside selectivity of vcCNT. A panel of five physiological purine (adenosine, guanosine, and inosine) and pyrimidine (cytidine and thymidine) nucleosides were individually and simultaneously added with 1 μM ^{3}H-labelled uridine in Na^+-containing transport medium (200 μM; 100 mM NaCl; pH 7.5) and compared to the uptake of uridine alone. The ability to inhibit uridine influx provides indirect evidence that the nucleoside examined is a permeant of the transporter, and the extent of that inhibition indicates the apparent affinity of the transporter for that nucleoside (Figure A-5). In comparison to the ^{3}H-labelled uridine influx alone (0.35 ± 0.05 pmol/oocyte.10min^{-1}), the co-application of 200 μM adenosine, guanosine, inosine, cytidine or thymidine yielded influx values between 0.09 - 0.11 pmol/oocyte.10min^{-1}: adenosine - 0.09± 1.1 pmol/oocyte.10min^{-1}, guanosine - 0.10 ± 0.01 pmol/oocyte.10min^{-1}, inosine - 0.10 ± 0.01 pmol/oocyte.10min^{-1}, cytidine - 0.09 ± 0.01 pmol/oocyte.10min^{-1}, and thymidine - 0.11 ± 0.01

pmol/oocyte.10min^{-1}. Consistent with essentially complete inhibition of uridine influx, these values were not significantly different from that observed in control water-injected oocytes [F(5, 66) = 0.81, p = 0.55], suggesting that all fivenucleosides are vcCNT permeants, and that vcCNT therefore exhibits broad nucleoside selectivity.

Effects of nucleobases on uridine transport - Figure A-6 further investigated the permeant selectivity of vcCNT by examining the effects of co-application of a panel of nucleobases on uridine influx, using the same cross-inhibition strategy applied in Figure A-5. vcCNT-mediated influx of 1 μM ^{3}H-labelled uridine uptake was examined either alone, or with the co-application of 200 μMadenine, cytosine, thymine, uracil, hypoxanthine, or guanine. In comparison to the^{3}H-labelled uridine influx alone (0.27 ± 0.02 pmol/oocyte.10min^{-1}), the co-application ofadenine(0.30 ± 0.02 pmol/oocyte.10min^{-1}), cytosine (0.29 ± 0.03 pmol/oocyte.10min^{-1}), thymine (0.26 ± 1.2 pmol/oocyte.10min^{-1}), uracil (0.25 ± 0.03 pmol/oocyte.10min^{-1}), hypoxanthine (0.28 ± 0.03 pmol/oocyte.10min^{-1}), or guanine (0.31 ± 0.03 pmol/oocyte.10min^{-1}) did not alter uridine transport, and values were not significantly different from the application of uridine alone [F(6, 67) = 0.67, p = 0.67], indicating that vcCNT does not mediate nucleobase transport.

Na^{+}-activation kinetics - Na^{+}-activation of vcCNT-mediated uridine uptake was investigated using 1 μM ^{3}H-labelled uridine in 100 mM NaCl pH 7.5 transport medium, with Na^{+} concentrations ranging from 0 - 100 mM. Figure A-7 depicts mediated uridine influx, defined as the difference in influx values between vcCNT-producing oocytes and control water-injected oocytes. The relationship between Na^{+}-concentration and uridine influx was hyperbolic for vcCNT-mediated transport, with a K_{50} value for Na^{+} of 5.6 ± 2.3 and a V_{max} value of 0.78 ± 0.07. The Hill coefficient was 0.64 ± 0.31, consistent with a Na^{+}:nucleoside stoichiometry of 1:1.

Uridine influx of vcCNT-N149 mutants - Previous studies of hCNT3 demonstrated the importance of residue N336 in Na^{+}/H^{+} coupling; thus, by analogy, the equivalent vcCNT residue, N149, was examined for its potential role in mediating vcCNT Na^{+}-dependent nucleoside transport. The experiments of Figure A-8 examined the uridine transport activity of vcCNT-WT and a series of vcCNT-N149 mutants in either Na^{+}-containing transport medium (100 mM NaCl; pH 7.5) pr Na^{+}-depleted, H^{+}-enriched medium (100 mM ChCl; pH 5.5). In 100 mM NaCl pH

7.5, uridine influx in the vcCNT-N149 mutants (0.07 ± 0.03 pmol/oocyte.10min^{-1} for vcCNT-N149S; 0.09 ± 0.01 pmol/oocyte.10min^{-1} for vcCNT-N149T; 0.04 ± 0.01 pmol/oocyte.10min^{-1} for vcCNT-N149A) was significantly lower than that observed in vcCNT-WT (0.35 ± 0.03 pmol/oocyte.10min^{-1}); specifically, 80 %, 74 %, and 89 % reductions in uridine influx were observed for vcCNT-N149S, vcCNT-N129T, and vcCNT-N149A mutants, respectively, in comparison to vcCNT-WT. Influx values, however, were still greater than that observed in control water-injected oocytes (0.03 ± 0.01 pmol/oocyte.10min^{-1}). In contrast, uridine influx values were low for both the vcCNT-WT (0.04 ± 0.01 pmol/oocyte.10min^{-1}) and vcCNT-N149 mutants in 100 mM ChCl pH 5.5 medium (0.05 ± 0.01 pmol/oocyte.10min^{-1} forvcCNT-N149S; 0.04 ± 0.01 pmol/oocyte.10min^{-1} for vcCNT-N149T; 0.03 ± 0.01 pmol/oocyte.10min^{-1} for vcCNT-N149A) and not significantly different [$F(3, 41) = 2.25$, $p = 0.096$] from each other, butstill greater than that observed in control water-injected oocytes (0.01 ± 0.01 pmol/oocyte.10min^{-1}). Comparing the two transport media used, greater uridine influx was observed in 100 mMNaCl pH 7.5, further validating vcCNT as a Na^+-dependent transporter.

Discussion

Although the vcCNT crystal structure has been solved (Johnson *et al*., 2012), its transport characteristics have not yet been defined. The primary objective of the research described here was to characterize transport mediated by vcCNT using the *Xenopus laevis* oocyte expression system in combination with radioisotope flux assays. The initial rate of uridine transport was determined by examining the time course of uridine uptake mediated by vcCNT (Figure A-2). Uridine uptake was linear for the first ten minutes of transport; thus, subsequent radioisotope influx experiments used ten minute uptake intervals to ensure that initial rates of transport were measured. Comparisons of uridine uptake in various transport media (Figures A-2, A-3) suggest that vcCNT is Na^+-dependent, in agreement with previously published observations (Johnson *et al*., 2012; Feng *et al*., 2013), and H^+-independent, similar to its human orthologs hCNT1/2, and different from hCNT3, which is additionally capable of utilizing H^+ electrochemical gradients to drive nucleoside transport (Smith 2004, 2005, 2007).

Kinetic studies examined the concentration dependence of vcCNT-mediated uridine influx (Figure A-4). A hyperbolic relationship indicative of saturable uridine transport and consistent with simple Michaelis-Menten kinetics was observed. vcCNT transported uridine with higher apparent affinity than hCNT1-3 (5.1 ± 1.0 μM versus 33, 40, and 15 μM for hCNT1-3, respectively) (Young *et al*., 2013). Further, Na^+-activation kinetics demonstrated functionally, for the first time, the Na^+:nucleoside coupling ratio of vcCNT. A hyperbolic relationship between Na^+ concentration and uridine influx was observed, and yielded a Hill coefficient consistent with a Na^+:nucleoside stoichiometry of 1:1. These results are in agreement with those of Johnson *et al*. (2012) who reported only a single Na^+-binding site within the vcCNT crystal structure, but contrasts with Feng *et al*. (2013) who predicted two Na^+-binding sites using molecular dynamic simulations.

The permeant selectivity of vcCNT was examined through nucleoside and nucleobase inhibition studies (Figures A-5 and A-6, respectively). In nucleoside inhibition studies, co-application of five physiological purine and pyrimidine nucleosides (adenosine, guanosine, inosine, cytidine, or thymidine) resulted in essentially complete inhibition of uridine influx, with values that were not significantly different from those observed in control water-injected oocytes. The ability of these nucleosides to essentially abolish uridine influx demonstrates that

they effectively compete with uridine for the vcCNT permeant binding site, and suggests that, similar to hCNT3, vcCNT exhibits broad selectivity for both purine and pyrimidine nucleosides. Although no evidence exists that the hCNTs are involved in nucleobase transport, the capability of vcCNT to transport nucleobases was also examined. In contrast to results obtained in the nucleoside inhibition studies, the co-application of six nucleobases (adenine, cytosine, thymine, uracil, hypoxanthine, or guanine) had no significant effect on uridine transport, suggesting that vcCNT, like hCNT1-3, functions exclusively as a nucleoside transporter.

Similar to hCNT1 and hCNT3 (Chapters 3 - 5), selection of the appropriate vcCNT-mutants to generate was based upon structural considerations as well as sequence alignments performed to determine the residues commonly located at the corresponding positions in various CNT family members (S.A. Baldwin, personal communication). The high sequence conservation and location of HP1 in both vcCNT and hCNT3 were of particular interest. According to the membrane topology of vcCNT and, by inference, other CNT family members, the tip of HP1 is located at the center of the transport domain, and is suggested to participate in the formation of the nucleoside binding pocket and, as well, the Na^+-binding site. Within this region, previous studies have highlighted the functional importance of hCNT3-N336 and hCNT1-N315 inmediating cation-dependent nucleoside transport (Chapters 3 - 5). Any alterations in this positionare thought to be critical because both the backbone and side-chain oxygen of the residue,according to the vcCNT topology model, are involved in the coordination of the Na^+ ion, whichwould have implications for the octahedral geometry of the vcCNT Na^+-binding site (Johnson *etal*., 2012). As such, the functional importance of the corresponding residue in vcCNT (N149) was chosen for investigation in the present study. It was postulated that the presence of aserine/threonine residue rather than an asparagine at this position may elicit H^+-driven rather than Na^+-driven transport, providing the rationale behind generating the vcCNT mutants vcCNT-N149S and vcCNT-N149T. A null vcCNT-N149A mutant was also generated.

Characterization of the vcCNT-N149 mutants (vcCNT-N149S, vcCNT-N149T, and vcCNT-N149A) and comparison to vcCNT-WT involved measurements of uridine influx in both Na^+-containing transport medium and in Na^+-depleted, H^+-enriched media (Figure A-8). A significant reduction in uridine transport activity was observed for all three mutants, with observed values greater than those in control water-injected oocytes, suggesting functional expression of the transporters (Figure A-8A). vcCNT-N149T exhibited the greatest uridine

influx, followed by vcCNT-N149S and vcCNT-N149A. Substitution to alanine removed any possibility of hydrogen bonding with Na^+. The dramatic reduction in uridine influx in the vcCNT-N149A mutant likely resulted from disruption of coordination of the Na^+ ion, providingevidence that the vcCNT-N149 residue plays an important role in cation-binding. Since all three vcCNT-N149 mutations produced a significant reduction in uridine influx compared to the wild- type protein, experiments to determine cell-surface expression are needed to exclude the possibility that mutation of the vcCNT-N149 residue impaired correct protein folding andtrafficking to the plasma membrane.

In Na^+-depleted, H^+-enriched medium, no significant difference in uridine transport activity was observed between vcCNT-WT and the vcCNT-N149 mutants, with uridine influx for all of the mutants being significantly greater than that in control water-injected oocytes, indicative of functional transporter expression (Figure A-8B). Comparing the two transport media used, the Na^+-containing transport medium resulted in greater transport activity, both forwild-type and vcCNT mutants, supporting the observation that vcCNT-mediated nucleosidetransport is Na^+-dependent. Although it was postulated that the presence of either a serine orthreonine in place of asparagine at this position might result in H^+-dependent transport, this was not the case (see also Chapters 4 and 5 for corresponding data for hCNT3 and hCNT1 mutants, respectively). This is potentially because H^+ coupling of CNTs might involve hydronium ions,which would bind to the transporter through potential interaction with three, not just one aminoacid residue.

In conclusion, this Appendix has described the functional expression and characterization of vcCNT, a bacterial member of the CNT nucleoside transporter family from the pathogenic bacterium *Vibrio cholerae*, in the *Xenopus oocyte* heterologous expression system. Transport properties, including kinetics of uridine transport, cation specificity, nucleoside selectivity, and coupling ratio were analyzed. Mutations of residue vcCNT-N149 to alanine, serine, and threonine resulted in substantial reductions in uridine transport in Na^+-containing transport medium, suggesting its role incation-binding.

References

Feng, Z., Hou, T., and Li, Y. 2013. Transport of nucleosides in the vcCNT facilitated by sodium gradients from molecular dynamics simulations. *Mol. Biosyst.* 9:2142-2153.

Johnson, Z.L., Cheong, C., and Lee, S. Crystal structure of a concentrative nucleoside transporter from *Vibrio cholerae* at 2.4 Å. *Nature* 483:489-493.

Mulinta, R., Slugoski, M.D., Ng, A.M.L., Yao, S.Y.M., Cass, C.E., Baldwin, S.A., and Young, J.D. Substituted cysteine accessibility method (SCAM) analysis of transport domain of human concentrative nucleoside transporter 3 (hCNT3) reveals features of structural and functional importance. *Unpublished observations*.

Smith, K.M., Ng, A.M., Yao, S.Y., Labedz, K.A., Knaus, E.E., Wiebe, L.I., Cass, C.E., Baldwin, S.A., Chen, X.Z., Karpinski, E., and Young, J.D. 2004. Electrophysiological characterization of a recombinant human Na^+-coupled nucleoside transporter (hCNT1) produced in *Xenopus* oocytes. *J. Physiol.* 558:807-823.

Smith, K.M., Slugoski, M.D., Loewen, S.K., Ng, A.M.L., Yao, S.Y.M., Chen, X., Karpinski, E., Cass, C.E., Baldwin, S.A., Young, J.D. 2005. The broadly selective human Na^+/nucleoside cotransporter (hCNT3) exhibits novel cation-coupled nucleoside transport characteristics. *J. Biol. Chem*. 280:25436-25449.

Smith, K.M., Slugoski, M.D., Cass, C.E., Baldwin, S.A., Karpinski, E., and Young, J.D. 2007. Cation coupling properties of human concentrative nucleoside transporters hCNT1, hCNT2 and hCNT3. *Mol. Membr. Biol*. 24:53-64.

Yao, S.Y.M., Ng, A.M.L., Ritzel, M.W.L., Gati, W.P, Cass, C.E., and Young, J.D. 1996. Transport of adenosine by recombinant purine- and pyrimidine-selective sodium/nucleoside cotransporters from rat jejunum expressed in *Xenopus laevis* oocytes. *Mol. Pharmacol.* 50:1529-1535.

Young, J.D., Yao, S.Y.M., Baldwin, J.M., Cass, C.E., and Baldwin, S.A. 2013. The human concentrative and equilibrative nucleoside transporter families, SLC28 and SLC29. *Mol. Aspects Med.* 34:529-547.

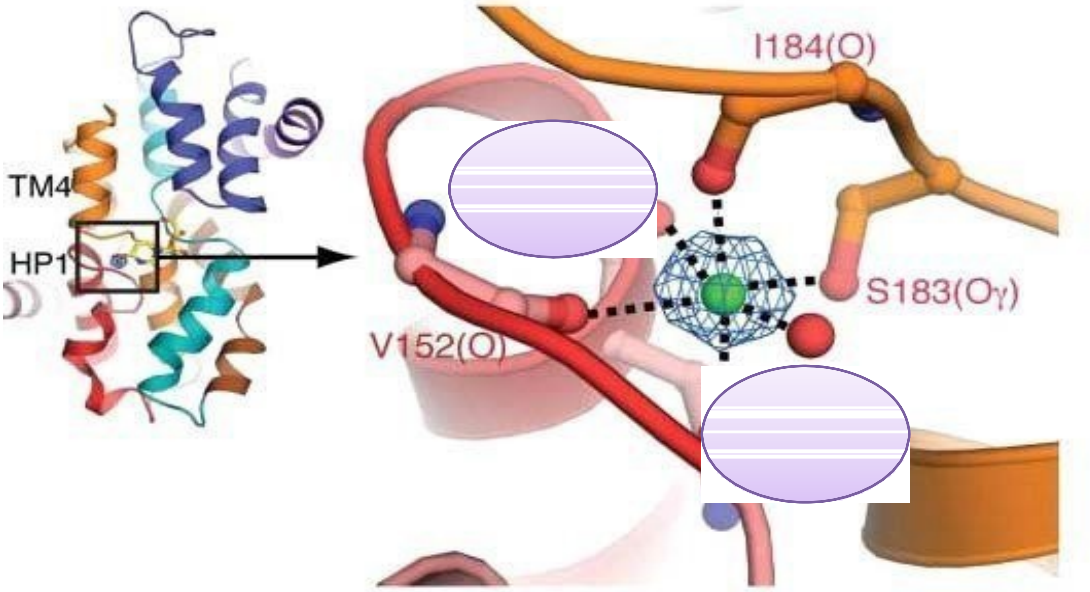

Figure A-1: Modelled structure of the Na^+-binding site in vcCNT. The Na^+-binding site, located between HP1 and the unwound region of TM4 in vcCNT, is coordinated in an ideal octahedral coordination site with N149, V152, S183, and I184 and a water molecule (shown in *red*). Coordination of the Na^+ ion is shown as dashed lines. vcCNT residue N149 is highlighted.

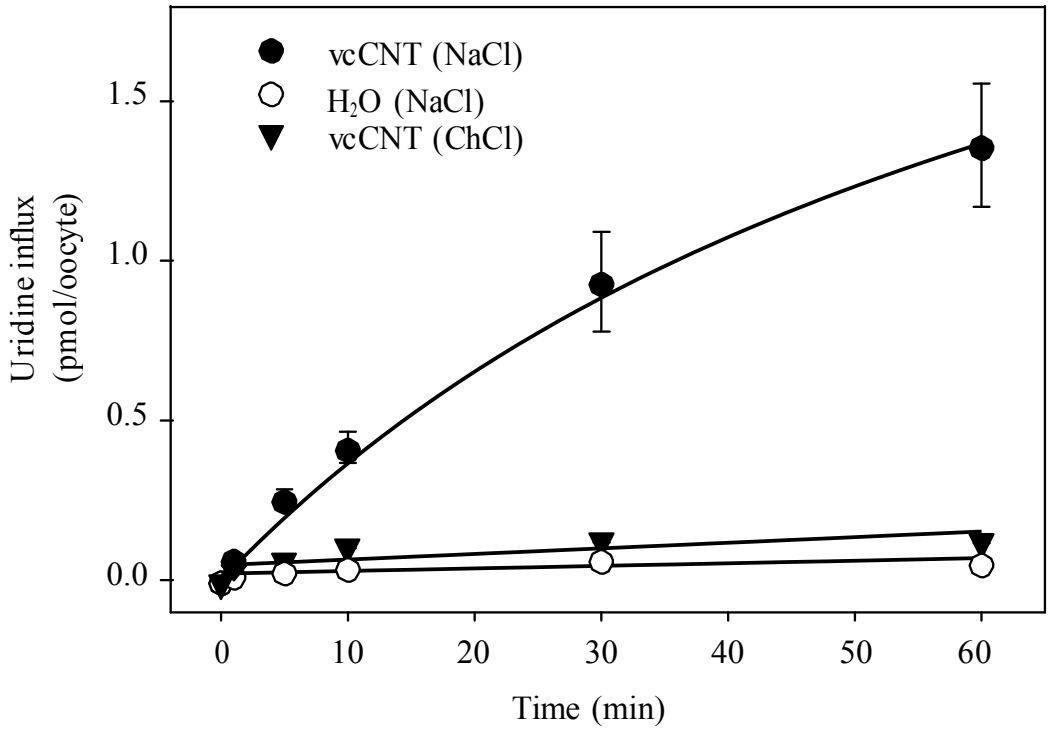

Figure A-2: Time course of uridine uptake by recombinant vcCNT produced in *Xenopus laevis* oocytes. Oocytes were injected with 10 - 20 nl vcCNT RNA transcripts (1µg/µl) or 10 -20 nl water and incubated for 5 days at 18 °C in MBM. Uptake of ^{3}H-labelled uridine (1 µM; 20 °C) for vcCNT-expressing oocytes was measured in transport medium containing either 100 mMNaCl pH 7.5 (*solid* circles) or 100 mM ChCl pH 5.5 (*solid* triangles), and compared to uptake by control water-injected oocytes (*open* circles; 100 mM NaCl; pH 7.5). Uridine uptake valuesrepresent the means ± SEM of data obtained from 10 - 12 oocytes.

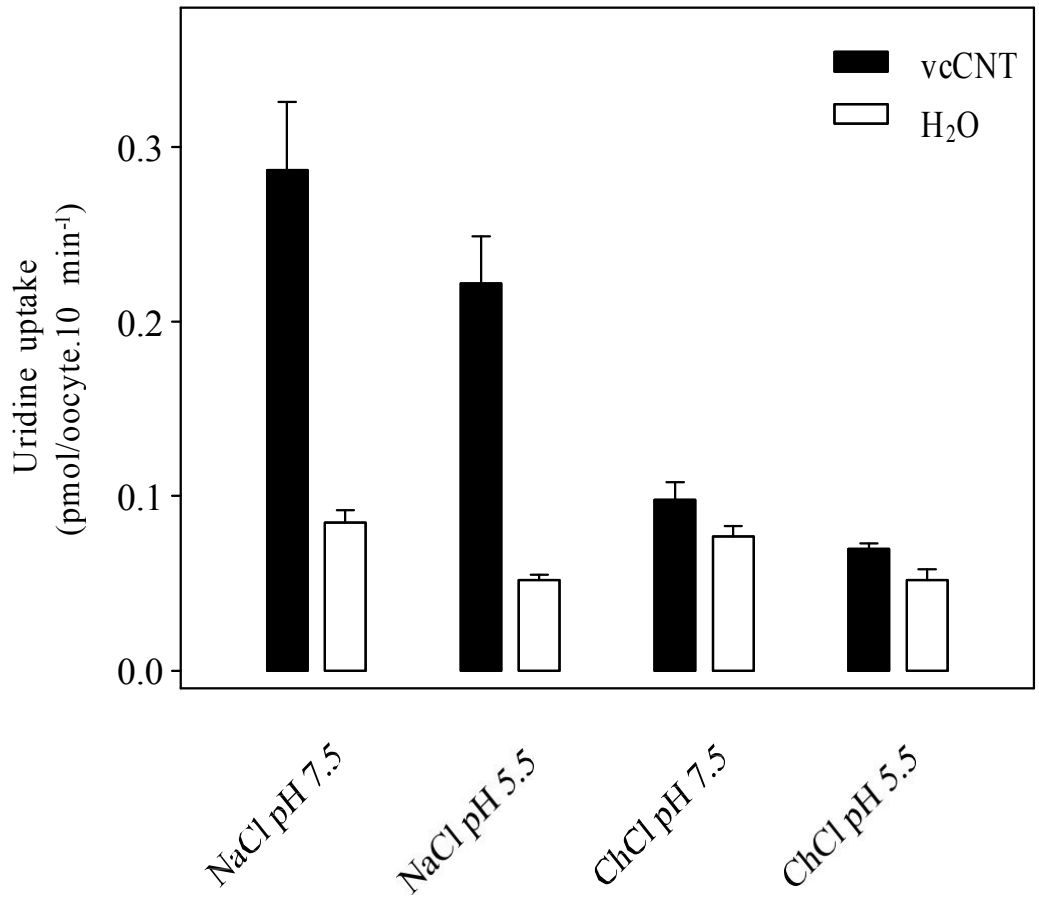

Figure A-3: Cation dependence of recombinant vcCNT produced in *Xenopus laevis* oocytes. Oocytes were injected with 10 - 20 nl of vcCNT RNA transcripts (1µg/µl; *black* bars) or 10 - 20 nl of water (*white* bars) and incubated for 5 days at 18 °C in MBM. Uptake of ^{3}H-labelled uridine (1 µM; 10 min flux; 20 °C) was measured in transport medium containing either 100 mM NaCl or ChCl at pH 5.5 and 7.5, and compared against uridine uptake in control water-injected oocytes. Uridine uptake values represent the means ± SEM of data obtained from 10 - 12 oocytes.

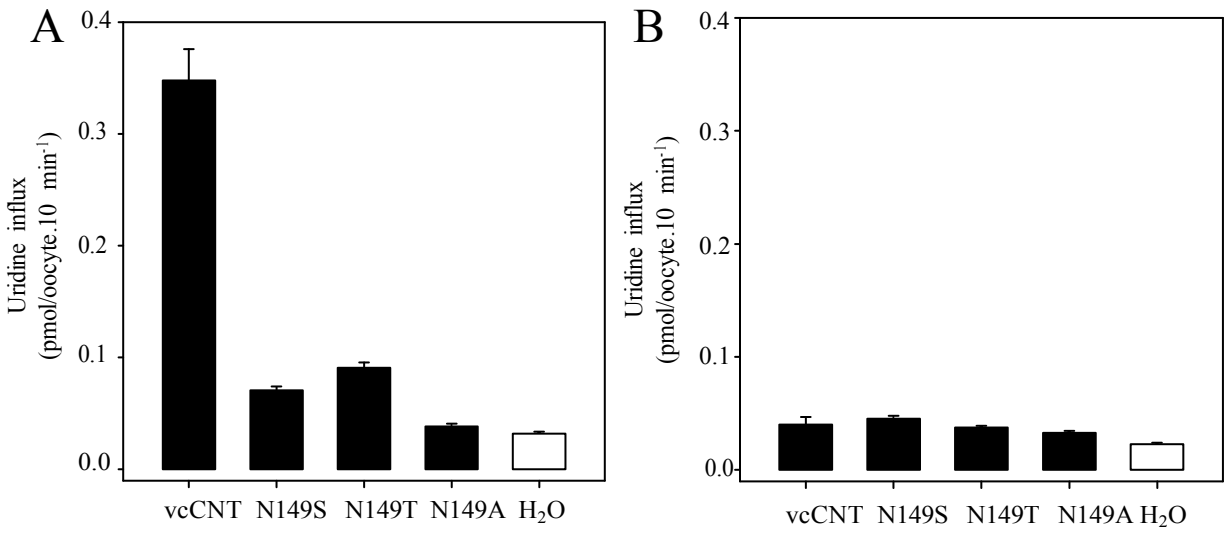

Figure A-4: Concentration dependence of uridine influx by recombinant vcCNT produced in *Xenopus laevis* oocytes. Oocytes were injected with 10 - 20 nl vcCNT RNA transcripts (1µg/µl) or 10 - 20 nl water and incubated for 5 days at 18 °C in MBM. Influx of ^{3}H-labelled uridine (1 µM; 10 min flux; 20 °C) for vcCNT-producing oocytes was measured in transport medium containing 100 mM NaCl pH 7.5 (*solid* circles) and compared with control water-injected oocytes (*open* circles) in panel **A**. Mediated uridine influx, representing the difference between uridine influx in control water-injected oocytes and vcCNT-producing oocytes is shown in panel **B**, yielding a uridine apparent affinity (K_m) of 5.1 ± 1.0 µM and a V_{max} of 2.4 ± 0.12 pmol/oocyte.10.min^{-1}, consistent with simple Michaelis-Menten kinetics. Uridine influx values represent the means ± SE of data obtained from 10 - 12 oocytes.

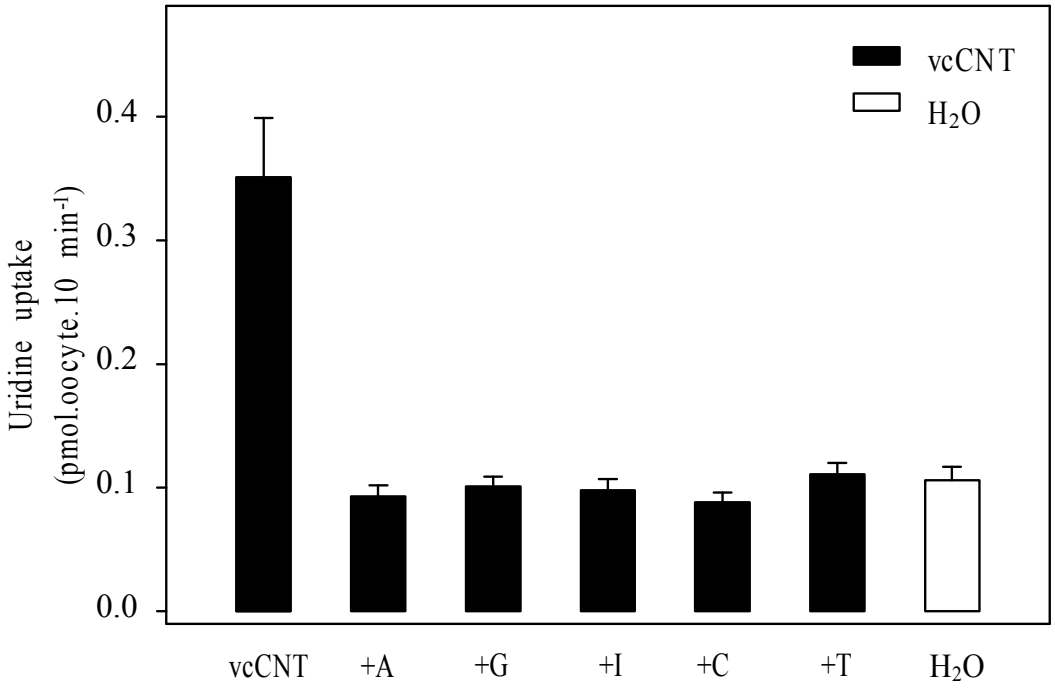

Figure A-5: Nucleoside selectivity of recombinant vcCNT produced in *Xenopus laevis* oocytes. Oocytes were injected with 10 - 20 nl of vcCNT RNA transcripts (1µg/µl) or 10 - 20 nl of water and incubated for 5 days at 18 °C in MBM. Uptake of ^{3}H-labelled uridine (1 µM; 10min flux; 20 °C) alone, or with the co-application of 200 µM physiological nucleosidesadenosine (A), guanosine (G), inosine (I), cytidine (C) or thymidine (T) was measured intransport medium containing 100 mM NaCl pH 7.5, and compared against uridine influx incontrol water-injected oocytes. Nucleoside co-application resulted in a complete attenuation of vcCNT-mediated uridine influx, and resultant uridine influx values were not significantly different from that observed in control water-injected oocytes [$F(5, 66) = 0.81$, $p = 0.55$]. Uridine influx values represent the means ± SEM of data obtained from 10 - 12 oocytes.

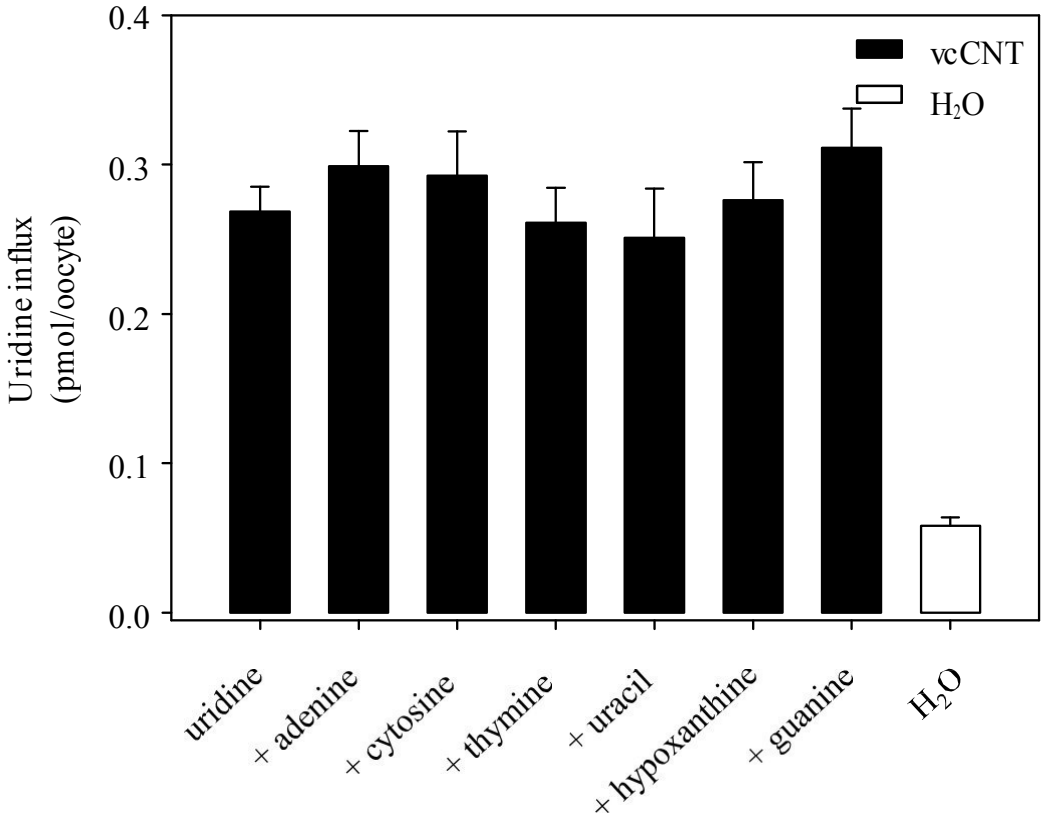

Figure A-6: Effects of nucleobases on uridine transport by recombinant vcCNT produced in *Xenopus laevis* oocytes. Oocytes were injected with 10 - 20 nl vcCNT RNA transcripts (1µg/µl) or 10 - 20 nl water and incubated for 5 days at 18 °C in MBM. Uptake of ^{3}H-labelled uridine (1 µM; 10 min flux; 20 °C) alone, or with the co-application of a panel of nucleobases(200 µM) was measured in transport medium containing 100 mM NaCl pH 7.5, and comparedagainst uridine uptake in control water-injected oocytes. vcCNT-mediated uridine influx was not significantly different in vcCNT RNA transcript-injected oocytes alone, or with nucleobase co-application [$F(6, 67) = 0.67$, $p = 0.67$]; thus, nucleobase co-application did not have a significant effect on vcCNT-mediated uridine influx. Uridine uptake values represent the means ± SEM of data obtained from 10 - 12 oocytes.

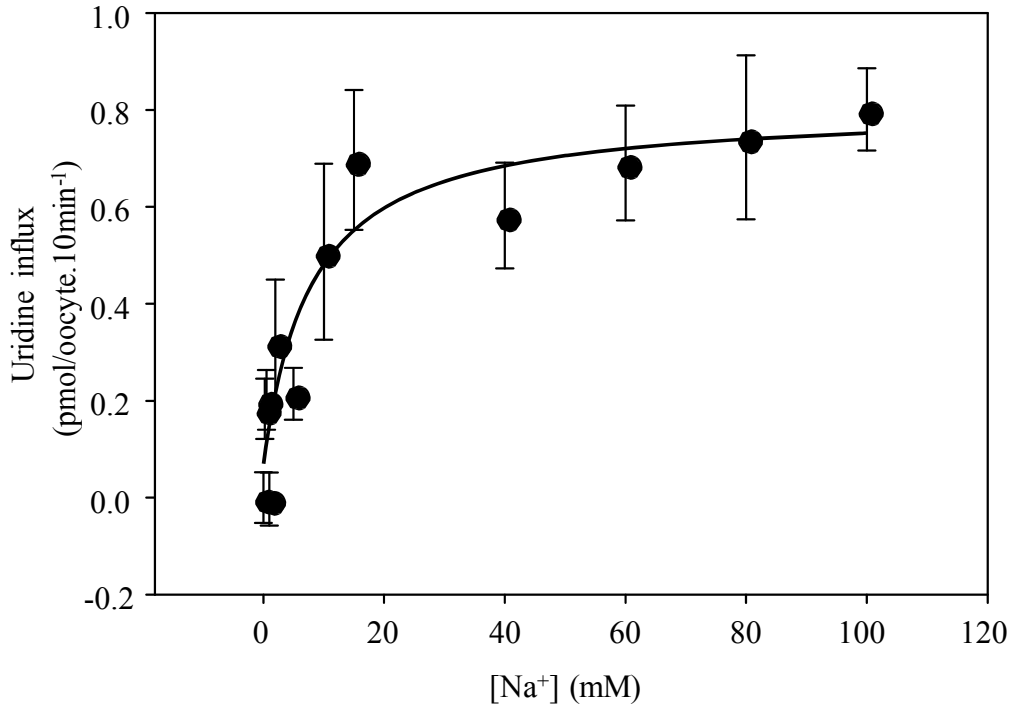

Figure A-7: Na^+-activation of vcCNT. Oocytes were injected with 10 - 20 nl of vcCNT RNA transcripts (1µg/µl) or 10 - 20 nl of water and incubated for 5 days at 18 °C in MBM. Influx of ^{3}H-labelled uridine (1 µM; 10 min flux; 20 °C) was measured in transport medium containing 0 - 100 mM NaCl pH 7.5, and values were corrected for basal non-mediated uridine influx in control water-injected oocytes. The K_{50} was 5.6 ± 2.3 mM and the Hill coefficient was 0.6 ± 0.3, which is consistent with a Na^+:uridine stoichiometry of 1:1. Uridine influx values are means ± SE ofdata obtained from 10 - 12 oocytes.

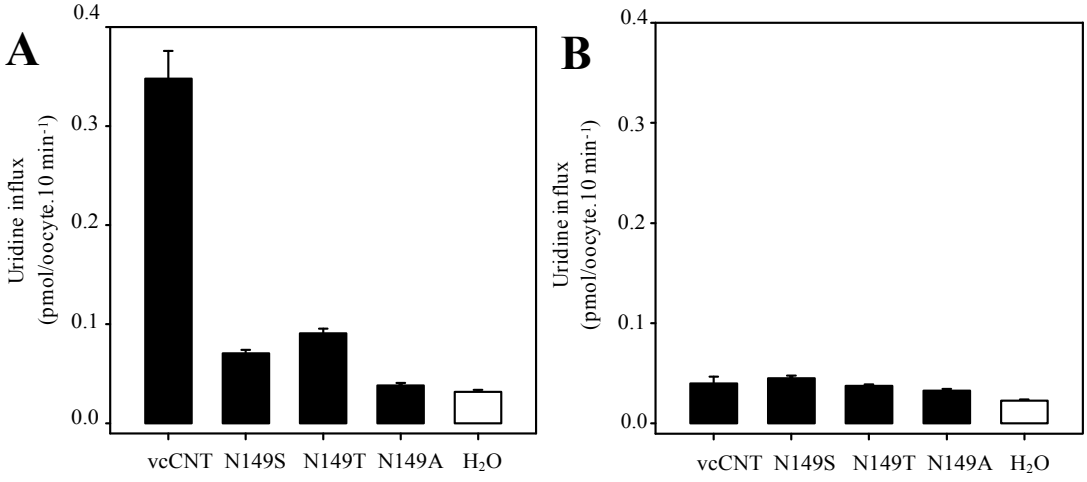

Figure A-8: Uridine influx by recombinant vcCNT-WT and vcCNT-N149 mutants produced in *Xenopus laevis* oocytes. Oocytes were injected with 10 - 20 nl vcCNT RNA transcripts (WT or N149 mutant) (1μg/μl) or 10 -2 0 nl water and incubated for 5 days at 18 °C in MBM. Influx of ^{3}H-labelled uridine (1 μM; 10 min flux; 20 °C) was measured in transport medium containing either 100 mM NaCl pH 7.5 (panel **A**) or 100 mM ChCl pH 5.5 (panel **B**). In the Na^{+}-containing transport medium (100 mM NaCl; pH 7.5), all vcCNT-N149 mutants exhibited a decrease in uridine influx. In the Na^{+}-depleted, H^{+}- enriched medium (100 mM ChCl; pH 5.5), uridine influx values of vcCNT-WT and the vcCNT-N149 mutants were not significantly different [$F(3, 41) = 2.25$, $p = 0.096$], although influx was significantly greater thanthat observed in the control water-injected oocytes. Uridine influx values are means ± SEM ofdata obtained from 10 - 12 oocytes.